Annual Report
Jahresbericht

2000

WALTHER-MEISSNER-INSTITUT
für Tieftemperaturforschung
Bayerische Akademie der Wissenschaften

Walther-Meissner-Institut für Tieftemperaturforschung
Bayerische Akademie der Wissenschaften
Walther-Meissner Str. 8
D - 85748 Garching

Phone: **+49 - (0)89 289 14202**
Fax: **+49 - (0)89 289 14206**
e-mail: **Emel.Doenertas@wmi.badw.de**
WWW: **http://www.wmi.badw.de**

Preface

The Walther-Meissner-Institute for Low Temperature Research (WMI) of the Bavarian Academy of Sciences carries out research projects at low and ultra-low temperatures and supplies liquid helium to both universities in Munich. The research program of the WMI is devoted to fundamental and applied research in the field of low temperature solid state physics with the main focus on superconductivity and superfluidity, magnetism and magneto-electronics, mesoscopic systems as well as on the general properties of metallic systems at low and very low temperatures. It also conducts applied research into methods of generating and using low temperatures. With respect to materials the research program is focused on superconducting and magnetic materials, both in bulk and thin films.

The year 2000 was an important year for the WMI. After the former director Prof. Dr. Klaus Andres retired in March 1999, Prof. Dr. Gerhard Abstreiter from the Walter-Schottky Institute was the acting head of the institute until June 2000. In July 2000, Prof. Dr. Rudolf Gross became the new director of the Walther-Meissner Institute and at the same time obtained the chair for Technical Physics (E23) at the Technical University of Munich.

With the change of director there has been also a shift of research priorities at the WMI and an extension of the activities to new fields. However, the general focus of the research program of the WMI is still on low temperature solid state physics and the development of low and ultra-low temperature techniques. The research activities can be subdivided into (i) basic research, (ii) application oriented research and (iii) materials and low temperature techniques. With respect to basic research, the future research activities are devoted to the phenomena superconductivity and magnetism, ordering phenomena in correlated electron systems as well as to the physics of low dimensional and mesoscopic systems. In the field of application oriented basic research the focus of the WMI will be on superconducting and magneto-electronic devices as well as novel devices based on quantum phenomena. With respect to low temperature techniques, the WMI develops new methods and techniques for experiments at low and ultra-low temperatures. The materials oriented work represents a new research area at the WMI. Here, our activities are devoted to the development of techniques for the growth of thin films and single crystals of superconducting and magnetic materials with special focus on complex transition metal oxides. In this area the transfer of innovative materials technology to applications is a key issue of our research with new functional materials and multi-functional thin film structures playing a central role.

The research at the WMI has been very successful in 2000 as demonstrated by a large number of scientific papers and invited presentations at international conferences. This is a good piece of news since the change of director and the reorientation of the research program were related to substantial building activities unavoidably disturbing the research work. However, also in this transitional stage the ongoing research projects have been successfully continued and new projects have been started. This Annual Report gives an overview on the scientific results which in many cases have been obtained in collaboration with international guests. Within this year the international collaboration again has been extended. At the suggestion of the WMI, Prof. V. L. Ginzburg, Russian Academy of Sciences, received the Humboldt Research Award in 2000. The WMI is very pleased to be able to welcome this outstanding physicist for a longer research stay within the next year.

There is no doubt that the success of the research at the WMI is based on the outstanding competence and experience of the staff having long-standing experience in the field of low temperature research. However, for the continuous development of the research program and the scientific progress the impetus and new scientific accents of young scientists and Ph.D. students is important. In this respect the year 2000 was very successful, since the WMI could win 4 young scientists (Dr. habil. Lambert Alff, Dr. habil. Andreas Erb, Dr. Achim Marx, Dr. Matthias Opel) and 6 Ph.D. students as new members of the scientific staff. These young researchers are highly important for the further development of the institute and the future success of our research program.

Our 2000 Annual Report is intended to provide an overview of our work to our friends and partners in research and industry and thereby to intensify our numerous cooperations. I would be particularly pleased if the report stimulates new collaborations. In order to be useful also for our numerous international partners, especially within EU projects, the report is now entirely in English. I would like to thank all authors and editors of this Annual Report for their effort and careful work.

I finally would like to thank all the colleagues, guests and cooperating partners who contributed to the success of our work within the last year and last but not least our ministry and administration for their trust and support.

Garching, December 2000

Rudolf Gross

Contents

Preface **1**

Reports: **5**

Basic Research **5**

Superconductivity and Superfluidity 5

Electronic Raman Response in Anisotropic Normal Metals 6

Collective Spin Fluctuation Mode and Raman Scattering in Superconducting Cuprates 8

Antiferromagnetism and Pseudogap in Y-123 and Bi-2212 11

Doping-dependent Pair Breaking in Y-123 and Bi-2212 14

Symmetry of the order parameter in hole and electron doped high-temperature superconductors 17

Pseudogap in electron doped cuprate high-temperature superconductors 19

Competition between the Pauli and orbital effects of magnetic field on the low-temperature electronic state of the organic metal α-(BEDT-TTF)$_2$KHg(SCN)$_4$ 21

Magnetisation studies of α-(BEDT-TTF)$_2$KHg(SCN)$_4$ at fields almost or exactly parallel to the layers 24

Anisotropy of high mobility electron systems at millikelvin temperatures 27

Tunneling between Quantum Hall Edge Channels in non Planar Geometry 30

Magnetotransport investigation of type-III modulation doped HgTe single quantum wells . . . 32

Studying the interaction of coupled quantum dots in the few electon limit 34

Local Magnetic Order in Manganite Thin Films Studied by $1/f$ Noise Measurements 36

DC Magnetic penetration depth of UPt_3 and Sr_2RuO_4: implications for the superconducting order parameters 39

Viscoelastic Model of Normal ^{3}He in Aerogel 41

Application Oriented Basic Research **43**

Shot noise and conductance fluctuations in mesoscopic metallic nanowires 43

Transport and Noise Characteristics of Submicron High-Temperature Superconductor Grain-Boundary Junctions 46

Tunneling magnetoresistance in doped manganite grain boundary junctions 49

Heteroepitaxial growth of high-temperature superconductors and doped manganites in ramp type geometry 52

Materials and Experimental Techniques **55**

$^{3}He/^{4}He$ dilution refrigerator with pulse tube refrigerator 55

Epitaxial thin films of ordered double perovskite materials with magnetoresistance at room temperature 57

Crystal growth and bulk materials of transition metal oxides 59

Mössbauer Spectroscopic Investigation of Redox Reactions in Vermiculites from Santa Olalla (Huelva, Spain) 60

Electrochemical Intercalation of Alkylammonium Ions into the Isostructural Layered Dichalcogenides 2H-NbS_2 and 2H-TaS_2 63

Computing, Network, and Internet Services 66

Publications **68**

Completed Diploma and Ph.D. Theses **71**

Research Projects and Cooperations **72**

Invited Talks **74**

Seminars **77**

Staff of the WMI **80**

Guest Researchers **81**

Commission for Low Temperature Physics **82**

Superconductivity and Superfluidity

Dietrich Einzel

This project, part of which is published in ref. [1], deals with a unified theoretical treatment of weakly coupled pair–correlated Fermi systems, and includes metallic superconductivity as well as the superfluidity of neutral Fermi liquids. Both the equilibrium properties and the response of these systems to weak external perturbations are discussed.

The pair– correlated Fermi systems investigated include, besides the conventional superconductors of the old days, the superfluid phases of liquid ^{3}He (–A,B, ...), heavy electron superconductors (for example UBe_{13}, UPt_3, ...), organic superconductors (for example κ–$(BEDT–TTF)_2Cu(NCS)_2$, ...), cuprate (high–T_c) superconductors, and the Ruddlesden–Popper system Sr_2RuO_4.

As a first step, the different flow resistance mechanisms in charged (Drude's law) and neutral systems (Hagen–Poiseuille's law) in their normal conducting or fluid state are explained and contrasted with that of the superconductor or superfluid.

The next step is a systematic classification of the pair–correlated Fermi sytems with respect to the symmetry of their respective ground state order. The classification adresses both the spin (singlet vs. triplet pairing) and the orbital (gap nodes, conventional vs. unconventional) structure of the order parameter.

The equilibrium properties are reflected in analytical results for the generalized universal BCS–Mühlschlegel parameters like the normalized zero temperature energy gap maximum $\Delta_0(0)/k_BT_c$ and the specific discontinuity at the transition $\Delta C/C_N$ for the various pairing symmetries under consideration.

Finally the response of the systems to weak external perturbations such as a temperature change $\delta T(\mathbf{r},t)$, the electromagnetic scalar $\phi(\mathbf{r},t)$ and vector $\mathbf{A}(\mathbf{r},t)$ potentials, and a magnetic field $\mathbf{B}(\mathbf{r},t)$ is investigated. The corresponding response functions are the heat capacity $C_B(T)$, the spin susceptibility $\chi_B(T)$ and the London–BCS magnetic field penetration depth $\lambda_L(T)$, in which both the properties of the gas of thermal excitations (Bogoliubov quasiparticles) and the condensate (Cooper pairs) are reflected. Again, analytical results for the asymptotic low T (activated vs. power law) behavior of these response functions are given for various gap anisotropies.

The result is a complete weak coupling BCS two–fluid description of singlet and triplet conventional and unconventional superconducters and superfluids. A comparison of the theoretical predictions for $C_B(T)$, $\chi_B(T)$ and $\lambda_L(T)$ with experimental observations can help to identify the symmetry of the superconducting and superfluid ground state.

References

[1] D. Einzel, *Lexikon der Physik*, Spektrum Akademischer Verlag, 2000, S. 228 – 235

Electronic Raman Response in Anisotropic Normal Metals

Dietrich Einzel

This project extends a treatment of the electronic Raman response of anisotropic normal metals with impurities [1] to finite wavenumbers ($|\mathbf{q}| \ll k_{\mathrm{F}}$). A second momentum relaxation mechanism (for example inelastic electron–electron or spin fluctuation scattering) is incorporated on a phenomenological level. The theory makes use of the Landau–Boltzmann equation for anisotropic metals. The calculations account for the long–range Coulomb interaction of the electrons within the RPA and treat the collision operator, in which elastic and inelastic processes are assumed to add up linearly, within a (charge) conserving relaxation time approximation. The generalization of the Lindhard density response function [2] to the Raman case is the main purpose of this work.

We consider an anisotropic normal metal in which the electronic states are characterized by a momentum $\hbar\mathbf{k}$, an energy dispersion $\varepsilon_{\mathbf{k}} = \mu + \xi_{\mathbf{k}}$ (with μ the Fermi energy), a group velocity $\mathbf{v}_{\mathbf{k}} = (1/\hbar)\nabla_{\mathbf{k}}\varepsilon_{\mathbf{k}}$, an inverse effective mass tensor $M_{ij}^{-1}(\mathbf{k}) = \partial^2\varepsilon_{\mathbf{k}}/\hbar^2\partial k_i \partial k_j$, and an equilibrium Fermi distribution $n_{\mathbf{k}}$ with derivative $\varphi_{\mathbf{k}} = -\partial n_{\mathbf{k}}/\partial\xi_{\mathbf{k}}$. Next we consider an external perturbation appropriate for a treatment of the electronic Raman response within the effective mass approximation:

$$U_{\mathbf{k}}^{\mathrm{ext}} = \underbrace{m\hat{\mathbf{e}}^{\mathrm{S}} \cdot \mathbf{M}^{-1}(\mathbf{k}) \cdot \hat{\mathbf{e}}^{\mathrm{I}}}_{\gamma_{\mathbf{k}}} \cdot \underbrace{\frac{e^2}{mc^2}|\mathbf{A}^{\mathrm{I}}||\mathbf{A}^{\mathrm{S}}|}_{u_\gamma^{\mathrm{ext}}} \tag{1}$$

The response of the electronic system to this perturbation is described within the the quasiclassical limit of the kinetic equation:

$$\omega\delta n_{\mathbf{k}} - \mathbf{q}\cdot\mathbf{v}_{\mathbf{k}} h_{\mathbf{k}} = i\sum_{\nu=\mathrm{e,i}} \delta I_{\mathbf{k}}^{\nu} \tag{2}$$

Here $h_{\mathbf{k}} = \delta n_{\mathbf{k}} + \varphi_{\mathbf{k}}\delta\xi_{\mathbf{k}}$, $\delta\xi_{\mathbf{k}} = U_{\mathbf{k}}^{\mathrm{ext}} + V(\mathbf{q})\delta n_1$ and $\delta n_b = \sum_{\mathbf{p},\sigma} b_{\mathbf{p}}\delta n_{\mathbf{k}}$. $V(\mathbf{q}) = 4\pi e^2/\mathbf{q}^2$ is the Fourier transform of the long range Coulomb interaction. The collision integrals for elastic (ν =e) and inelastic (ν =i) have the form (conserving relaxation time approximation)

$$\delta I_{\mathbf{k}}^{\nu} = -\Gamma_{\mathbf{k}}^{\nu} h_{\mathbf{k}} + \sum_{\mathbf{p}\sigma} C_{\mathbf{kp}}^{\nu} h_{\mathbf{p}} \quad ; \quad C_{\mathbf{kp}}^{\nu} \approx \varphi_{\mathbf{k}} \sum_b \lambda_b^{\nu} \frac{b_{\mathbf{k}}\Gamma_{\mathbf{k}}^{\nu} b_{\mathbf{p}}\Gamma_{\mathbf{p}}^{\nu}}{\sum_{\mathbf{p}\sigma}\varphi_{\mathbf{p}} b_{\mathbf{p}}^2 \Gamma_{\mathbf{p}}^{\nu}} \tag{3}$$

The scattering parameters λ_b^{ν} allow for a classification of the macroscopic moments δn_b into conserved ($\lambda_b^{\nu} = 1$) and nonconserved ($\lambda_b^{\nu} < 1$) quantities. In what follows, we will, for the sake of simplicity, restrict ourselves to the case of charge conservation $\lambda_1^{\nu} = 1$, $\lambda_b^{\nu} = 0\ \forall b \neq 1$. The Raman response, as obtained from Eqs. (1)–(3) is then of the form

$$\begin{aligned} \delta n_\gamma(\mathbf{q},\omega) &= L_{\gamma\gamma}(\mathbf{q},\omega) u_\gamma^{\mathrm{ext}}(\mathbf{q},\omega) \\ L_{\gamma\gamma} &= M_{\gamma\gamma}^* - \frac{M_{\gamma 1}^{*2}}{M_{11}^*}\left(1 - \frac{1}{\varepsilon}\right) - \Xi_{\gamma\gamma}^* + \frac{\Xi_{\gamma 1}^{*2}}{\Xi_{11}^*} + \frac{\Xi_{11}^*\zeta_{\gamma\gamma}^*}{\varepsilon} + O\left(\mathbf{q}^2, \frac{1}{\varepsilon}\right) \end{aligned} \tag{4}$$

Here M_{ab}^* is the generalization of the Lindhard function to arbitrary vertices $q_{\mathbf{k}}$, $b_{\mathbf{k}}$ and to the inclusion of collision effects:

$$M_{ab}^* = \frac{\mathbf{q}\cdot\left(\mathbf{T}_{ab}^{(0)*} + \zeta_{ab}^*\mathbf{T}_{11}^{(1)*} - \mathbf{T}_{ab}^{(1)*}\right)\cdot\mathbf{q}}{i\omega - \mathbf{q}\cdot\mathbf{D}_{11}^{(1)*}\cdot\mathbf{q}} \tag{5}$$

$\mathbf{T}_{ab}^{(\mu)*}$ are generalizations of the electronic conductivity to general vertices a, b:

$$\begin{aligned}
\mathbf{T}_{ab}^{(\mu)*} &= \sum_{\mathbf{p}\sigma}\left(-\frac{\partial n_{\mathbf{p}}}{\partial \xi_{\mathbf{p}}}\right) f_{\mathbf{p}} \frac{a_{\mathbf{p}}\mathbf{v}_{\mathbf{p}} : b_{\mathbf{p}}\mathbf{v}_{\mathbf{p}}}{-i\omega+\Gamma_{\mathbf{p}}^*}\left(\frac{i\Gamma_{\mathbf{p}}^*}{\omega+i\Gamma_{\mathbf{p}}^*}\right)^{\mu} \\
f_{\mathbf{p}} &= = \frac{(\omega+i\Gamma_{\mathbf{p}}^*)^2}{\left(\omega+i\Gamma_{\mathbf{p}}^*\right)^2-(\mathbf{q}\cdot\mathbf{v}_{\mathbf{p}})^2} \\
\Gamma_{\mathbf{p}}^* &= \sum_{\nu=\mathrm{e,i}} \Gamma_{\mathbf{p}}^{\nu} = \Gamma_{\mathbf{p}}^{\mathrm{e}} + \Gamma_{\mathbf{p}}^{\mathrm{i}}
\end{aligned}$$

The quantities $\mathbf{D}_{ab}^{(\mu)*}$ are generalized diffusion tensors

$$\mathbf{D}_{ab}^{(\mu)*} = \frac{\mathbf{T}_{ab}^{(\mu+1)*}}{N_{ab}^*} \quad ; \quad N_{ab}^* = \sum_{\mathbf{p}\sigma}\left(-\frac{\partial n_{\mathbf{p}}}{\partial \xi_{\mathbf{p}}}\right)\frac{i\Gamma_{\mathbf{p}}^*}{\omega+i\Gamma_{\mathbf{p}}^*} a_{\mathbf{p}} b_{\mathbf{p}}$$

Ξ_{ab}^* are the collision–limited Raman response function which have a finite $\mathbf{q}\to 0$ limit:

$$\Xi_{ab}^* = \sum_{\mathbf{p}\sigma}\left(-\frac{\partial n_{\mathbf{p}}}{\partial \xi_{\mathbf{p}}}\right) f_{\mathbf{p}} \frac{i\Gamma_{\mathbf{p}}^*}{\omega+i\Gamma_{\mathbf{p}}^*} a_{\mathbf{p}} b_{\mathbf{p}} \tag{6}$$

and the objects ζ_{ab}^* describe the mixing of elastic and inelastic scattering processes and hence deviations from Matthiessen's rule within the conserving relaxation time approximation:

$$\begin{aligned}
\zeta_{ab}^* &= \frac{\Xi_{a1}^*\Xi_{1b}^*}{\Xi_{11}^{*2}} + \frac{\omega}{\omega+i\gamma^*}\frac{\Xi_{11}^{\mathrm{e}}\Xi_{11}^{\mathrm{i}}}{\Xi_{11}^{*2}}\left(\frac{\Xi_{a1}^{\mathrm{e}}}{\Xi_{11}^{\mathrm{e}}}-\frac{\Xi_{a1}^{\mathrm{i}}}{\Xi_{11}^{\mathrm{i}}}\right)\left(\frac{\Xi_{b1}^{\mathrm{e}}}{\Xi_{11}^{\mathrm{e}}}-\frac{\Xi_{b1}^{\mathrm{i}}}{\Xi_{11}^{\mathrm{i}}}\right) + O(\mathbf{q}^2) \qquad (7) \\
\gamma^* &= \frac{\Xi_{11}^*}{\Xi_{11}^{\mathrm{e}}\Xi_{11}^{\mathrm{i}}}\sum_{\mathbf{p}\sigma}\left(-\frac{\partial n_{\mathbf{p}}}{\partial \xi_{\mathbf{p}}}\right) f_{\mathbf{p}} \frac{i\Gamma_{\mathbf{p}}^{\mathrm{e}}\Gamma_{\mathbf{p}}^{\mathrm{i}}}{\omega+i\Gamma_{\mathbf{p}}^*} \\
\Xi_{ab}^{\nu} &= \sum_{\mathbf{p}\sigma}\left(-\frac{\partial n_{\mathbf{p}}}{\partial \xi_{\mathbf{p}}}\right) f_{\mathbf{p}} \frac{i\Gamma_{\mathbf{p}}^{\nu}}{\omega+i\Gamma_{\mathbf{p}}^*} a_{\mathbf{p}} b_{\mathbf{p}} \quad ; \quad \nu = \mathrm{e,i}
\end{aligned}$$

Finally $\varepsilon = \varepsilon(\mathbf{q},\omega) = 1 - V(\mathbf{q})M_{11}^*(\mathbf{q},\omega)$ is the dielectric function of the electronic system. It has thus been shown that the mixing terms $\propto \zeta_{ab}^*$ of the two separate scattering mechanisms occur in the Lindhard function $M_{ab}^*(\mathbf{q},\omega) = O(\mathbf{q}^2)$ and in terms which are screened $\propto \varepsilon^{-1}$ by the long range Coulomb interaction. For practical applications of the result (4) to the cuprate systems, say, where $\mathbf{q}\to 0$ and $\varepsilon \approx 10^4$ may be assumed, one may use the $\mathbf{q}\to 0, \varepsilon\to\infty$ limit of $L_{\gamma\gamma}$ and the contributions from mixing $\propto \zeta_{ab}^*$ are hence irrelevant. Therefore, the scattering mechanisms can be linearly combined, leading to the exclusive occurrence of $\Gamma_{\mathbf{p}}^* = \Gamma_{\mathbf{p}}^{\mathrm{e}} + \Gamma_{\mathbf{p}}^{\mathrm{i}}$ in the Raman response function. A numerical analysis of the Raman response function $L_{\gamma\gamma}$ for various models particularly for the inelastic scattering rate $\Gamma_{\mathbf{k}}^{\mathrm{i}}$ is in preparation [3].

References

[1] Zawadowski und Cardona, Phys. Rev. **42**, 10732 (1990)
[2] N. D. Mermin, Phys. Rev. **1**, 2362 (1970)
[3] D. Einzel and D. Manske, *to be published*

Collective Spin Fluctuation Mode and Raman Scattering in Superconducting Cuprates

F. Venturini [1]

Electronic Raman scattering has proven to be a useful tool in exploring the superconducting state in the cuprate materials. The possibility of probing selectively electronic excitations in different regions of the Brillouin zone by the choice of polarization geometries has allowed to explore the superconducting gap anisotropy. The successful explanation of the Raman data in B_{1g} and B_{2g} scattering geometries has provided one piece of evidence for the by now widely accepted $d_{x^2-y^2}$ pairing symmetry in hole-doped cuprate superconductors.

However up to now the discrepancy between Raman data in A_{1g} and B_{1g}, B_{2g} geometries has remained unresolved [1]. Also, previous results for the A_{1g} scattering geometry were found to be very sensitive to changes in the Raman vertex function making a comprehensive explanation difficult for the experimental data in different cuprate materials [2].

Recent inelastic neutron scattering (INS) experiments have shown that the sharp magnetic collective mode, first observed in the superconducting state of Y-123, also exist in Bi-2212 and at all doping levels [3, 4]. This resonance occurs at an energy of ~ 40 meV and at a wave vector (π,π), and it is believed to be fundamental for the understanding of the interrelation between antiferromagnetism and superconductivity in high-T_c cuprates.

In this work we present calculations suggesting that the A_{1g} peak position is largely controlled by the strength and frequency of the collective spin fluctuation (SF) mode which on the other hand does not affect the Raman response in the B_{1g} and B_{2g} channels.

The bilayer structure of CuO_2 planes of the cuprates is modeled by a tight binding band structure with a nearest (t) and a next nearest neighbor hopping (t') parameter and an inter-plane hopping given by

$$t_\perp(\mathbf{k}) = 2t_\perp \cos(k_z)[\cos(k_x)-\cos(k_y)]^2. \tag{1}$$

k_z is 0 or π for the bonding or anti-bonding bands of the bilayer, respectively.

The spin susceptibility (χ_s) is constructed by extending the weak coupling form of a $d_{x^2-y^2}$ superconductor to include antiferromagnetic spin fluctuations by an RPA form with an effective interaction$\bar{U}$; i.e. $\chi_s = \chi^0/(1-\bar{U}\chi^0)$ where χ^0 is the bare BCS propagator. This form of the spin susceptibility contains a strong magnetic resonance peak at (π,π,π) which was proposed [5] to explain the resonance observed by INS experiments.

The spin fluctuation scattering produces an additional contribution to the Raman response via a two-magnon-like process as shown diagrammatically in Fig. 1 [6].

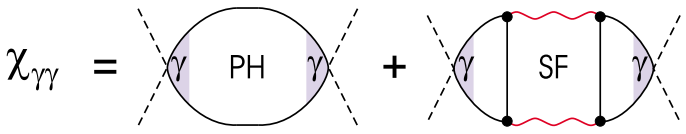

Figure 1: Feynman diagram considered for the particle-hole (PH) and the spin fluctuation (SF) contributions. Dashed, wiggly and solid lines represent photon, SF and electronic propagators, respectively.

The Raman response function at finite temperature is therefore given by the sum of a particle-hole (PH) and a SF contribution

$$\chi_{\gamma\gamma}(\mathbf{q},i\omega) = \chi^{PH}_{\gamma\gamma}(\mathbf{q},i\omega) + \chi^{SF}_{\gamma\gamma}(\mathbf{q},i\omega) \tag{2}$$

[1] In collaboration with U. Michelucci, A.P. Kampf (Universität Augsburg), T.P. Devereaux (University of Waterloo, Canada).

with the Raman vertex γ specifying the scattering geometry [7]. For the electronic propagators we have used the bare BCS Green's functions with a d-wave superconducting gap. Finally, the total Raman response is calculated in the gauge invariant form which results from taking into account the long wavelength fluctuations of the order parameter [8].

The first important result is that in the B_{1g} and B_{2g} geometries the SF term introduces vanishingly small corrections to the total response, rendering the presence of the SF term important only in the A_{1g} geometry. This is due to the sharpness in momentum space of the resonance peak at (π, π) in the SF propagator. Therefore for the B_{1g} and B_{2g} channels the response is given by the PH term alone.

Within our model the problem of the sensitivity of the result to changes in the bare Raman vertex is solved. In fact, in order to investigate the effect of changes of the vertex function, we have calculated the final response using the three different forms for the vertex which posses the correct transformation properties required by symmetry. The result is that the strong sensitivity to changes of the bare Raman vertex is much reduced when the SF term is added [7].

The comparison between the calculated Raman response and the experimental spectra of an optimally doped Bi-2212 sample is shown in Fig. 2 [7]. Adding the SF contribution leads to a shift of the peak position to higher frequencies, allowing a better agreement with the experimental relative positions of the peaks in A_{1g} and B_{1g} geometries.

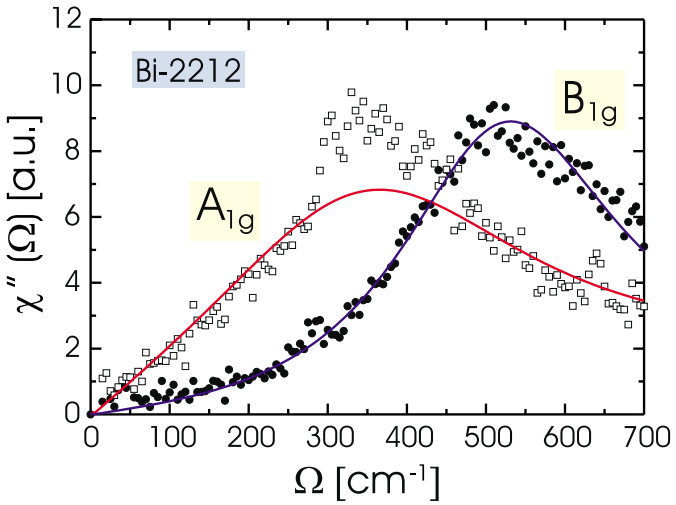

Figure 2: Comparison of the A_{1g} and B_{1g} calculated response (solid lines) with experimental data of optimally doped Bi-2212.

From this work we conclude that including the SF contribution in the Raman response solves the previously unexplained sensitivity of the A_{1g} response to small changes in the Raman vertex. Also, within our model it is now possible to obtain the correct relative peak positions of the A_{1g} and the B_{1g} scattering geometry. Whereas the SF (two-magnon) contribution controls the A_{1g} peak, the B_{1g} and B_{2g} scattering geometries are essentially unaffected and determined by particle-hole processes alone.

References

[1] F. Wenger and M. Käll, Phys. Rev. B **55**, 97 (1997); T. Strohm and M. Cardona, *ibid*. **55**, 12725 (1997); **58**, 8839 (1998); D. Manske, C. Rieck, R. Das Sharma, A. Bock, and D. Fay, *ibid*. **56**, R2940 (1997); **58**, 8841 (1998); A.V. Chubukov, D.K. Moor, and G. Blumberg, Solid State Commun. **112**, 183 (1999).

[2] T.P. Devereaux, A. Virosztek, and A. Zawadowski, Phys. Rev. B **54**, 12523 (1996).

[3] H.A. Mook, M. Yethiraj, G. Aeppli, T.E. Mason, and T. Armstrong, Phys. Rev. Lett. **70**, 3490 (1993).

[4] H.F. Fong, B. Keimer, P.W. Anderson, D. Reznik, F. Dogan, and I.A. Aksay, Phys. Rev. Lett. **75**, 316 (1995); H.F. Fong, P. Bourges, Y. Siddis, L.P. Regnault, A. Ivanov, G.D. Gu, N. Koshizuka, and B. Keimer, Nature **398**, 588 (1999).

[5] N. Bulut and D.J. Scalapino, Phys. Rev. B **53**, 5149 (1996).
[6] F. Venturini, U. Michelucci, T.P. Devereaux, A.P. Kampf, Physica C **341-348**, 2265 (2000).
[7] F. Venturini, U. Michelucci, T.P. Devereaux, A.P. Kampf, Phys. Rev. B **62**, 15204 (2000).
[8] T.P. Devereaux and D. Einzel, Phys. Rev. B **51**, 16336 (1995); **54**, 15547 (1996).

Antiferromagnetism and Pseudogap in Y-123 and Bi-2212

M. Opel, F. Venturini, A. Erb, R. Hackl [2]

Cuprate systems are characterized by a generic doping-temperature phase diagram (Fig. 1). The normal metallic and superconducting phases evolve from an antiferromagnetic (AF) insulating one upon increasing carrier concentration. For a wide doping range AF fluctuations are observed in the metallic and superconducting states. Especially at low doping, the normal state does not behave like a simple metal, and a temperature range with qualitatively different properties has recently been identified in various experiments [1]. It is characterized by a partial suppression of the electronic density of states at the Fermi energy below a doping-dependent temperature $T^*(p)$. This pseudogap and its doping dependence have also been observed in Raman experiments. The spectra show a suppression of spectral weight below a frequency of 800 cm^{-1}. Its value is independent of both doping and temperature [3, 4].

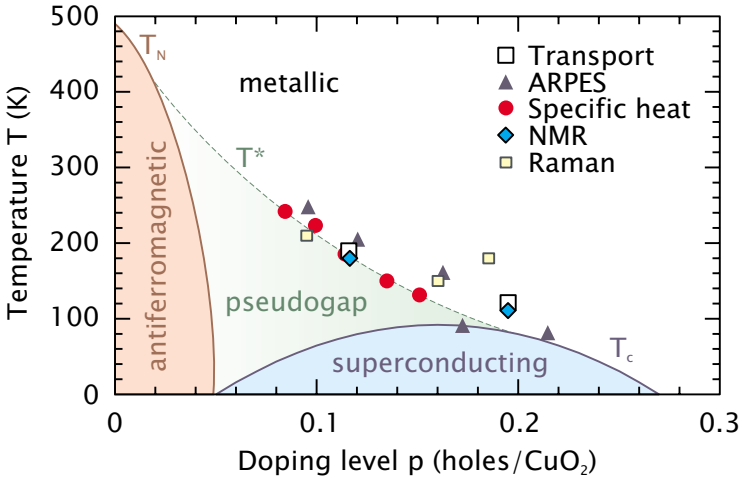

Figure 1: Generic phase diagram for p-doped cuprate superconductors. The symbols for transport, ARPES, specific heat and NMR measurements were taken from [1], the Raman data were obtained at the WMI [2].

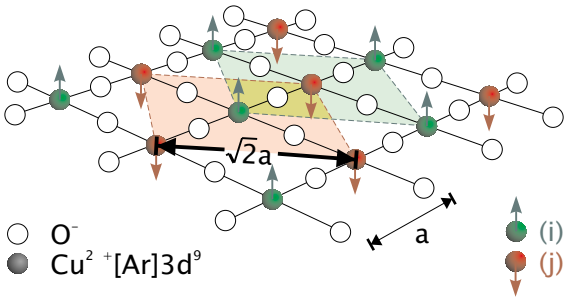

Figure 2: The copper-oxide plane of cuprate superconductors. The Cu^{2+} spins order antiferromagnetically.

The mechanism leading to the opening of the pseudogap is not clear. Therefore we looked for a relation between this phenomenon and magnetic excitations in the cuprates. We will first focus on magnetic properties of the undoped parent compounds ($p = 0$). The Cu^{2+} spins in the copper-oxide planes represent a two-dimensional antiferromagnetically ordered spin system (Fig. 2). It consists of two ferromagnetic sublattices with opposite spin orientation. In this spin system there exist magnons as elementary excitations which can be observed using Raman spectroscopy [5]. Because of the small momentum transfer $\vec{q} \to 0$ of the photons the interaction of light with single magnons is restricted to the center of the Brillouin zone where their density of states (DOS) is low because of their dispersion. However, if a magnon-pair with $\pm\vec{k}$ is created simultaneously (one magnon in each sub-lattice) it is possible to observe magnons at the boundaries of the Brillouin zone with a high DOS and thus a high peak intensity in the Raman experiment (two-magnon scattering). The peak position should be $\hbar\omega_{2M} = 2.8J$ where J is the magnetic exchange energy [6].

In the following, we present recent results from light scattering experiments on undoped, AF insulating $YBa_2Cu_3O_6$ (Y-123) and $Bi_2Sr_2YCu_2O_{8+\delta}$ (Bi-2212) single crystals. The polarizations of the incoming

[2] In collaboration with H. Berger and L. Forró (Lausanne)

and outgoing photons were always in the planes and are represented symbolically in the figures with respect to the CuO_2 planes. At low temperatures, the Raman spectra clearly show the two-magnon peak at approx. 3000 cm^{-1} for both compounds (Fig. 3) [7]. Its lineshape is asymmetric. Next to the maximum at $\hbar\omega_{2M}$ there is a shoulder seen at higher Raman shifts. It is addressed to a so-called "triple resonance" at $\hbar\omega_{3R} \simeq 4J$ [6].

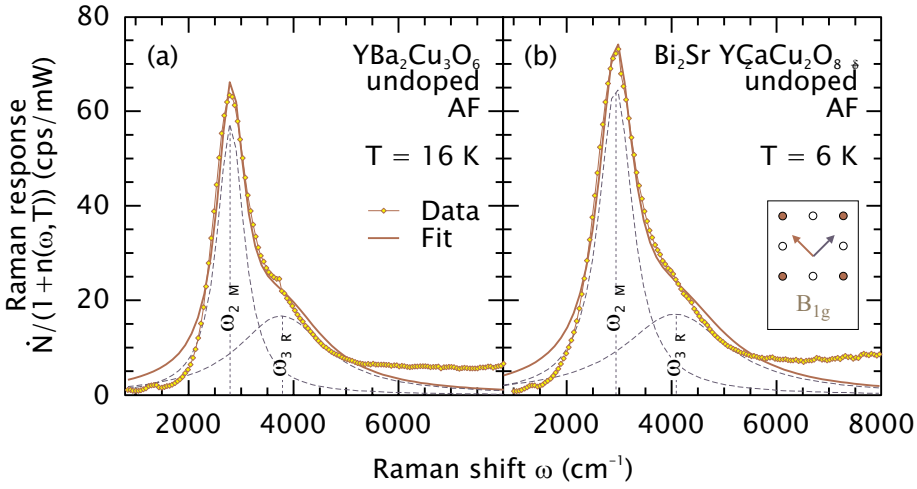

Figure 3: The two-magnon peak in undoped Y-123 (a) and Bi-2212 (b). The experimental data (symbols) were fitted using a 2-band Lorentzian (lines).

To determine values for both $\hbar\omega_{2M}$ and $\hbar\omega_{3R}$ the spectra (symbols) were fitted using a 2-band Lorentzian (lines). From the position $\hbar\omega_{2M}$ of the maximum of the first Lorentzian one can calculate the magnetic exchange energy J using $\hbar\omega_{2M} = 2.8J$ (Tab. 1). The results are in agreement with the values obtained in NMR or inelastic neutron scattering experiments [8]. Together with the position $\hbar\omega_{3R}$ of the maximum of the second Lorentzian one can test the relation $\hbar\omega_{3R} \simeq 4J$. The results are compiled in Table 1.

Table 1: Position of the two-magnon peak $\hbar\omega_{2M}$ and of the triple resonance $\hbar\omega_{3R}$ in undoped Y-123 and Bi-2212 and calculated values for the magnetic exchange energy J.

	$\hbar\omega_{2M}$	J	$\hbar\omega_{3R}$
Y-123	2773 cm^{-1}	124 meV	3739 $cm^{-1} = 3.78J$
Bi-2212	2954 cm^{-1}	132 meV	4093 $cm^{-1} = 3.88J$

In real space, two-magnon scattering can be described as simultaneous spin-flip of two neighboring Cu^{2+} spins. For this process it is necessary to move one electron with charge and spin between the copper and the oxygen sites and to overcome the charge-transfer gap $2\Delta_{CT}$ in these materials. Therefore the probability of this process strongly depends on the energy $\hbar\omega^I$ of the incoming photon. The maximum effect is expected for $\hbar\omega^I = 2\Delta_{CT} + 8J$ [6]. In fact, one finds that the intensity of the two-magnon peak shows clear resonance when observed at different excitation energies (Fig. 4). Both in Y-123 and Bi-2212 the intensity of the scattered light decreases with increasing wavelength while the spectral shape remains unchanged [7]. More detailed studies between 400 and 700 nm (3.0 and 1.8 eV) show a maximum peak intensity for 458 nm ($\hbar\omega^I = 2.71$eV). With $2\Delta_{CT} \simeq 1.7$eV [9] this resonance effect gives another independent estimate for the magnetic exchange energy of $J = 126$meV. This is in excellent agreement with the values calculated above.

In summary, the magnetic exchange energy J represents a microscopic energy scale of 125 meV (1000 cm^{-1}) for both Y-123 and Bi-2212 which is independent of temperature and doping. On the other hand, we find evidence for the opening of a pseudogap in the same compounds. The related suppression of spectral weight has been observed below an energy of 800 cm^{-1} which is very close to J

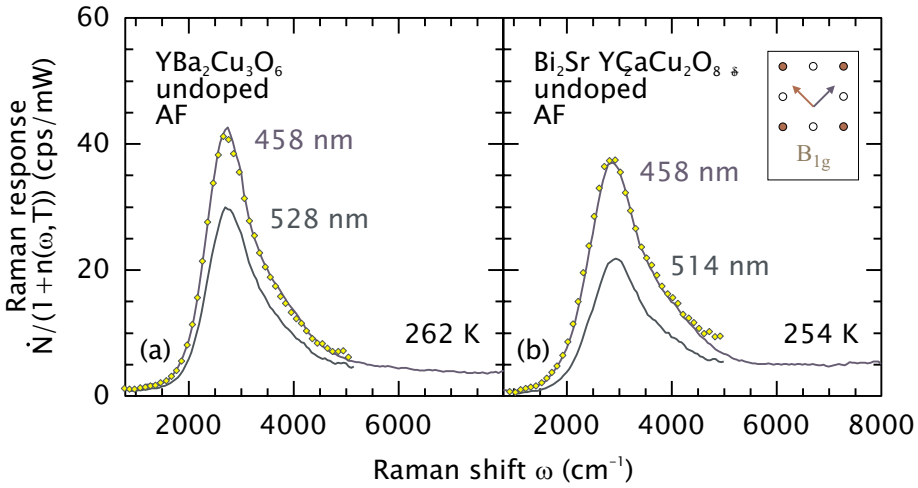

Figure 4: Resonance properties of the two-magnon peak at room temperature. At lower excitation energies (528 nm or 514 nm instead of 458 nm) the peak intensities are reduced. However, the spectra can be scaled to each other by multiplicative factors of 1.38 (a) and 1.73 (b) (symbols).

and also independent of temperature and doping [3, 4]. This leads to the conclusion that the pseudogap phenomenon may have a magnetic origin.

References

[1] T. Timusk and B.W. Statt, Rep. Prog. Phys. **62**, 61-122 (1999).

[2] M. Opel, M. Götzinger, C. Hoffmann, R. Nemetschek, R. Philipp, F. Venturini, R. Hackl, A. Erb, and E. Walker, J. Low Temp. Phys. **117**, 347 (1999).

[3] M. Opel, R. Nemetschek, F. Venturini, I. Tüttő, A. Erb, H. Berger, L. Forró, R. Hackl, WMI Jahresbericht **1999**, 6 (1999).

[4] M. Opel, R. Nemetschek, C. Hoffmann, R. Philipp, P.F. Müller, R. Hackl, I. Tüttő, A. Erb, B. Revaz, E. Walker, H. Berger, and L. Forró, Phys. Rev. B **61**, 9752 (2000).

[5] P.A. Fleury and R. Loudon, Phys. Rev. **166**, 514 (1968).

[6] D.K. Morr and A.V. Chubukov, Phys. Rev. B **56**, 9134 (1997).

[7] M. Opel, *Eigenschaften des Elektronensystems und seiner Wechselwirkungen in antiferromagnetischen und supraleitenden Kupraten: Eine Raman-Sudie*, PhD thesis TU München, Shaker Verlag Aachen (2000).

[8] S.M. Hayden, G. Aeppli, R. Osborn, A.D. Taylor, T.G. Perring, S.-W. Cheong, and Z. Fisk, Phys. Rev. Lett. **67**, 3622 (1991); T. Imai, C.P. Slichter, K. Yoshimura, and K. Kosuge, Phys. Rev. Lett. **70**, 1002 (1993)

[9] R. Liu, M.V. Klein, D. Salamon, S.L. Cooper, W.C. Lee, S.-W. Cheong, and D.M. Ginsberg, J. Phys. Chem. Solids **54**, 1347 (1993).

Doping-dependent Pair Breaking in Y-123 and Bi-2212

M. Opel, F. Venturini, A. Erb, R. Hackl [3]

The electronic Raman spectra of superconductors show a characteristic redistribution of the intensity of the scattered light in the superconducting state. This effect is caused by the existence of a gap in the carrier excitation spectrum which leads to a suppression of inelastic scattering at low frequencies. On the other hand, a peak in the Raman spectra develops if the energy transfer is high enough to break a Cooper pair. In combination with selection rules which depend on the polarizations of the incoming and the scattered light, this "pair-breaking Raman effect" gave valuable contributions for the investigation of the $\vec{k}$-dependence of the superconducting order parameter [1].

Most recent results from differently doped $Bi_2Sr_2(Y_{1-x}Ca_x)Cu_2O_{8+\delta}$ (Bi-2212) single crystals are compiled in Fig. 1 [2]. The figure shows difference spectra (superconducting minus normal state). In B_{2g} symmetry (right) which is most sensitive around $(\pm\frac{\pi}{2},\pm\frac{\pi}{2})$ in $\vec{k}$-space the pair-breaking peaks can be clearly observed at all doping levels at the same value of $\omega_p \simeq 6kT_c$. In B_{1g} symmetry (left), however, which is most sensitive around $(\pm\pi,0)$ and $(0,\pm\pi)$ both the pair-breaking intensity and the peak position ω_p depend strongly on the doping level. In the underdoped compound, we could not find any evidence for pair-breaking at all. Similar results have been obtained for $YBa_2Cu_3O_{6+x}$ (Y-123) [2].

The doping dependence of the peak frequency $\omega_p(p)$ in absolute units (cm^{-1}) is summarized in Fig. 2. While in the overdoped regime the values for B_{1g} and B_{2g} symmetry are comparable to each other a significant anisotropy develops towards lower doping levels p. In B_{2g} symmetry, the position of the pair-breaking peak scales with the transition temperature $T_c(p)$. Its value $\omega_p^{B_{2g}}(p) \simeq 6kT_c$ in both compounds is independent of the doping level. This result is in agreement with other low-energy methods like measurements of the magnetic penetration depth and zero-bias tunneling [3], or Andreev reflection [4] (Tab. 1). In the B_{1g} channel, however, the peak energy $\omega_p^{B_{1g}}(p)$ is increasing with decreasing doping level (Fig. 2). This observation is in agreement with the results from high-energy methods like angle-resolved photoemission [5] or tunneling spectroscopy [6] (Tab. 1). Surprisingly, $\omega_p^{B_{1g}}(p)$ shows a behavior similar to the one of the pseudogap temperature $T^*(p)$.

In summary, using Raman spectroscopy one seems to be able to determine two different energy scales which are relevant for superconductivity. As $\omega_p^{B_{2g}}(p)$ is directly related to the doping dependence of the transition temperature it could represent the energy scale which is responsible for phase coherence in the cuprates. On the other hand, one can speculate whether $\omega_p^{B_{1g}}(p)$ could be a measure for the maximum binding energy of the Cooper pairs as the B_{1g} channel is most sensitive around the maxima of the order parameter. However, these subjects are still discussed controversially. Up to now the Raman experiment is the only experiment where both energy scales can be observed separately in one single experiment - and in the same sample.

Table 1: Scaling behavior of the doping-dependent position of the pair breaking peak $\omega_p(p)$.

	$\omega_p(p)$ scales like ...	experiments with comparable results
B_{1g}	$\ldots T^*(p)$	angle-resolved photoemission spectroscopy, tunneling spectroscopy
B_{2g}	$\ldots T_c(p)$	magnetic penetration depth, zero-bias tunneling, Andreev reflection

References

[1] T.P. Devereaux, D. Einzel, B. Stadlober, R. Hackl, D.H. Leach, and J.J. Neumeier, Phys. Rev. Lett. **72**, 396 and 3291 (1994).

[3] In collaboration with H. Berger and L. Forró (Lausanne)

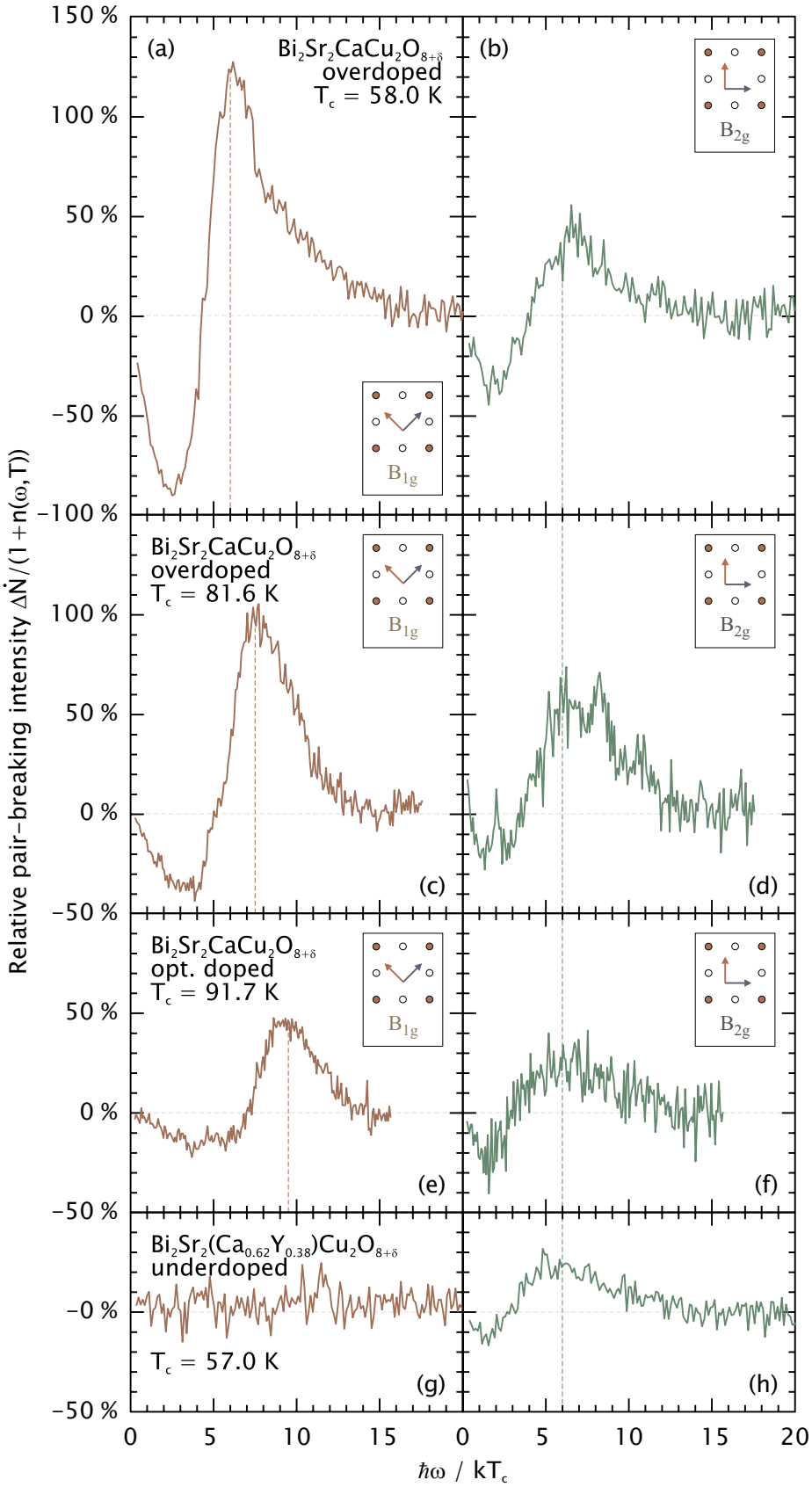

Figure 1: Difference spectra from Bi-2212 (superconducting minus normal state), normalized to the average intensity at 1000 cm^{-1}.

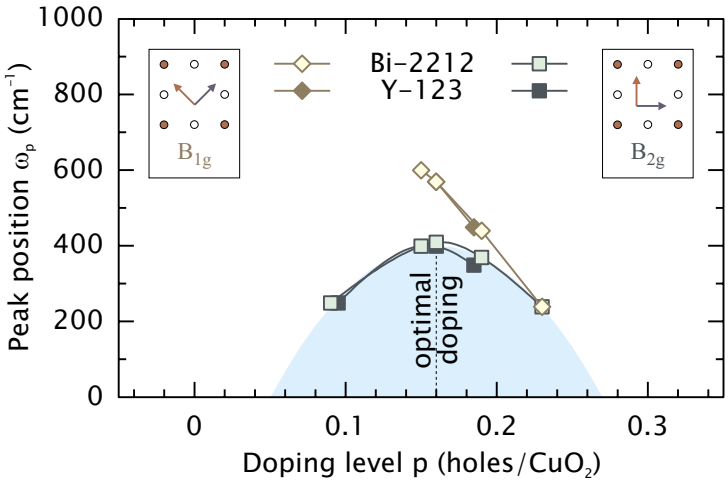

Figure 2: Position ω_p of the pair breaking peak as a function of doping for both Bi-2212 and Y-123. The superconducting phase is given by the shaded area ($\hbar\omega_p = 6.3kT_c$, cyan).

[2] M. Opel, *Eigenschaften des Elektronensystems und seiner Wechselwirkungen in antiferromagnetischen und supraleitenden Kupraten: Eine Raman-Sudie*, PhD thesis TU München, Shaker Verlag Aachen (2000).

[3] C. Panagopoulos and T. Xiang, Phys. Rev. Lett. **81**, 2336 (1998).

[4] G. Deutscher, Nature **397**, 410 (1999).

[5] H. Ding, J.C. Campuzano, M.R. Norman, M. Randeria, T. Yokoya, T. Takahashi, T. Takeuchi, T. Mochiku, K. Kadowaki, P. Guptasarma, and D.G. Hinks, J. Phys. Chem. Solids **59**, 1888 (1998).

[6] C. Renner, B. Revaz, J.-Y. Genoud, K. Kadowaki, and Ø. Fischer, Phys. Rev. Lett. **80**, 149 (1998).

Symmetry of the order parameter in hole and electron doped high-temperature superconductors

B. Welter, L. Alff, A. Marx, R. Gross [4]

The determination of the symmetry of the superconducting order parameter is an important step towards the understanding of the physics of high-temperature superconductors (HTS). Any microscopic mechanism leading to the phenomenon of high-temperature superconductivity must prove to be consistent with the given symmetry of the superconducting state. Meanwhile, there is general agreement that the *hole* doped HTS have a $d_{x^2-y^2}$-wave symmetry of the order parameter with nodes and a sign change under $\pi/2$ rotation. However, the doping dependence of the symmetry of the order parameter has not yet been settled sufficiently. For the hole doped HTS the existence of a quantum critical point (QCP) has been proposed [1]. For the electron doped HTS a particularly important question is whether or not hole and electron doped HTS have the same symmetry type [2, 3].

In Fig. 1 (left) a schematic phase diagram of the hole and electron doped HTS is shown. There are two possible ways of looking at this phase diagram: On the one hand, one can stress the strong similarities of both doping types. On both the hole *and* electron doped side there is a close vicinity of the superconducting phase to an antiferromagnetic (AFM) phase, which has been discussed in several theories as related to the origin of superconductivity in the HTS [4, 5]. It is therefore natural to assume the same mechanism of superconductivity for both hole and electron doping and, hence, the same symmetry of the superconducting order parameter. On the other hand, one could also stress the phenomenological differences of the doping types: While already for low hole doping the AFM state is strongly suppressed due to magnetic frustration, electron doping produces a clearly weaker suppression of the AFM phase by dilution of antiferromagnetism. The extension of the superconducting phase is much wider on the hole doped side as compared to the electron doped side. The transition region between AFM and superconducting phase is still controversially discussed for the hole doped side, and is even less explored for electron doping. Independent of the theoretical point of view one might have on this question, a convincing body of experiments is required to settle this issue. Unfortunately, at present the experimental situation is contradictory. There are experiments giving evidence for either *s*-wave [2, 6, 7] or *d*-wave type [3, 8] symmetry of the order parameter of the electron doped HTS.

For the hole doped HTS the experiments give consistent results and can all be interpreted within a $d_{x^2-y^2}$-symmetry of the order parameter. With respect to the electron doped HTS, experiments have been performed on the system $Ln_{2-x}\mathrm{Ce}_x\mathrm{CuO}_4$ (here $Ln = \mathrm{Nd}, \mathrm{Pr}, x = 0.15$) with the so-called T' structure. However, these experiments give contradictory results. In our experiments we have focused on tunneling studies and measurements of the London penetration depth. We note that there have been experiments on electron doped HTS favoring *s*-wave symmetry as for example Raman scattering [9]; for further references see [2]. The hall mark of *d*-wave symmetry, the sign change under rotation of $\pi/2$, gives rise to surface bound states depending on the surface orientation [10]. These states are also called Andreev bound states (ABS) and can be detected in several types of experiments. ABS in *d*-wave superconductors result e. g. in zero energy states in the quasiparticle spectrum of superconductor - insulator - normal metal /superconductor (SIN or SIS) junctions. For hole doped HTS a zero bias conductance peak has been consistently observed in several junctions and the results of temperature and surface orientation dependent tunneling studies have been interpreted as a strong argument for *d*-wave symmetry. However, for the electron doped HTS in the same class of experiments no ABS could be detected in the tunneling spectra giving evidence for *s*-wave symmetry. A comparison of tunneling spectra of hole and electron doped HTS is shown in Fig. 1 (right) [11].

[4] In collaboration with S. Kleefisch, U. Schoop (II. Physikalisches Institut, Universität zu Köln) and M. Naito, H. Sato (NTT Basic Research Laboratories, Japan).

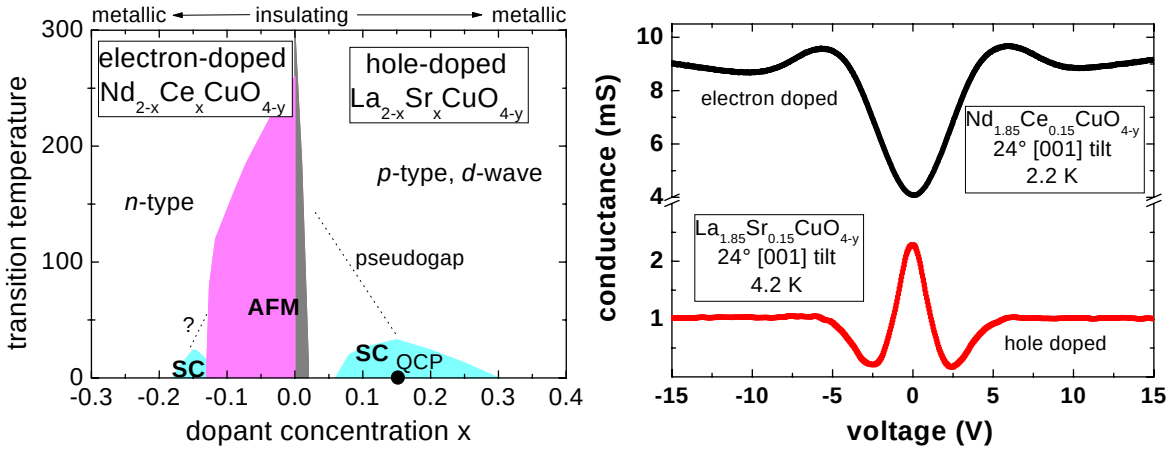

Figure 1: Left: Schematic phase diagram of hole and electron doped HTS. The T_c values are taken from the indicated superconductors. The dotted line representing the pseudogap temperature is still speculative. Right: Comparison of the tunneling spectra of hole and electron doped HTS [11].

In order to further clarify this unsatisfying experimental situation, more detailed and also new types of experiments are needed. In our work we are presently performing a systematic study of the *doping dependence* of the relevant properties of electron doped HTS. A doping dependence of the superconducting order parameter (that also might have two-components) could be a possible solution for the existing controversy.

References

[1] R. B. Laughlin, Phys. Rev. Lett. **80**, 5188 (1998).
[2] L. Alff, S. Meyer, S. Kleefisch, U. Schoop, A. Marx, H. Sato, M. Naito, and R. Gross, Phys. Rev. Lett. **83**, 2644 (1999).
[3] C. C. Tsuei and J. R. Kirtley, Phys. Rev. Lett. **85**, 182 (2000).
[4] D. Scalapino, Phys. Rep. **250**, 329 (1995).
[5] E. Demler and S.-C. Zhang, Nature **396**, 733 (1998).
[6] L. Alff, H. Takashima, S. Kashiwaya, N. Terada, T. Ito, K. Oka, Y. Tanaka, and M. Koyanagi, Physica **C 282-287**, 1485 (1997); L. Alff, H. Takashima, S. Kashiwaya, N. Terada, T. Ito, K. Oka, M. Koyanagi, and Y. Tanaka, in *Advances in Superconductivity IX*, edited by S. Nakajima and M. Murakami, Springer-Verlag, Tokyo (1997), pp. 49 - 52.
[7] S. Kashiwaya, T. Ito, K. Oka, S. Ueno, H. Takashima, M. Koyanagi, Y. Tanaka, and K. Kajimura, Phys. Rev. B **57**, 8680 (1998).
[8] R. Prozorov, R. W. Giannetta, P. Fournier, and R. L. Greene, Phys. Rev. Lett. **85**, 3700 (2000).
[9] B. Stadlober, G. Krug, R. Nemetschek, R. Hackl, J. L. Cobb, and J. T. Markert, Phys. Rev. Lett. **74**, 4911 (1995).
[10] C. R. Hu, Phys. Rev. Lett. **72**, 1526 (1994).
[11] L. Alff, A. Beck, R. Gross, A. Marx, S. Kleefisch, Th. Bauch, H. Sato, M. Naito, and G. Koren, Phys. Rev. B **58** (1998) 11197; L. Alff, S. Kleefisch, U. Schoop, M. Zittartz, T. Kemen, T. Bauch, A. Marx, and R. Gross; Eur. Phys. J. B **5**, 423 (1998).

Pseudogap in electron doped cuprate high-temperature superconductors

L. Alff, B. Welter, A. Marx, R. Gross [5]

The existence of a pseudogap in hole doped high-temperature superconductors (HTS) has been established over the recent years. The physical origin of the pseudogap state, however, is still one of the most debated topics for HTS (for a recent review see e. g. [1]). In different types of experiments including tunneling spectroscopy it has been found that the pseudogap feature and the superconducting energy gap merge smoothly into each other at the critical temperature T_c [2–6]. Even more, from angle-resolved photoemission experiments it has been suggested that the pseudogap has the same $d_{x^2-y^2}$-symmetry as the superconducting gap in the hole doped HTS [2, 3]. It has also been observed that the temperature $T^\star$ associated with the appearance of the pseudogap state roughly becomes equal to T_c around optimum doping or in the slightly overdoped regime, but is considerably larger than T_c in the underdoped regime. The evident question arising from these experimental observations is whether or not there is a relation between the physical origin of the superconducting gap and the pseudogap. Such a scenario has been proposed within theories involving so-called preformed pairs or at least dynamical pair correlations above T_c [7].

With respect to different HTS, the hole doped system $La_{2-x}Sr_xCuO_4$ seems to be a special case. For this material, the behavior of the pseudogap has been reported to be different compared to the other hole doped HTS, e. g. the size of the pseudogap may be much larger than the superconducting gap [8]. However, the experimental situation is not well settled and more experiments are needed to further clarify this point. For the electron doped HTS of the class $Ln_{2-x}Ce_xCuO_4$ (Ln = Nd, Pr) with T' structure, up to now no low-energy spectroscopic experiments probing the pseudogap state have been reported. There is no doubt that experiments on electron doped HTS are important and highly desired with regard to the question whether hole and electron doped HTS have the same underlying mechanism of superconductivity and the pseudogap state. Furthermore, controversial experimental results on the symmetry of the superconducting order parameter in the electron doped HTS have been published recently [9–12]. That is, both the symmetry of the order parameter and the question whether there is a normal state pseudogap are under discussion for electron doped HTS.

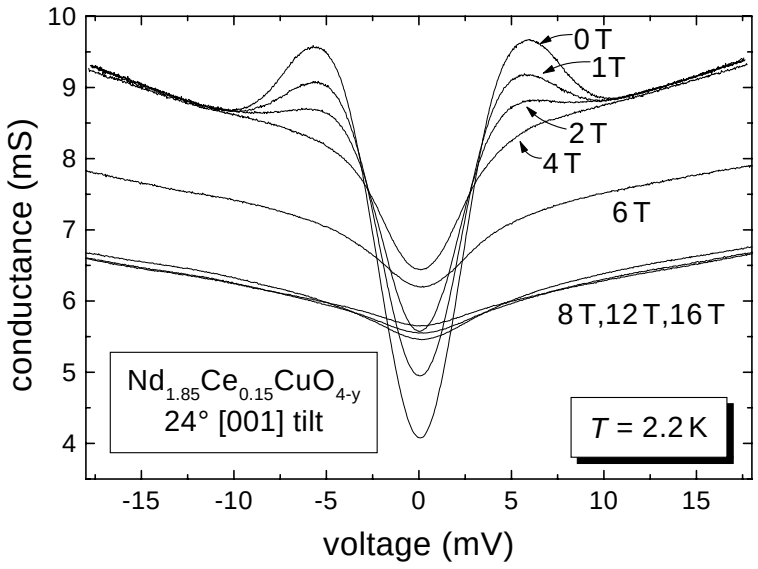

Figure 1: Conductance vs. voltage curves of a symmetric 24° [001] tilt NCCO-GBJ measured at 2.2 K in different applied magnetic fields applied parallel to the *c*-axis.

In our ongoing research, we have measured tunneling spectra using superconductor - insulator - superconductor junctions based on bicrystal grain boundary junctions (GBJs). The samples have been

[5] In collaboration with S. Kleefisch, U. Schoop (II. Physikalisches Institut, Universität zu Köln) and M. Naito (NTT Basic Research Laboratories, Japan).

fabricated in collaboration with the NTT Basic Research Laboratory (Japan) [13]. The temperature and magnetic field dependence of the tunneling spectra has been studied up to 16 T for the optimum electron doped HTS $Nd_{1.85}Ce_{0.15}CuO_{4-y}$ (NCCO) and $Pr_{1.85}Ce_{0.15}CuO_{4-y}$ (PCCO). The key result of our study up to now is that while above $T_c(B=0)$ no pseudogap feature could be observed, where B is the applied magnetic field. In contrast, below $T_c(B=0)$ a pseudogap around the Fermi level is clearly present for applied magnetic fields larger than the resistively determined upper critical field B_{c2}^{ρ} (see Fig. 1). This suggests that similar to the hole doped HTS, there is a pseudogap state also for the electron doped HTS. However, the presence of a non-uniform superconducting state may also be consistent with our observations.

In order to further clarify the experimental situation as well as to provide more insight into the nature of the superconducting and, in particular, the possible pseudogap state in the electron doped HTS, more measurements at lower temperatures, higher fields, and for different electron doping levels (especially for the under(electron)doped case) are required. For the hole doped HTS, in the underdoped regime the pseudogap phenomenon is clearly present at temperatures above $T_c(B=0)$. The goal of our present work is the clarify the question whether or not a similar pseudogap feature is present also for electron doped HTS in the underdoped regime, i.e. to settle the question whether or not there is a corresponding behavior for both doping types.

References

[1] T. Timusk and B. Statt, Rep. Prog. Phys. **62**, 61 (1999).
[2] H. Ding, T. Yokoya, J. C. Campuzano, T. Takahashi, M. Randeira, M. R. Norman, T. Mochiku, K. Kadowaki, and J. Giapintzakis, Nature **382**, 51 (1996).
[3] A. G. Loeser, Z.-X. Shen, D. S. Dessau, D. S. Marshall, C. H. Park, P. Fournier, A. Kapitulnik, Science **273**, 325 (1996).
[4] Ch. Renner, B. Revaz, J.-Y. Genoud, K. Kadowaki, and Ø. Fischer, Phys. Rev. Lett. **80**, 149 (1998).
[5] Y. DeWilde, N. Miyakawa, P. Guptasarma, M. Iavarone, L. Ozyuzer, J. F. Zasadzinski, P. Romano, D. G. Hinks, C. Kendziora, G. W. Crabtree, and K. E. Gray, Phys. Rev. Lett. **80**, 153 (1998).
[6] N. Miyakawa, P. Guptasarma, J. F. Zasadzinski, D. G. Hinks, and K. E. Gray, Phys. Rev. Lett. **80**, 157 (1998).
[7] V. J. Emery and S. A. Kivelson, Nature **374**, 434 (1995); V. J. Emery, S. A. Kivelson, and O. Zachar, Phys. Rev. B **56**, 6120 (1997).
[8] T. Sato, T. Yokoya, Y. Naitoh, T. Takahashi, K. Yamada, and Y. Endoh, Phys. Rev. Lett. **83**, 2254 (1999).
[9] S. Kashiwaya, T. Ito, K. Oka, S. Ueno, H. Takashima, M. Koyanagi, Y. Tanaka, and K. Kajimura, Phys. Rev. B **57**, 8680 (1998).
[10] L. Alff, A. Beck, R. Gross, A. Marx, S. Kleefisch, Th. Bauch, H. Sato, M. Naito, and G. Koren, Phys. Rev. B **58**, 11197 (1998).
[11] L. Alff, S. Meyer, S. Kleefisch, U. Schoop, A. Marx, H. Sato, M. Naito, and R. Gross, Phys. Rev. Lett. **83**, 2644 (1999).
[12] C. C. Tsuei and J. R. Kirtley, Phys. Rev. Lett. **85**, 182 (2000).
[13] M. Naito and H. Sato, Appl. Phys. Lett. **67**, 2557 (1995); H. Yamamoto, M. Naito, and H. Sato, Phys. Rev. B **56**, 2852 (1997).

Competition between the Pauli and orbital effects of magnetic field on the low-temperature electronic state of the organic metal α-(BEDT-TTF)$_2$KHg(SCN)$_4$

D. Andres, W.Biberacher and M. Kartsovnik [6]

A common feature of all BEDT-TTF-based salts (where BEDT-TTF stands for the organic molecule bis(ethylenedithio)-tetrathiafulvalene) is the layered structure of the crystal, consisting of conducting BEDT-TTF sheets, which are separated by insulating anion layers [1]. This separation leads to a strongly anisotropic conductivity. In the title compound the Fermi surface reveals itself in a unique coexistence of open sheets and cylindrical components, both parts being slightly corrugated in the direction perpendicular to the layers, reflecting a mixture of quasi-one-dimensional (Q1D) and quasi-two-dimensional (Q2D) electron systems. During the last years α-(BEDT-TTF)$_2$KHg(SCN)$_4$ has become a material of intense interest due to its unconventional ground state existing at $T < T_p \approx 8$ K. To the moment there are strong arguments for a density wave formation at T_p [2, 3] that causes the nesting of the Q1D parts of the Fermi surface. However, the exact nature of the low temperature (LT) state is still under debate. In particular, up to now there is no direct evidence for either a charge or magnetic modulation at low temperatures, respectively corresponding to a charge-(CDW) or spin-density wave (SDW). In order to clarify the real nature of this unconventional ground state we have studied the magnetic field-temperature (B-T) phase diagram at various pressures.

The CDW phase diagram is known to strongly differ from the SDW one, basically because a CDW is destroyed by the paramagnetic Pauli effect at high enough magnetic fields while a SDW is not sensitive to this effect [1]. The B-T phase diagram at ambient pressure, measured by means of magnetic torque and interplane resistance measurements with the magnetic field applied almost perpendicular to the highly conducting layers shows a decreasing transition temperature with field [4]. At high fields (≈ 24 T) there exists a transition from a low temperature low field (LTLF) state into a low temperature high field (LTHF) state accompanied by a hysteresis in the field sweeps at constant temperature. This phase diagram turns out to be very similar to the one proposed theoretically for a well nested CDW system [5]: At small fields the Pauli effect leads to a quadratic decrease of the transition temperature; when the Zeeman energy approaches the zero temperature energy gap of the density wave, there is a first order transition from the initial CDW into a CDW$_x$ state, which is actually a CDW with a spatially modulated order parameter. Noteworthy, the LTHF state would be the first example of such a CDW$_x$ phase.

We expect quasi-hydrostatic pressure to increase the molecular orbital overlap. This should cause a stronger warping of the Q1D sheets of the Fermi surface and thus less perfect nesting conditions. We therefore studied the B-T phase diagrams of α-(BEDT-TTF)$_2$KHg(SCN)$_4$ at various pressures via the interplane magnetoresistance to see how the phase lines will be affected by changing the nesting properties. The resulting phase diagrams for four different pressures and the magnetic field directed perpendicular to the layers are depicted in Fig. 1. For clarity only points from the very same experiment for each pressure are plotted. The solid lines illustrate the behaviour observed on several samples from different batches. As can be seen, the transition temperature moves gradually to lower values with enhancing the pressure. Remarkably, the phase boundary changes its shape under pressure: the field dependence of the transition temperature in a certain field interval turns from negative to positive. Further, we see that the LTHF/NM (NM $\equiv$ normal metallic state) boundary shows a much weaker pressure dependence than the LTLF/NM one, that leads to the observation that at 3.6 kbar the LTHF state still exists while there are no indications for the LTLF state any more. Another important result is the establishment of the LTHF state at lower fields under pressure that makes it easier to investigate in reachable static magnetic fields.

[6] High quality samples were provided by N. Kushch and H. Müller; part of the work was done at the HMFL in Grenoble

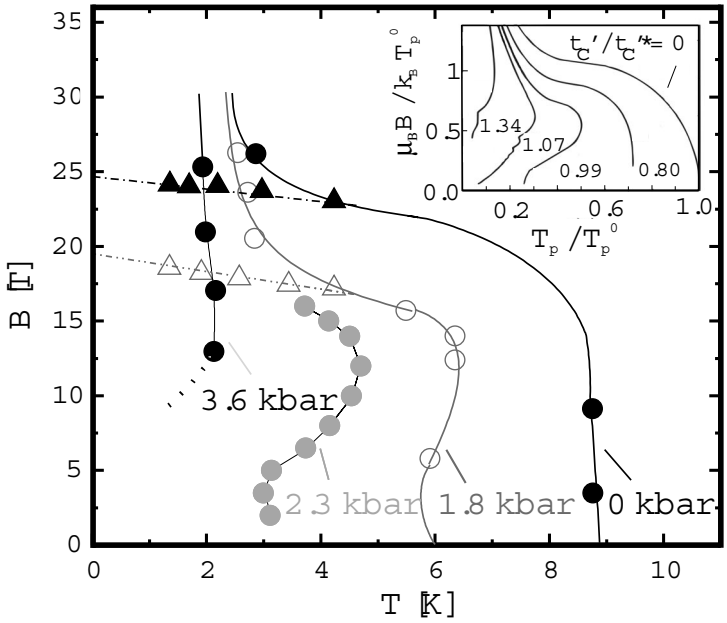

Figure 1: B-T phase diagrams measured at different pressures. Circles correspond to the boundary between the NM and the LT states, triangles to the transition from the LTLF to the LTHF state. The inset shows theoretically proposed phase diagrams of a CDW system at different nesting conditions [5].

Qualitatively, the measured phase diagrams closely resemble those predicted theoretically for a CDW system at different nesting conditions [5] which are shown in the inset of Fig. 1. A deterioration of the nesting conditions reduces the energy gain of the system on crossing the NM/LTLF boundary and thus decreases the transition temperature. In the extended Hubbard mean field calculations the imperfect nesting is parameterized by the ratio $t_c' / t_c'^*$, where t_c' is the second order transfer-integral in the dispersion relation of the Q1D electron system:

$$\varepsilon = v_F(|k_x| - k_F) + t_c \cos(k_c c) + t_c' \cos(2k_c c), \tag{1}$$

and $t_c'^*$ is the value of t_c' at which the zero-field transition temperature exactly vanishes. In the case of an imperfectly nested system a competition between the Pauli effect and another, so-called orbital effect comes into play. The latter is due to the fact that at the given field direction perpendicular to the conducting planes the electrons are forced to move perpendicular to the field on the Q1D sheets of the Fermi surface. Then, in real space the inplane electron motion has a constant component along the 1D axis and an oscillating component in the perpendicular direction. The amplitude of this oscillation is $\propto B^{-1}$. The resulting restriction of the electron motion to one dimension with field causes an increase of the density wave transition temperature. Thus, there will exist a competition between the Pauli and orbital effects in a CDW system. The observed enhancement of the transition temperature with field at 2.3 kbar would be the first clear manifestation of the orbital effect in a CDW system. Although our organic system appears to be fairly well described by the CDW model there are still some remaining questions. In particular, we cannot explain to the moment a difference (by factor of ≈ 2) in the absolute field scales between experiment and theory.

Another interesting observation is shown in Fig. 2. Under pressure of 2.3 kbar at $T \lesssim 2$ K a broad hysteresis emerges in the magnetic field sweeps of the magnetoresistance below 12 T, indicating a first order transition. This is accompanied with an additional weak feature at low fields that can be seen in Fig. 2a, where the beginning and the end of the hysteresis are marked by vertical arrows. With increasing the pressure further to 3 kbar, already two pronounced features are present at low fields as shown in Fig. 2b. These anomalies, at first glance unexpected, might turn out to be a sign of a new quantum

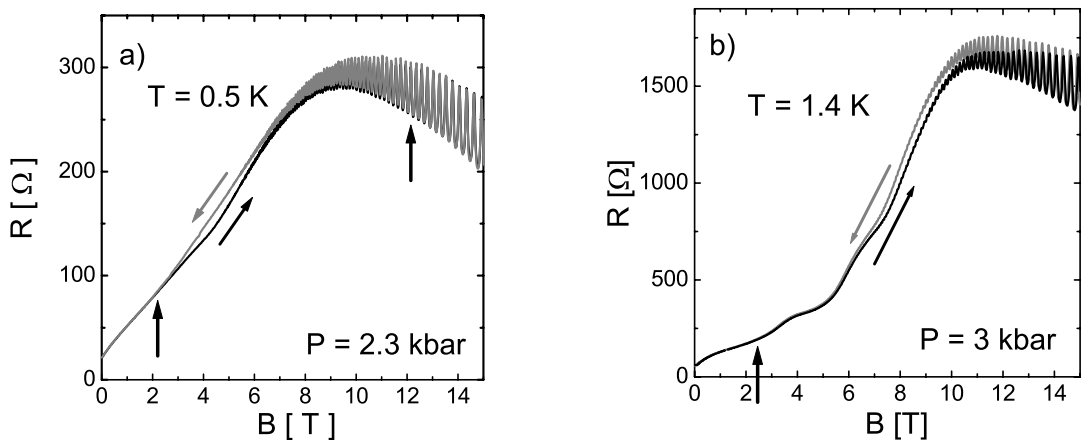

Figure 2: Field dependence of the magnetoresistance at constant temperatures. The vertical arrows mark the boundaries of the hysteresis region: a) under pressure of 2.3 kbar at T = 0.5 K, b) under pressure of 3 kbar at T = 1.4 K.

phenomenon. For certain nesting conditions, i.e. when t_c' becomes comparable to t_c^{l*}, the theory proposes the existence of successive field-induced CDW transitions (FICDW) [5]. This phenomenon is analogous to already known FISDW, where the adjustment of the nesting vector serves to keep the Fermi energy level between the Landau levels, in order to stabilize the DW in a changing magnetic field [6]. Jumps of the nesting vector will then cause a cascade of first order transitions between different SDW states. Up to now, FICDW have not been observed in any kind of material. Although we cannot state yet an unambiguous detection of FICDW, the obtained similarities between the theoretical CDW model and the ground state of this organic compound let the latter be a prominent candidate for the realization of this new quantum phenomenon.

References

[1] T. Ishiguro, K. Yamaji, and G.Saito. Organic superconductors, 2^{nd} edition. *Springer-Verlag Berlin Heidelberg* (1998).
[2] M. V. Kartsovnik, A. E. Kovalev, and N. D. Kushch. *J. Phys. I France* **3**, 1187 (1993).
[3] M. Basletić, B. Korin-Hamzić, M. V. Kartsovnik, and H. Müller. *to be published in Synth. Met.*.
[4] P. Christ, W. Biberacher, M. V. Kartsovnik, E. Steeb, E. Balthes, H. Weiss, and H. M"uller. *JETP Lett.* **71**, 303 (2000).
[5] D. Zanchi, A. Bjelis, and G. Montambaux. *Phys. Rev. B* **53**, 1240 (1996).
[6] P. M. Chaikin. *J. Phys. I France* **6**, 1875 (1996).

Magnetisation studies of α-(BEDT-TTF)$_2$KHg(SCN)$_4$ at fields almost or exactly parallel to the layers

W. Biberacher, D. Andres and M. Kartsovnik

Recent extensive studies of the "magnetic field – temperature " ($B-T$) phase diagram of the layered organic metal α-(BEDT-TTF)$_2$KHg(SCN)$_4$ have given strong arguments in favour of the charge-denisty-wave (CDW) nature of the low-temperature electronic state of this material [1]. The very low critical temperature of the phase transition, $T_p \cong 8$ K, provides a unique opportunity to study the competition between different mechanisms of the influence of magnetic field on the CDW state in a wide range, far beyond the low-field limit. Although many of the experimental results can be very well explained by the superposition of the Pauli and orbital effects of the magnetic field, there still remain some important questions which are difficult to understand within the existing CDW theories. In particular, unexpected for the CDW transition is the anisotropic change of the magnetic susceptibility: When the field is applied parallel to the highly conducting plane (crystallographic *ac*-plane) of the sample, the susceptibility exhibits a prominent drop independent of the field direction in the plane; at the same time, no change in the magnetisation, within the experimental resolution, has been found for the field perpendicular to the *ac*-plane [2].

So far, most of the studies of magnetic field effects on the title material have been done with the field either aligned perpendicular to the *ac*-plane or tilted by a moderate angle, up to $\simeq 40^\circ$, from this direction. In the present work, we have studied the magnetisation and magnetoresistance under the field almost or exactly parallel to the conducting layers.

High-quality single crystals of α-(BEDT-TTF)$_2$KHg(SCN)$_4$ with typical masses of 150 to 500 μg were grown electrochemically by H. Müller (ESRF, Grenoble, France) and N. Kushch (IPCP, Chernogolovka,Russia). For the magnetisation measurements, a sample was fixed by a small amount of Apiezon grease on a cantilever beam magnetometer, with an *in situ* rotation facility. This device was used in the center of the magnet as a torquemeter and 4 cm above as a Faraday forcemeter. A part of the experiments was carried out in a simultaneous torque and interlayer magnetoresistance configuration. In that case, annealed Pt wires of 10-μm diameter were attached with a graphite paste to both sides of the sample parallel to the *ac*-plane, before fixing it to the cantilever. The resistance was measured by a standard 4-probe a.c. technique. The experiments were performed at the High Magnetic Field Facility in Grenoble.

As will be shown below, the change in the magnetic susceptibility due to the phase transition can be described by a tensor with the principal axes determined by the layered structure of the material. In that case, the magnetic torque is given by:

$$\tau_a = (V/\mu_0)(\chi_{b^*} - \chi_c)B^2 \sin\theta\cos\theta, \qquad (1)$$

where V is the volume of the sample, b^* is the normal to the *ac*-plane and θ is the angle between the b^*-direction and the magnetic field B. For magnetic fields along the principal axes the signal becomes zero. The normal to the layers could be exactly determined by studying the vanishing of the de Haas-van Alphen oscillations.

The theoretical dependence $\tau \propto B^2$ is only fulfilled at temperatures above the phase transition. The additional anisotropy of the susceptibility below 8 K shows strong deviations from the the B^2 law. To extract this low temperature part we performed angular dependent measurements around the parallel ($\theta = 90^\circ$) direction at about 10 K. For this temperature one of the principal axes was found to be shifted by $7 \pm 0.5^\circ$ from the crystal *a*-axis and the other by $2 \pm 0.2^\circ$ from the *c*-axis. The high temperature torque was then subtracted from the low temperature data. The resulting torque of the low-temperature

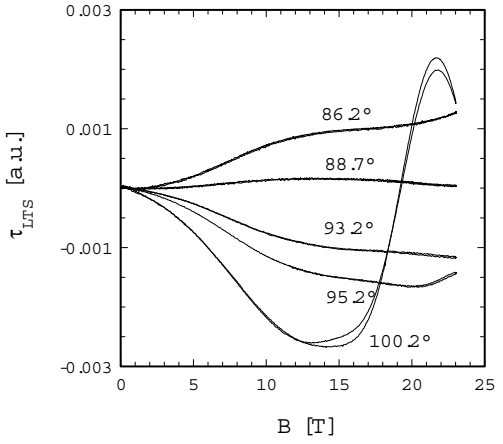

Figure 1: Field dependence of the magnetic torque in the LT state at T = 1.4 K.

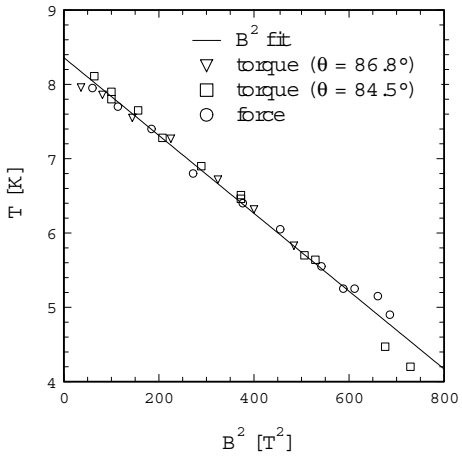

Figure 2: Transition temperatrure as determined by temperature sweeps plotted versus the square of the magnetic field

state (LTS) is shown in Fig. 1. This part vanishes exactly for the field direction parallel to the layers, meaning that the principal axes of the additional low temperature anisotropy are connected with the layer structure.

To study the transition from the normal state to the LTS we performed temperature sweeps of the torque at fixed magnetic fields oriented almost parallel to the conducting layers. In addition, similar temperature sweeps were performed in the Faraday force configuration with the field parallel to the *c*-axis. A clear transition could be observed up to 28 T. The field dependence of the transition temperatures of 3 different samples are shown in Fig. 2. The data can be well described by a B^2 law with a slope of $(5.2 \pm 0.4)10^{-3}$ [K/T^2]. This is in very good agreement with former specific heat measurements at lower magnetic fields [3]. There are clear differences to the phase diagram for magnetic fields perpendicular to the layers: (i) the field dependence of the transition temperature is considerably stronger than in the latter case; (ii) there is no clear indication of the so-called kink transition into the low-temperature–high-field (LTHF) state which is supposed to be a CDW with a spatially modulated order parameter; (iii) the phase line shows a B^2-dependence up to the highest fields, i.e. well above the low-field limit. While the first observation can be naturally explained by a strong reduction of the orbital effect on the CDW state at turning the field towards the conducting layers, the other two are not understood so far.

As seen in Fig. 1, the field dependence of the torque becomes non-monotonic and displays a hysteresis with respect to the field sweep direction when the field is tilted from the *ac*-plane by more than 5°. We have carried out detailed studies of the structure in the field sweeps of the torque and magnetoresistance at the angles $40^\circ \leq \theta \leq 90^\circ$. At $\theta > 60^\circ$ both quantities are found to display a series of irregular oscillations with a strong hysteresis. The amplitude of the oscillations and the hysteresis rapidly grow with decreasing the temperature. An example of the evolution of the structure in the field sweeps within a narrow interval of angles θ is given in Fig. 3. With increasing θ, the oscillations gradually shift to lower fields and fade out below $\sim$10 T. Simultaneously, new features emerge at the higher fields. The rate of the changes in the structure rapidly increases as θ approaches 90°. At angles very close to 90° the features become less pronounced; at $\theta > 88.5^\circ$ they could not be resolved in our experiment.

The positions of local maxima in the torque signal are plotted against $1/\cos(\theta)$ in Fig. 4. Such a scale is chosen because of the very rapid angular dependence of the structure at $\theta > 80^\circ$. The behaviour shown in Fig. 4 is characteristic of all the extreme points in the torque and magnetoresistance.

The strong irreversibility of the observed structure with respect to the field sweep direction suggests that it is probably associated with a series of first order phase transitions. At present we cannot specify which

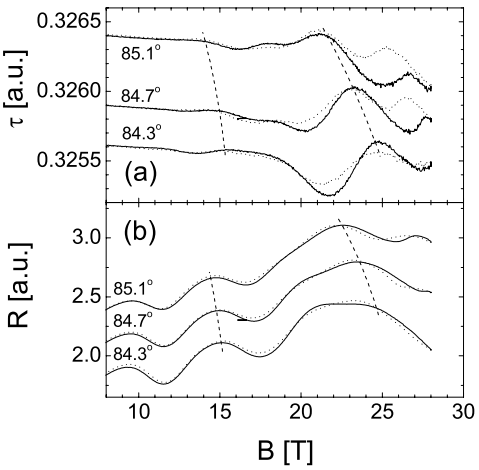

Figure 3: Up (solid lines) and down (dotted lines) field sweeps of the torque (a) and resistance (b) at high angles at T = 0.4 K. Dashed lines are guides to the eye.

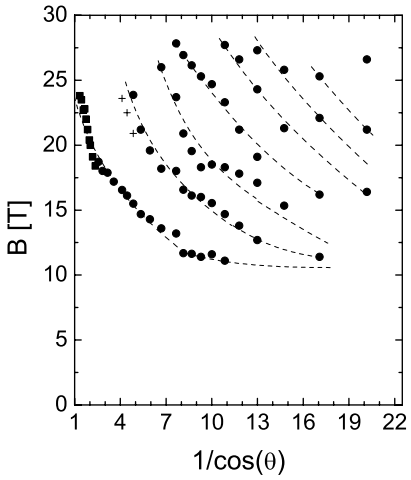

Figure 4: Angular dependence of the positions of local maxima in the field sweeps of the torque. Dashed lines are guides to the eye.

features in the torque or resistance exactly correspond to the transition points. Nevertheless some conclusions can be already derived from the present data. First, the obtained behaviour is more complicated than just a splitting of the kink transition due to an additional subphase, as proposed recently [4]. Second, the sensitivity of the structure to slight changes of the angle at θ near to 90° points to a crucial role of the field component perpendicular to the layers, $B_\perp \equiv B\cos\theta$. One can suppose that the observed phenomenon originates from an interplay between the Pauli and orbital effects of magnetic field. It should be noted that the orbital effect in the present compound may be more complicated than in purely Q1D materials: here it can also involve cyclotron orbits on the Q2D part of the Fermi surface [5]. The latter mechanism becomes increasingly important in high fields due to a growing probability of the magnetic breakdown between the Q2D and Q1D Fermi surfaces. The impact of the orbital effect is determined by $B_\perp$ while the Pauli effect is isotropic. From our experiment it follows that $B_\perp$ should be sufficiently small, however finite in order to induce the observed structure.

References

[1] M.V. Kartsovnik et al., Synth. Met. **86**, 1933 (1997); N. Biskup et al., Solid State Commun., **107**, 503 (1998); S. Hill et al., Synth. Met. **103**, 1807 (1999); C. Proust et al., Phys. Rev. B **62**, 2388 (2000); P. Christ et al., JETP Lett., **71**, 303 (2000); D. Andres et al., this proceedings, rep. No....? or ICSM'2000, to be published in Synt. Met.

[2] T. Sasaki et al., Synth. Met. **41-43**, 2211 (1991); P. Christ et al., Synth. Met. **86**, 2057 (1997).

[3] A. Kovalev et al., JETP **86**, 578 (1998).

[4] C. Proust et al., Phys. Rev. B **62**, 2388 (2000); J. Qualls et al., Phys. Rev. B 62, 1008 (2000).

[5] K. Kishigi et al., J Supercond. **12**, 485 (1999).

Anisotropy of high mobility electron systems at millikelvin temperatures

Cooperation between Walter-Schottky-Institut, Technical University of Munich:
O. Jaeger, F. Ertl, R. A. Deutschmann, M. Bichler and G. Abstreiter
and WMI:
E. Schuberth and C. Probst

During the last decade the purity and crystal quality of MBE deposited $Al_xGa_{1-x}As$ compounds has continuously been improved. As a result low-temperature peak mobilities beyond $10^7\,cm^2/Vs$ have been achieved in modulation doped heterostructures. The discovery, further exploration and understanding of the FQHE resulted from this development. Two years ago Eisenstein et al. discovered evidence of a new anisotropic state in higher Landau-levels [1], which shows up only in the best samples and only at temperatures below 150 mK. The anisotropy in magnetoresistance was attributed to the formation of a striped phase whose origin however remains unclear. In order to gain insight into the relation between the orientation of the stripes and the crystallographic axes, we investigated the influence of a slightly miscut substrate on the transport anisotropy.

Samples are grown in the EPI MBE (molecular beam epitaxy) system at WSI which is equipped with three large cryopumps and all full metal valves at the growth chamber. Furthermore the liquid nitrogen shrouds are continuously operated, resulting in a background pressure in the 10^{-12} mbar range at standby. Standard high mobility samples were grown on (001)-GaAs substrates at a temperature of $640^{\circ}C$ as measured by a pyrometer. Samples are rotated during growth. The layer structure for the high mobility samples consists of a modulation doped $GaAs/Al_xGa_{1-x}As$ single interface heterojunction (x=0.3) using Si d-doping. After a thick GaAs buffer and a $GaAs/Al_xGa_{1-x}As$ superlattice the $GaAs/Al_xGa_{1-x}As$ interface is grown with a spacer layer of $800\mathring{A}$. Square samples of $4\,mm \times 4\,mm$ are cleaved out of the middle of the wafer and contacted at the 4 corners and 4 side midpoints using indium. Our standard high mobility samples typically show mobilities of $10^7\,cm^2/Vs$ with an electron density in the sheet of $2.1 \cdot 10^{11} cm^{-2}$ at 1.4 K. The low temperature experiments were carried out in the nuclear demagnetization cryostat "BMM2" at the Walther Meissner Institut which allows for a base sample temperature below 1 mK. A photograph of the sample mount is shown in fig. 1. Great care was taken to ensure excellent thermal anchoring of the 8 measuring leads at the temperature of the nuclear stage and to appropriately shielding of HF radiation and vibrational damping of the cryostat. A low excitation current of 4 nA is used to avoid electron heating. The final temperature of the electron gas was certainly below 10 mK and probably as low as 5 mK.

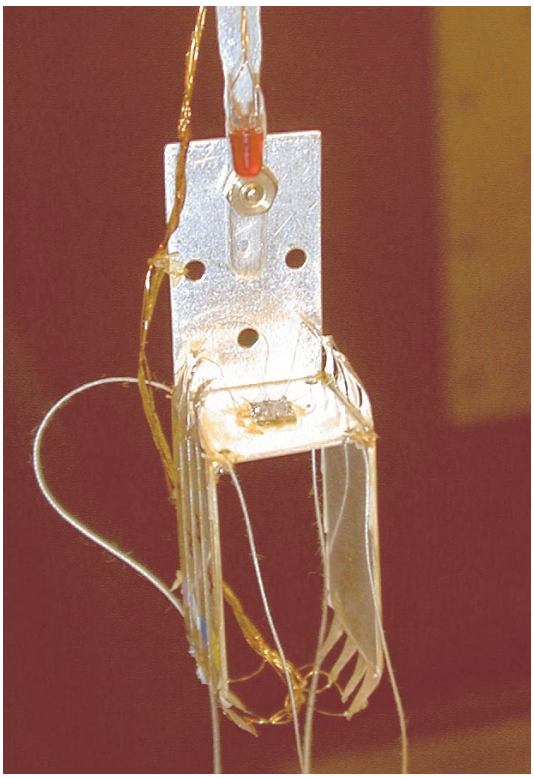

Figure 1: Sample mount and thermal anchoring of the GaAs-specimen. The red LED provides the illumination of the sample.

We took measurements of the longitudinal and Hall voltage while sweeping the magnetic field up to 5 T. The Shubnikov-de Haas-oscillations commence around 60 mT and even fragile FQHE states like $\frac{5}{2}$ are visible, which is a sign for the high quality of the growth. Most interestingly the samples exhibit the transport anisotropy, of which a temperature study is shown in Fig. 2 and whose dependence on the substrate misorientation was subject of our investigations which are still in progress.

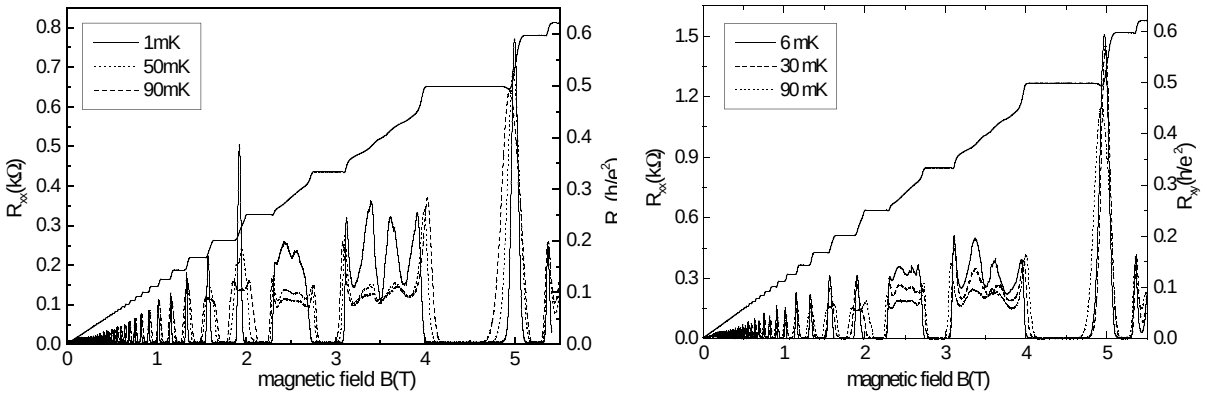

Figure 2: temperature dependent Shubnikov-de Haas and Hall measurements with current flowing in (011) direction (hard direction,left) and in $(01\bar{1})$ direction (easy direction,right)

(001)-GaAs substrates with miscut angles of $1\pm0.5/1.5\pm0.5/2\pm0.5$ and miscut orientation towards the (111)/(110) plane have been investigated, growing the same layer sequence as for high mobility samples. In order to guarantee identical growth conditions three different $\frac{1}{4}$ wafers of one miscut orientation and one $\frac{1}{4}$ standard (001) wafer piece were overgrown simultaneously. We examine the surface morphology after growth by AFM, a typical image of an overgrown piece is shown in fig. 3.

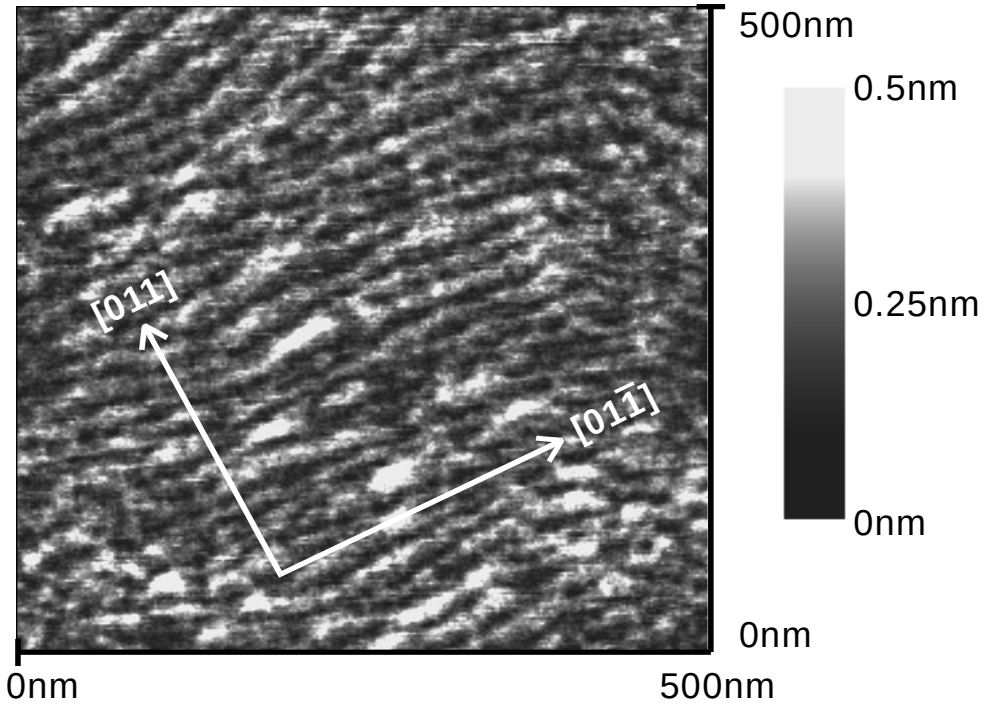

Figure 3: AFM image of the (001)surface with $1^\circ \pm 0.5^\circ$ miscut orientated towards the (111) plane after growth

On a small scale the surface structure of the substrate is apparent even after growth. The orientation and the average step distance is in agreement with the expected value from the specification. The mobilities for all samples are listed in table 1. The electron density is unaltered, while we observe an overall higher mobility of the (111) plane misoriented wafers, which decreases with increasing miscut angle. The wafers miscut towards the (110) plane also show a reduced mobility with respect to the reference wafer. This fact may be due to the growth conditions at the presence of monoatomic steps. We plan to

miscut orientation to (111) plane		miscut orientation to (110) plane	
miscut angle (°)	mobility $(10^6 cm^2/Vs)$	miscut angle (°)	mobility $(10^6 cm^2/Vs)$
reference 0	7.1	reference 0	10.3
1	11.3	1	9.2
1.5	9	1.5	8.0
2	8.5	2	6.7

Table 1: Electron mobilities

investigate also these samples at millikelvin temperatures in order to study the influence of the miscut angle on the anisotropic states.

References

[1] M. P. Lilly, K. B. Cooper, J. P. Eisenstein, L. N. Pfeiffer, and K. W. West, Phys. Rev. Lett. **82**, 394 (1999).

Tunneling between Quantum Hall Edge Channels in non Planar Geometry

M. Huber[*], *M. Rother*[*], *W. Biberacher, M. Grayson*[*], *R. Deutschmann*[*], *M. Bichler*[*] *und G. Abstreiter* [*]

The well established epitaxial growth of GaAs/AlGaAs heterostructures relies heavily on high crystalline interface quality. The resulting high electron mobility makes this material system favorable for investigation of fundamental electron-electron interaction in quantum transport. In collaboration with the Walter Schottky Institute from the Technical University in Munich in this project we want to measure tunneling currents in the quantum hall regime.

Therefore high magnetic fields and low temperature are essential. A cryostat with a superconducting magnet provides the required magnetic fields up to 14/16 Tesla. With a ^{3}He-system in combination with a rotatable mounted sample holder we obtained temperatures down to below 450 mK. Under these conditions in high electron mobility GaAs/AlGaAs heterostructures the integer and fractional quantum hall regimes are accessible.

The samples consist of two perpendicular high mobility two dimensional electron systems (2DEGs). These 2DEGs are realized as 200 Å thick quantum wells epitaxially grown with the method of cleaved edge overgrowth: a (001) quantum well sample is cleaved along the perpendicular (110) plane and overgrown with an (110) quantum well in a second expitaxial growth step (Fig. 1 inset). In the samples measured the quantum wells are additionally separated by a 50Å thick AlGaAs barrier. Applying bias voltages of up to 0.4 V we measured the tunneling current between the two 2DEGs.

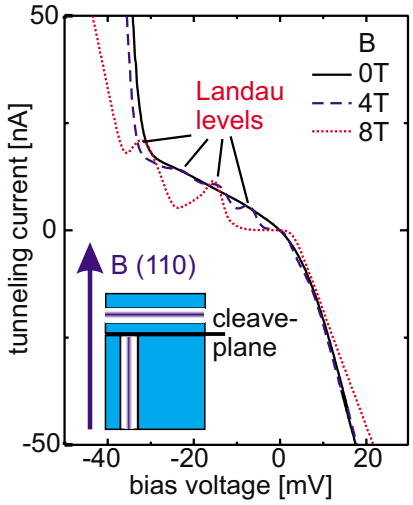

Figure 1: Tunneling current versus bias at a magnetic field of 0, 4 and 8 Tesla perpendicular to the [110]-plane. With an applied magnetic field clear peak structures arise in the I-V curves, which can be ascribed to Landau levels.

A magnetic field perpendicular to one of the quantum wells causes Landau quantization, with chiral edge states near the tunnel junction. The variation in the density of states affects the tunneling current (Fig. 1). Especially for higher magnetic fields the resonances in the tunneling current due to Landau levels become clearly visible.

For higher bias voltages a negative differential resistance appears. The subband structure of the quantum wells might possibly cause such an effect. For further analysis we have to investigate samples with various quantum well widths.

For this sample geometry it is of special interest to measure under simultaneous magnetic quantization in both quantum wells. As a relevant prerequisite for such investigations we use a rotatable mounted sample holder here in the institute. This allows computer controlled tilting of the sample *in situ* at low temperature and applied magnetic field.

[*] In collaboration with Walter Schottky Institut, Technische Universität München

We showed that it is possible to bring both quantum wells into a quantized state at the same time, where in each case the perpendicular component of the magnetic field is responsible for the Landau quantization. Depending on the exact strength, angle and orientation of the magnetic field the tunneling between different filling factors, i.e. different quantum hall and fractional quantum hall states can be studied. We also can compare the parallel edge channel propagation with the antiparallel one for the same filling factors.

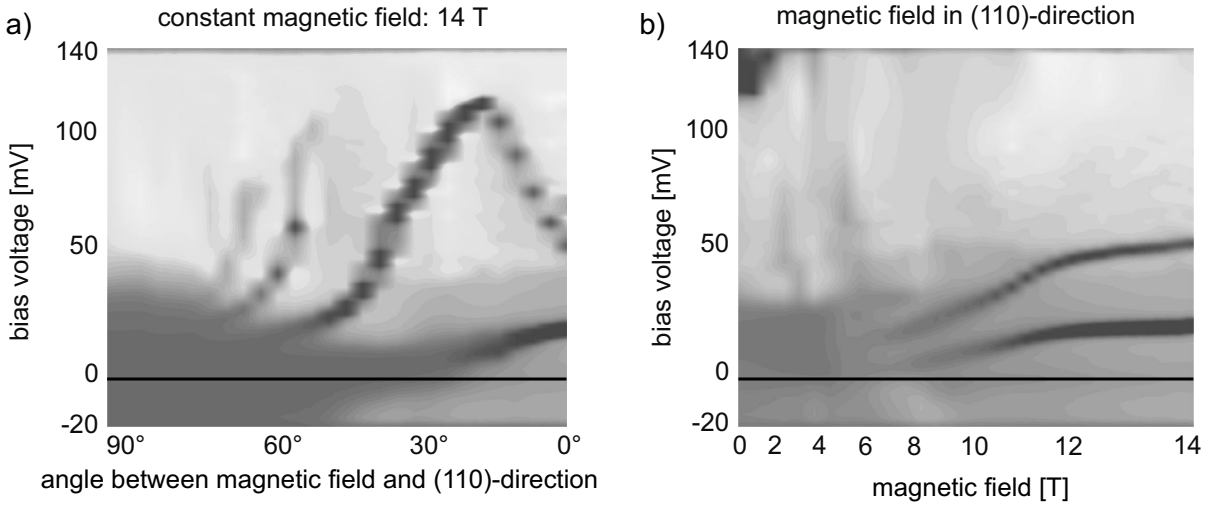

Figure 2: In grayscale plot of I-V curve as function of tilt angle with constant magnetic field (a) and as function of the magnetic field at constant angle perpendicular to the [110]-cleave plane (b). Dark areas represent an enhancement in the tunneling current.

For a fixed orientation of the magnetic field perpendicular to the [110]-plane in a plotting of the tunneling current as a function of bias voltage and magnetic field the Landau splitting of the electronic states is obvious (Fig. 2b). The fan like structure formed by the dark areas in the gray scale plot represents the well known Landau fan.

At a constant magnetic field strength the effective component in (110)-direction also changes by tilting the sample. Fig. 2a) shows the corresponding plot, where the angle scale is equivalent to the scale of the effective (110)-component in plot b). Tilting the sample produces an additional field component in (001)-direction, causing a quantization in the [001]-quantum well. This (001)-component of the magnetic field changes the tunneling current significantly, as the two plots in Fig. 2 show. The right edge of the two plots represent the same I-V-curve. With increasing angle, however, one of the resolved resonances shifts to higher bias and reaches its maximum at about 18° before it returns to the normal Landau fan at about 45°. At angles above 45° additional resonances evolve, which indicate similar behavior. Further measurements with various quantum well and barrier parameters will show if this effect can be completely explained by the additional quantization in the [001] quantum well.

Magnetotransport investigation of type-III modulation doped HgTe single quantum wells

X. C. Zhang, K. Ortner, A. Pfeuffer-Jeschke, C. R. Becker, G. Landwehr, W.Biberacher and K. Neumaier [7]

1. *n*-type HgTe single quantum wells (QWs)

Magnetotransport investigation of both *n* and *p*-type modulation doped type-III HgTe/CdTe single quantum wells, which were grown by molecular beam epitaxy (MBE), were carried out over a temperature range of 50 mK-200K and magnetic fields up to 14 T in Würzburg and at the Walther Meissner Insitut (WMI).

The band structure of *n*-type HgTe single quantum wells is relatively well known. Earlier experimental work in Würzburg has been mainly focused on the effective mass m^*, effective g-factor g^* and Rashba spin splitting in asymmetrical QWs.

A systematic study of the effective mass m^* and g-factor g^* and their dependence on carrier density, well widths, which extended from the normal semiconductor to inverted semiconductor regime, and doping mode, i.e., symmetrically or asymmetrically doped, was carried out.

Zero field spin splitting has been observed in the inverted band regime: by using a gated Hall bar, Rashba spin splitting has been observed in wide HgTe QWs with an inverted band alignment which can be tuned from zero to large finite values for either gate voltage polarity. In order to interpret the experiment, band structure calculations based on an $8\times 8\,\mathbf{k}\cdot\mathbf{p}$ model have been performed, which show good agreement with experiment. Compared to the widely investigated III-V group type I heterojunctions whose conduction subband has the normal $\Gamma 6$ symmetry, the specific feature of zero field spin splitting is that the conduction subband of type III QWs is hole-like, which has $\Gamma 8$ symmetry, even though it is occupied by electrons. Furthermore the zero field spin splitting has been shown to depend on the well width. The larger the well width, the larger this effect.

For good quality n-type HgTe QWs, very well developed quantum Hall plateaus have been observed. A measurement on a *n*-type HgTe QW in Braunschweig reveals that the accuracy of the quantum Hall effect (QHE), i.e., ρ_{xy} for $\nu = 2$, is better than 10^{-6}. This provides another system in order to study the localization problem in the quantum Hall regime. Excellent scaling behavior has been observed only in an InGaAs/InP 2D electron gas [1]. Experimental studies which are being carried out on HgTe SQWs down to the milli-Kelvin range will shed new light on this topic. The sample mentioned above has also been measured at the WMI over a temperature range of 450 mK to 7.0 K in a He^3 cryostat. A preliminary analysis of the experimental data shows that the temperature dependence of both the maximum in $d\rho_{xy}/dB$ and the half-width ΔB for ρ_{xx} peaks is negligible, in contrast with the universal scaling power law $T^{-\kappa}$ with $\kappa = 0.42 \pm 0.04$. [1] This discrepancy suggests that more extensive experimental and theoretical studies on this issue should be carried out in the future.

2. *p*-type HgTe QWs

The difficulties in the ongoing investigation of *p*-type QWs lie in the growth of high mobility samples, making good ohmic contacts, fabricating good quality gates, as well as the difficulty of interpreting the irregular Shubnikov-de Haas (SdH) oscillations due to a complex band structure. Till now mobilities up

[7] In collaboration with Universität Würzburg

to 60,000 cm^2/Vs have been achieved at 4.2 K in arsenic modulation doped HgTe QWs with a well width of 150 Å.

Because of the much larger hole effective mass compared to that of the electron, the SdH oscillations have a very strong temperature dependence, and it is absolutely essential for temperatures in milli-Kelivin range in order to resolve the SdH oscillations particularly at low magnetic fields. Magnetotransport measurements were carried out from 100 mK to 1.6K at magnetic field up to 14 T in a dilution refrigerator of the WMI. The carrier concentration calculated from the Hall effect is about four times larger than that from the frequency of the SdH oscillations at low magnetic fields. This is in accordance with theoretical calculations which reveal that the Fermi surface consists of four separated regions which are shaped like distorted crescents at low hole density, and a single ring shaped surface when the hole density is high. In order to test the theoretical predictions, a measurement at 450 mK in a He^3 cryostat of WMI for a gated Hall bar, whose hole concentration could be varied by a factor of three, has also been carried out. An analysis of the experimental data is now being performed. A detailed Landau level fan chart in the framework of the $8 \times 8\,\mathbf{k} \cdot \mathbf{p}$ model will be calculated to compare with experimental results.

References

[1] H. P. Wei, D. C. Tsui, M. A. Paalanen, and A. M. M. Pruisken, Phys. Rev. Lett. **61**, 1294 (1988).

Studying the interaction of coupled quantum dots in the few electon limit

Andreas Hüttel, Hua Qin*, Robert Blick*, Karl Neumaier*

The continuing decrease of circuit size eventually will lead to the implementation of single electron electronics. The devices which allow to trap and manipulate single charges are called quantum dots. The dots used in this work are defined in a two dimensional electron gas (2DEG) of a GaAs/AlGaAs heterostructure with a mobility of 8×10^5 cm^2/Vs and a density of $n_S = 1.7 \times 10^{11}$ cm at a base temperature of $T_{bath} \approx 25$ mK. On the surface of this heterostructure Au electrodes are defined by electron beam lithography. By applying negative bias voltages to the gates the 2DEG underneath is depleted and the geometry of the gate structure is transferred to the 2DEG. Thus, we can form quantum dots of different geometry with tunable tunneling barriers. As an example a coupled quantum dot configuration is shown in the figure below. In total four dots can be tuned in: A1, A2, and B1, B2. Each of the pairs is connected to emitter/collector contacts, the two pairs couple capacitively. This ensures that the dots can be charged individually.

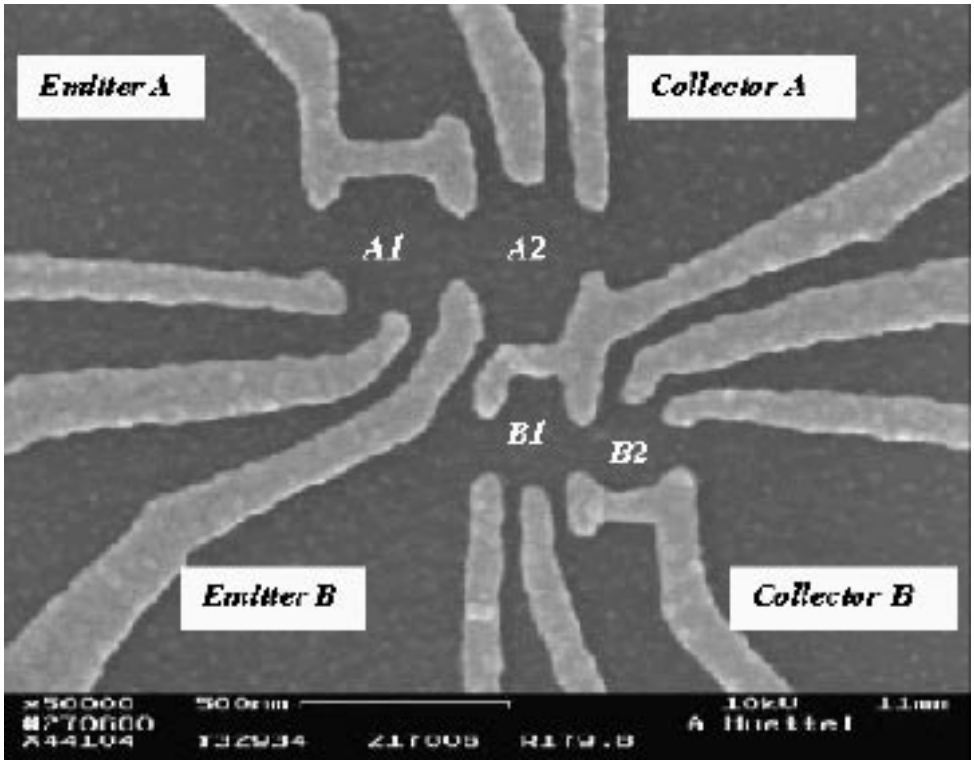

Generally, electron transport through quantum dots is characterized by the Coulomb blockade of transport. Adding additional electrons to a dot costs a charging energy E_C which can be higher than the thermal energy of the electrons at the Fermi-level in the 2DEG. It basically is governed by the total capacitance of the electron island $E_C = e^2/C_\Sigma$. Only at discrete levels, when the charging energy coincides with the energy provided by the electrons in the 2DEG, single charges can flow through the dots, otherwise the current is blocked. A necessary condition is a low temperature of operation, i.e. $E_C >> k_B T$. If this condition is satisfied the dots function as single electron transistors in which the flow of single charges can be minutely controlled. Obviously, the strength of this approach is the ease with which the electron-electron interaction can be accessed.

Naturally, for industrial applications a high operation temperature is desired. This we achieved not in GaAs/AlGaAs-heterostructures, but in dots formed in doped silicon nanostructures. However, the main objective in this experiments on coupled dots in 2DEGs is to go beyond the classical charge confinement

and focusing on phase coherence effects in electronic transport. The underlying idea of the apparatus shown in the figure is to confine single electrons in one of the coupled dots (system A) and minimizing the coupling to the environment (the leads), while the other dots (system B) is actuated as a detector. This is easily achieved, since quantum dots by definition are ultra sensitive electrometers. Thus, the charge configuration system A can be read out sensitively by system B.

*Center for Nanoscience, LMU Munich

Local Magnetic Order in Manganite Thin Films Studied by $1/f$ Noise Measurements

A. Marx, R. Gross [8]

The mixed-valence manganites $Ln_{1-x}D_xMnO_3$ (with Ln a rare earth and D a divalent alkaline earth) recently have attracted renewed interest because of their colossal magneto-resistance (CMR) [1, 2] and the interesting interplay between charge, spin, orbital, and structural degrees of freedom in these materials resulting in new ordering phenomena and very rich phase diagrams [3–5]. Both the fundamental mechanism of the CMR effect and its potential for device applications have been addressed in a large number of studies [6–9]. The charge transport mechanism in the doped manganites is still controversely debated. The question whether there is a phase separation in the ferromagnetic phase into insulating and highly conducting regions leading to a filamentary/percolative current flow is of primary interest.

In addition to standard transport measurements the detailed investigation of the $1/f$ noise is a well established, valuable tool for clarifying the charge transport mechanism in a variety of physical systems [10]. In previous measurements the $1/f$ noise in manganite thin films and single crystals was found to be orders of magnitude larger than in conventional metals or semiconductors and to display a broad spectrum of different temperature dependencies. The resistance fluctuations are intimately related to the conduction mechanism in different temperature regimes. Thus, the detailed investigation of the $1/f$ noise helps to clarify the interplay of polaronic charge transport with mainly localized charge carriers in the paramagnetic phase and charge transport mediated by double exchange in the ferromagnetic phase.

We have performed a detailed study of the temperature and magnetic field dependence of the low frequency resistance fluctuations in $La_{2/3}Ca_{1/3}MnO_3$ (LCMO) thin films of high epitaxial quality [11]. Film preparation on different substrates resulting in different amounts of lattice mismatch between film and substrate is found to have a tremendous effect on both the overall temperature dependence and the magnitude of the resistivity and the normalized resistance noise. The strikingly different magnitude and temperature dependence of the $1/f$ noise most likely originates from the different amount of local strain in the epitaxial films deposited on different substrates.

Our noise measurements have been performed in a five-probe configuration. The films have been deposited by pulsed laser deposition and patterned into microbridges using optical lithography and Ar ion beam etching.

Noise data of a strain free LCMO film

The temperature dependence of the resistivity of the LCMO film grown on a $NdGaO_3$ (NGO) substrate (nearly strain free, lattice mismatch 0.5%) is shown in Fig. 1 for different values of the applied magnetic field. The curves show a transition from a semiconducting to a metallic behavior which can be explained by a transition from a para- to ferromagnetic state in terms of the double exchange model with a high transition temperature $T_C \simeq 250\,\mathrm{K}$.

The temperature dependence of the normalized noise magnitude is shown in Fig. 2 for different values of the applied magnetic field. These values are by several orders of magnitude smaller than all data published so far for manganites, both for bulk samples and thin films and are comparable to the noise data found in conventional metals. These results suggest that the low resistance noise level is related to the high epitaxial quality and very low internal strain in the $La_{2/3}Ca_{1/3}MnO_3$ film grown on the NGO substrate.

The noise peak at $T_C \simeq 250\,\mathrm{K}$ for $B = 0$ can be suppressed by a small magnetic field. Furthermore, for zero applied magnetic field there is an increase of the normalized noise by a factor of about five going

[8] In collaboration with P. Reutler, F. Herbstritt, T. Kemen, Universität zu Köln

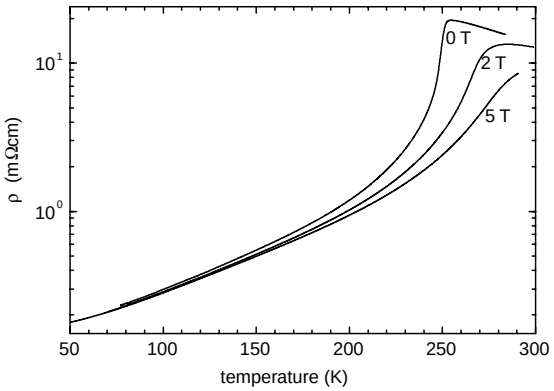

Figure 1: Temperature dependence of the resistivity of a $La_{2/3}Ca_{1/3}MnO_3$ film grown on a NGO substrate showing a transition from a semiconducting to a metallic behavior at $T_C \simeq 250\,\mathrm{K}$ in zero applied magnetic field.

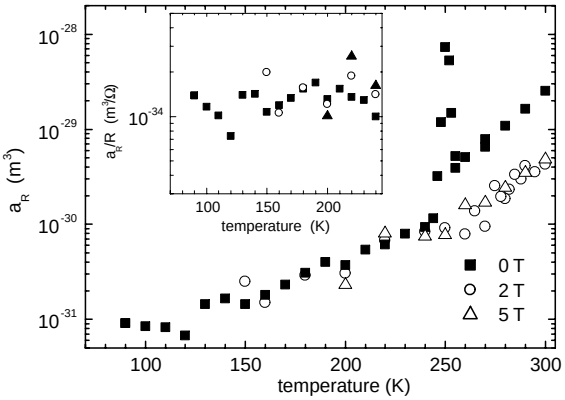

Figure 2: Temperature dependence of the normalized resistance noise amplitude a_R of a $La_{2/3}Ca_{1/3}MnO_3$ film grown on a NGO substrate for different applied magnetic fields. The inset shows a_R/R as a function temperature in the ferromagnetic phase.

from the ferromagnetic ($T < T_C$) to the paramagnetic phase ($T > T_C$). This increase is completely suppressed by an applied magnetic field. The significant reduction of the noise in the paramagnetic regime by an applied magnetic field suggests that the increased noise level in the paramagnetic as compared to the ferromagnetic regime is due to the existence of small ferromagnetically ordered clusters embedded into a paramagnetic environment. By the strong coupling of resistance to magnetization in the doped manganites, the fluctuating spin clusters directly give rise to low frequency resistance fluctuations. From the low value of the resistance noise in the ferromagnetic regime and from the negligible magnetic field dependence at temperatures below the transition we can conclude that for the ferromagnetic/metallic phase of the investigated $La_{2/3}Ca_{1/3}MnO_3$ film there is no significant contribution to the low frequency resistance noise due to fluctuations in the magnetic order.

Noise data of a highly strained LCMO film

Due to the considerable lattice mismatch between the film and the substrate (1.5%) the $La_{2/3}Ca_{1/3}MnO_3$ film grown under identical conditions on a $SrTiO_3$ substrate has significantly different transport and noise properties.

As shown in Fig. 3, due to the significant strain effect [12, 13], the film is characterized by a much lower value of $T_C \simeq 115\,\mathrm{K}$ and a significantly higher resistivity. Furthermore, in contrast to the film on $NdGaO_3$ the IVCs of the microbridge patterned into the $La_{2/3}Ca_{1/3}MnO_3$ film grown on $SrTiO_3$ were found to be non-linear in a temperature range close to T_C as shown in the inset of Fig. 3,

There is a strong difference both in the magnitude and the temperature dependence of the normalized low frequency resistance noise between the $La_{2/3}Ca_{1/3}MnO_3$ film grown on $SrTiO_3$ and $NdGaO_3$. As shown in Fig. 4, on decreasing temperature, a huge increase of the magnitude of the normalized resistance noise in a wide temperature range is observed just in the vicinity of the paramagnetic to ferromagnetic transition. The strong increase of the normalized noise by about 3 orders of magnitude takes place in a relatively wide temperature regime extending over about 40 K. The maximum value of the noise is measured at about 80 K, that is, at a temperature where the ferromagnetic/metallic phase is expected to be already well established. Obviously, the strain introduced in the $La_{2/3}Ca_{1/3}MnO_3$ film grown on $SrTiO_3$ due to the large lattice mismatch of 1.5% results in a strongly increased noise level both in the paramagnetic and ferromagnetic regime with a huge enhancement in the ferromagnetic regime (almost 10 orders of magnitude as compared to the strain free film). It is known that strain due to a large lattice mismatch between film and substrate causes significant local structural disorder in the doped manganites.

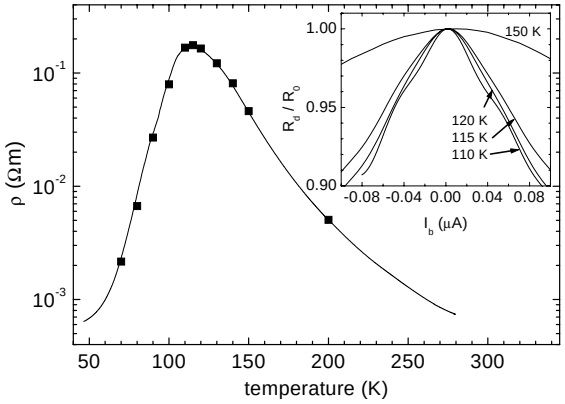

Figure 3: Temperature dependence of the resistivity of a $La_{2/3}Ca_{1/3}MnO_3$ film on a $SrTiO_3$ substrate. In the inset the differential resistance $R_d = \partial V/\partial I$ normalized to $R_0 = R_d(I_b = 0)$ is shown for temperatures close to $T_{\max}$.

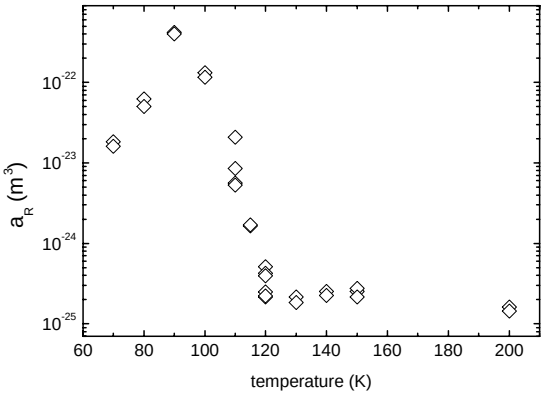

Figure 4: Temperature dependence of the normalized noise amplitude a_R of a $La_{2/3}Ca_{1/3}MnO_3$ film grown on a $SrTiO_3$ substrate showing a huge increase of the noise level in the vicinity of the transition from the paramagnetic/semiconducting to the ferromagnetic/metallic phase.

The observed huge increase of the resistance noise suggests that the resistance in the temperature range near the transition from the paramagnetic to the ferromagnetic phase is mostly determined by charge hopping between domains in an inhomogeneous, disordered magnetic material [14]. Such a transport mechanism is a likely source for both the noise peak and the non-linearity of the current-voltage characteristics. Low frequency fluctuations of domains are known to give rise to an anomalous high normalized low frequency noise level. Beyond the explanation of the noise data in terms of a disordered magnetic material, there is another possible scenario where the noise data are taken as evidence for a percolative nature of the charge transport in the ferromagnetic regime.

Our comparative study shows that there is a strong coupling between local magnetic disorder and structural disorder introduced by strain effects due to a large lattice mismatch between film and substrate. Judging from our noise analysis, the low-T_C film shows strong magnetic disorder, whereas the high-T_C film behaves more like a conventional ferromagnetic metal.

References

[1] R. von Helmolt, J. Wecker, B. Holzapfel, L. Schultz, and K. Samwer, Phys. Rev. Lett. **71**, 2331 (1993).
[2] S. Jin, T. H. Tiefel, M. McCormack, R. A. Fastnacht, R. Ramesh, and L. H. Chen, Science **264**, 413 (1994).
[3] M. Imada, A. Fujimori, and Y. Tokura, Rev. Mod. Phys. **70**, 1039 (1998).
[4] J. M. Coey, M. Viret, and S. von Molnár, Adv. Phys. **48**, 167 (1999).
[5] A. P. Ramirez, J. Phys.: Condens. Matt. **9**, 8171 (1997).
[6] A. J. Millis, P. B. Littlewood, and B. I. Shraiman, Phys. Rev. Lett. **74**, 5144 (1995).
[7] A. J. Millis, Nature **392**, 147 (1998).
[8] J. B. Goodenough and J.-S. Zhou, Nature **386**, 229 (1997).
[9] J. M. De Teresa, M. R. Ibarra, P. A. Algarabel, C. Ritter, C. Marquina, J. Blasco, J. Garcia, A. del Moral, and Z. Arnold, Nature **386**, 256 (1997).
[10] S. Kogan, *Electronic Noise and Fluctuations in Solids*, (University Press, Cambridge) (1996).
[11] P. Reuter, A. Bensaid, F. Herbstritt, C. Höfener, A. Marx, and R. Gross, Phys. Rev. B **62**, 11619 (2000).
[12] B. Wiedenhorst, C. Höfener, Y. Lu, J. Klein, L. Alff, R. Gross, B. H. Freitag, and W. Mader, Appl. Phys. Lett. **74**, 3636 (1999).
[13] B. Wiedenhorst, C. Höfener, Y. Lu, J. Klein, M. S. R. Rao, B. H. Freitag, W. Mader, L. Alff, and R. Gross, J. Magn. Magn. Mater. **211**, 16 (2000).
[14] H. T. Hardner, M. B. Weissman, M. Jaime, R. E. Treece, P. C. Dorsey, J. S. Horwitz, and D. B. Chrisey, J. Appl. Phys. **81**, 272 (1997).

DC Magnetic penetration depth of UPt_3 and Sr_2RuO_4: implications for the superconducting order parameters

Erwin A. Schuberth[1], *Stephan Schöttl*[1], *Karol Flachbart*[2], *and Takahiko Sasaki*[3]

In order to distinguish the superconducting phases of the title compounds we have studied their dc magnetic properties in low fields with a SQUID magnetometer. The magnetic penetration depth of UPt_3 shows the second superconducting transition at T_c^- when the field is applied along the c-axis, but not with H⊥c. This result, combined with a power law behavior of λ at low temperatures, is most consistent with the two-dimensional E_{2u} order parameter symmetry. Below 20 mK we find an additional diamagnetic signal which we ascribe to the normal state magnetism. For Sr_2RuO_4, supposedly a p-wave superconductor, we find a sharp single diamagnetic transition at 1.08 K showing that our sample is of high quality, but there is no indication of an unusual superconducting behavior.

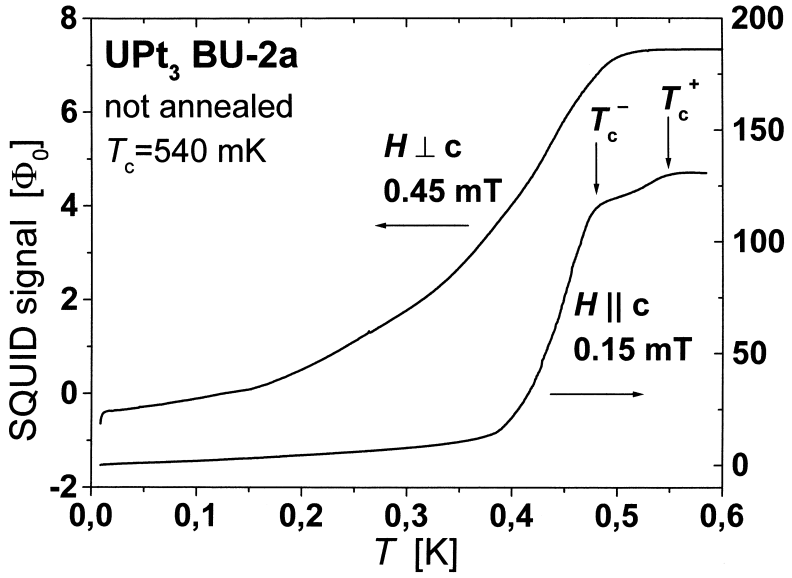

Figure 1: Temperature dependence of the s.c. penetration depth λ for sample BU-2a, for both H // c and H⊥ c. For the measurements with H ⊥ c, only a small slab cut from BU-2a was used resulting in a smaller signal (in spite of the higher measuring field)

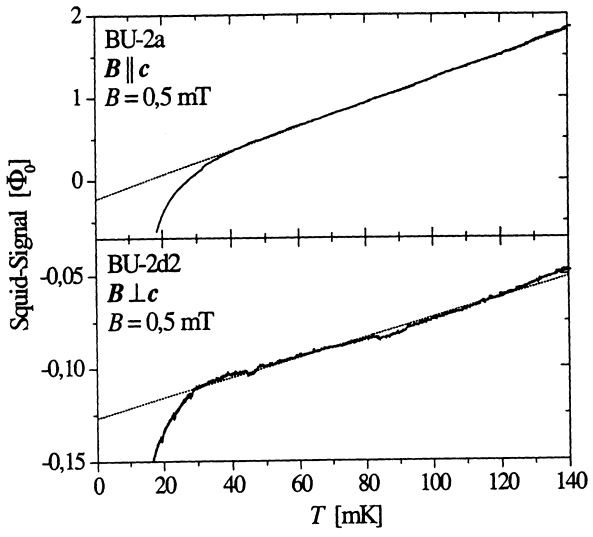

Figure 2: Low temperature part of λ from Fig. 1 showing a linear dependence for both field directions.

Among the Heavy-fermion superconductors UPt_3 is most widely studied because of its unconventional properties, such as the double superconducting (s.c.) transition in low fields and the three internal s.c. phases. However, there is still a lack of information on the differences between these phases. Here we re-investigated a single crystal grown by Bucher, Konstanz (see Ref. [1]) with SQUID magnetometry and confirmed results obtained from samples of excellent quality grown at Northwestern University [2]. This is especially remarkable since this sample was not annealed and did not show a double transition in specific heat measurements.

The SQUID signal from a superconductor in a constant external magnetic field reflects the temperature dependence of the penetration depth λ. To avoid contributions from flux creep processes, our experiments were performed in the field-cooled state. For UPt_3 the penetration depth λ drops steeply near T_c^+ and then tends to flatten out.

When H // c, a second steep drop appears below T_c^- as shown in Fig. 1. This second drop is not observed when H $\perp$c. At even lower T , λ obeys a power law $\lambda \propto T$ for both field directions, see Fig. 2. At 20 mK this power law is followed by an additional diamagnetic signal.

The results confirm previous ones from the Northwestern samples, except that for those a quadratic T-dependence was observed for H // c [1]. Since impurity scattering leads to higher power laws than linear, we believe that the Bucher sample is also of excellent quality, although it was not annealed. As we argued previously [1], the observation of the A-B transition in λ below T_c^-only with H // c implies an increase of the number of paired electrons with momentum in the a-b plane at these temperatures. This is consistent with the 2-dim E_{2u} [3] and E_{1g} [4] order parameters. The linear T-dependence at lower T favors the E_{2u} model, but due to our sample geometry we cannot fully exclude E_{1g}. The diamagnetic signal below 20 mK, also observed with the Northwestern samples, seems to be due to the magnetism of the vortex cores and points to antiferromagnetic ordering in the normal state, as it coincides with anomalies in thermodynamic and neutron data [5,6].

For Sr_2RuO_4 which is considered a p-wave superconductor, both zero field cooled and field cooled SQUID measurements on a sample grown at Tohoku University, showed a single, very sharp transition around 1.08 K, see Fig. 3. Although the Meissner signal was only a few % of the shielding transition, the sharpness of T_c shows that the crystal is of very high quality. We followed the Meissner signal down to 17 mK and found no unusual features, only a flat T-dependence at low temperatures.

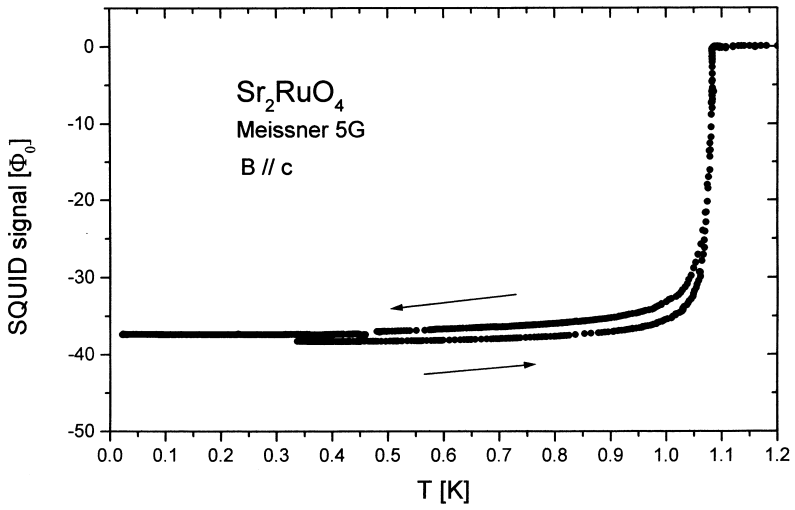

Figure 3: Meissner signal in a Sr_2RuO_4 sample in 0.5 mT. A small increase of the background below 100 mK has been subtracted.

We gratefully acknowledge financial support by DAAD.

References

[1] S. Schöttl et al., Phys. Rev. Lett. 82, 2378 (1999)
[2] J. B. Kycia et al., Phys. Rev. B 58 ,R603 (1998)
[3] J. A. Sauls, J. Low Temp. Phys. 95 , 153 (1994)
[4] K. A. Park and R. Joynt, Phys. Rev. B 53 , 12346 (1996)
[5] E. A. Schuberth et al., Phys. Rev. Lett. 68 ,117 (1992);
[6] A. Sawada et al., Czech. J. Phys. 46 , 803 (1996); Y. Koike et al., J. Phys. Soc. Jpn. 67 , 1142 (1998)

Viscoelastic Model of Normal ^{3}He in Aerogel

Dietrich Einzel

The sound propagation in a normal Fermi liquid such as ^{3}He can be viewed as viscoelastic behavior which is governed entirely by the conservation law for the momentum density and the viscous dissipation or the relaxation of the momentum current (stress tensor). This research project is devoted to a study of the alterations to the viscoelastic properties of normal liquid^{3}He in the presence of a dilute system of aerogel strands immersed into the bulk liquid. If the aerogel system behaves like a *rigid* random system of interconnected silica strands, it introduces an additional elastic scattering channel for the quasiparticle excitations of the Fermi liquid and breaks the momentum conservation law explicitly. In order to understand the physical consequences, we recall the essential equations of the hydrodynamic description of liquid ^{3}He, which start from the law of mass conservation

$$\frac{\partial}{\partial t}\delta\rho + \nabla\cdot\mathbf{g} = 0$$

Here $\delta\rho$ denotes the mass density and $\mathbf{g}$ the mass current or momentum density. $\mathbf{g}$ obeys the linearized Navier–Stokes equation

$$\left(\frac{\partial}{\partial t} + \frac{\Phi_1^{\rm s}}{\tau_1}\right)\mathbf{g} + \nabla\cdot\mathbf{\Pi} = n\mathbf{F}$$

Here $\mathbf{F} = -\nabla\phi - \partial\mathbf{A}/\partial t$ is an external force which may, as usual, be generated from a scalar potential ϕ and a vector potential $\mathbf{A}$. τ_1 describes the impurity–limited relaxation of the momentum density due to the presence of the aerogel, and $\Phi_\ell^{\rm s} = 1 + F_\ell^{\rm s}/(2\ell+1)$. The momentum current is, as usual, decomposed into a diagonal reactive (pressure) and a traceless (viscous dissipation) part:

$$\begin{aligned}
\mathbf{\Pi} &= \delta P\mathbf{1} + \mathbf{\Pi}' \\
\delta P &= c_1^2\delta\rho \\
\nabla\cdot\mathbf{\Pi}' &= -\frac{\eta^*(\omega)}{\rho}\left\{\nabla^2\mathbf{g} + \frac{1}{3}\nabla(\nabla\cdot\mathbf{g})\right\}
\end{aligned}$$

Here

$$\eta^*(\omega) = \frac{1}{5}\frac{np_{\rm F}v_{\rm F}\tau_2}{1 - i\omega\tau_2/\Phi_2^{\rm s}}$$

is the dynamic shear viscosity, in which τ_2 is the viscous relaxation time in the presence of aerogel:

$$\frac{1}{\tau_2} = \frac{1}{\tau_\eta} + \frac{1}{\tau_{\rm A}}$$

With this set of equations one may derive the following form for the density response (or Lindhard–Mermin) function in $(\omega,\mathbf{q})$–space $\mathbf{L}(\mathbf{q},\omega)$, which is consistent with density conservation [1]:

$$\begin{aligned}
\delta\rho &= i\mathbf{q}\cdot\mathbf{L}(\mathbf{q},\omega)\cdot\mathbf{F} \\
\mathbf{L}^*(\mathbf{q},\omega) &= m\frac{N_{\rm F}}{\Phi_0^{\rm s}}\frac{c_1^2 b_1^*(\omega)}{\omega^2 - c^2(\omega)\mathbf{q}^2 b_1^*(\omega)} \\
c(\omega) &= c_1 + (c_0 - c_1)b_2^*(\omega) \\
b_\ell^*(\omega) &= \frac{-i\omega}{-i\omega + \Phi_\ell^{\rm s}/\tau_\ell}
\end{aligned}$$

Here $N_{\rm F}$ is the density of states at the Fermi level for both spin projections. The functions $b_\ell^*(\omega)$ describe the viscoelastic transitions from a diffusive to a propagating sound mode ($\ell = 1$) and from first to zero

sound ($\ell = 2$). In order to emphasize the aspect of hydrodynamic diffusion $\mathbf{L}^*$ can be rewritten in the equivalent form

$$\begin{aligned} \mathbf{L}^*(\mathbf{q},\omega) &= m\frac{N_{\rm F}}{\Phi_0^{\rm s}}\frac{D_1^*(\omega)}{i\omega - D^*(\omega)\mathbf{q}^2} \\ D_1^*(\omega) &= \frac{c_1^2}{-i\omega + \Phi_1^{\rm s}/\tau_1} \quad ; \quad D^*(\omega) = \frac{c^2(\omega)}{-i\omega + \Phi_1^{\rm s}/\tau_1} \end{aligned}$$

Therefore, due to the breaking of the momentum conservation law in the presence of aerogel, the sound pole in the Lindhard function of the pure system has to be replaced by a diffusion pole in the Lindhard–Mermin function $i\omega = D^*(\omega)\mathbf{q}^{*2}(\omega)$ leading to a complex wave number

$$q^*(\omega) = \sqrt{\frac{i\omega}{D^*(\omega)}} = \frac{\omega}{c_1 + (c_0 - c_1)b_2^*(\omega)}\sqrt{1 + \frac{i\Phi_1^{\rm s}}{\omega\tau_1}} \tag{1}$$

Clearly, in the absence of aerogel $\tau_1 \to \infty$, the clean Fermi liquid result

$$\alpha(\omega) = \frac{2}{3}\frac{\omega^2}{\rho c_1^3}\mathrm{Re}\ \eta^*(\omega)$$

is recovered. A preliminary estimate, using an expression for the aerogel limited relaxation time $\tau_{\rm A}$ [2]

$$\tau_{\rm A} \approx \frac{1.2583}{c[\%]^{1.24}}10^{-8}\mathrm{sec}$$

shows, however, that $\omega\tau_1$ is not large in the sound case and one should use

$$\alpha^*(\omega) = \mathrm{Im}\ q^*(\omega) \tag{2}$$

for the analysis of the sound attenuation. The above investigations are based on the assumption of a rigid aerogel system. If, on the contrary, the aerogel system moves in phase with the density oscillation, the attenuation is governed by the viscous coupling of the ^{3}He to the aerogel [3]

$$\alpha^*(\omega) = \frac{\omega}{c_1 + (c_0 - c_1)b_2^*(\omega)} \tag{3}$$

It can be expected that there exists a crossover frequency ω_0, separating these two (rigid at higher vs. in–phase motion at lower frequencies) limiting behaviors of the aerogel system and the experiment can eventually fix ω_0. A numerical analysis of Eqs. (2) and (3) at various temperatures, pressures and aerogel concentrations is in preparation.

References

[1] N. D. Mermin, Phys. Rev. B **1**, 2362 (1970)
[2] J. V. Porto and J. M. Parpia, Phys. Rev. B **59**, 14583 (1999)
[3] D. Rainer and J. A. Sauls, J. Low Temp. Phys. **110**, 525 (1998)

Shot noise and conductance fluctuations in mesoscopic metallic nanowires

A. Marx, R. Gross [9]

The electronic transport properties of metallic nanostructures cannot be decribed solely within classical models. The quantum nature of the charge carriers and the discreteness of the elementary charge lead to macroscopically observable effects. If the lateral dimensions become comparable to the phase coherence length L_φ at low temperatures quantum interference effects considerably modify the conductance G. Within the Landauer description [1] the charge transport in a mesoscopic system is described as a quantum mechanical scattering problem. The scattering properties resulting from a quantum treatment determine the interference corrections to the conductance. Important examples of interference corrections are Universal Conductance Fluctuations (UCF) [2] and the Aharonov-Bohm effect [3]. By applying a magnetic field the conductance of a phase coherent sample becomes an aperiodic function of the magnetic field with an universal fluctuation amplitude $\delta G \simeq e^2/h$ even though the background conductance varies over several orders of magnitude.

On the other hand, Larkin and Khmel'nitskiĭ predicted an increase of the amplitude of the conductance fluctuations with an increasing electrical field for samples with lengths L comparable to L_φ [4]. So far, this increase has experimentally been found only in point contact-like structures [5, 6]. We have investigated the voltage dependence of the UCF in 2000 nm long gold wires. These experiments facilitate the analysis of phase breaking scattering processes which become important at finite voltage.

The shot noise S_I provides information about the electronic system beyond the conductance G: at finite voltage S_I mediates information about correlations between the charge carriers. Furthermore, from the shot noise the electron temperature in the sample can be determined. This is very important for the investigation of the voltage dependence of the phase breaking processes.

Sample preparation and experimental techniques

The gold nanowires were fabricated using eletron beam lithography and a lift off process. The figure shows a scanning electron micrograph of a 1000 nm long and 25 nm wide Au wire. The film thickness is 25 nm the thickness of the reservoirs is 100 nm. The experimental investigation of conductance fluctuations and shot noise in low-resistance metallic samples is challenging because a high voltage resolution is needed. By integrating a highly sensitive SQUID voltage amplifier into the dilution unit a signal to noise resolution well above 50 could be reached which is an order of magnitude larger compared to conventional lock-in techniques.

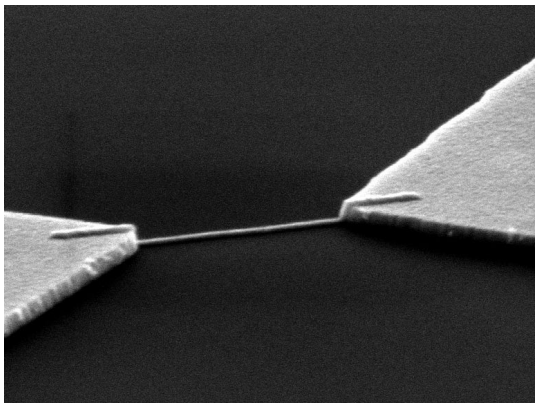

Shot noise

The spectral density of current fluctuations for a two probe geometry is given by [7]

$$S_I = 2\frac{2e^2}{h}\left[2k_BT\sum_n T_n^2 + eV\coth\left(\frac{eV}{2k_BT}\right)\sum_n T_n(1-T_n)\right]. \qquad (1)$$

The transmission coefficients T_n are evaluated at the Fermi energy E_F. For $T,V = 0$ the expression for thermal equilibrium noise is obtained from eq. (1). For small T_n the Poisson expression $S_P = 2eI$ is

[9] In collaboration with T. Bauch, T. Kemen, Universität zu Köln

obtained. The Fano factor $F = S_I/S_P$ describes the reduction of the shot noise by correlations between the charge carriers.

For diffusive metals theory predicts $F = 1/3$ and $F = \sqrt{3}/4$ for systems which are phase coherent ($L \ll l_{ee}, l_{ph}$) and for interacting systems (hot electrons), respectively [7]. To avoid excessive heating of the electronic system due to the applied voltage $V \gg k_B T/e$ the thickness of the reservoirs is 4 times the film thickness.

The knowledge of the electron temperature in the sample is crucial for interpreting the experimental current noise data. The voltage dependence of the electron temperature at the end of the wire can be approximated by [8]

$$T_{e,max}^2 = T_{ph}^2 + c\frac{R_\square}{R}V^2, \tag{2}$$

where $R_\square$ is the sheet resistance of the reservoirs, R the wire resistance, and c a constant. The phonon temperature T_{ph} can be approximated by the substrate temperature T_{sub} which can phenomenologically be described by $T_{sub} = (T_{MK}^4 + c(P_0 + P))^{1/4}$ (T_{MK} is the mixing chamber temperature, $P = V^2/R$, and c and P_0 are constants).

From eq. (2) it becomes obvious that in the non-interacting regime the current noise density strongly depends on the electronic temperature in the reservoirs (for $eV \gg k_B T$ the limit $S_I = \frac{2}{3}4k_B TG + \frac{1}{3}2eI$ is obtained). Furthermore, a large ratio $R_\square/R$ is desirable.

Figure 1 shows the dependence of the experimentally determined current noise S_I on the bias current (open symbols). In addition, the theoretically predicted $S_I(I)$ dependecies for the non-interacting regime (curves $S_{I1} + S_{I3}$) and for the interacting regime ($S_{I2} + S_{I4}$) are also plotted. The lower curves ($S_{I1} + S_{I2}$) only take an increased substrate temperature T_{sub} into account whereas the upper curves also consider electron heating according to eq. (2). It is obvious from fig. 1 that the increased noise is mainly due to heating of the electron system in the reservoirs. Unfortunately, these data are not yet eligible to validate the Fano factor $F = 1/3$ for the non-interacting regime. On the other hand, the high sensitivity of the SQUID amplifer should allow the proof of $F = 1/3$ for a *single* nanowire provided the ratio $R_\square/R$ is chosen large enough to cope with the heating problem.

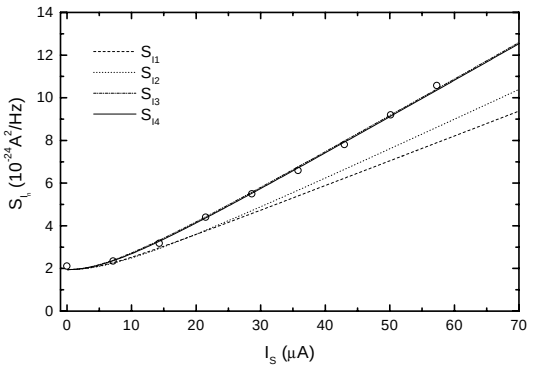

Figure 1: Current noise S_I vs current. Open symbols represent experimental data

Voltage dependence of conductance fluctuations amplitude

For independent electrons quantum interference effects in a phase coherent volume give rise to nonlinear contributions to the conductance fluctuations as has been predicted by Larkin and Khmel'nitskiĭ [4] for diffusive metallic samples with $L \gg l$, where l is the electron mean free path. For zero temperature the current voltage characteristics (CVC) is predicted to be linear if the voltage across the sample is much less than $V_c = E_c/e$. Here, $E_c = hd/L^2$ is the Thouless energy and D the diffusion constant. For $V < V_c$ only electrons with an energy inside an interval of width E_c around the Fermi energy contribute to the coherent transport that can be described by an average conductance G and an interference correction $\hat{e}/h$ through $I(V) = V[G \pm e^2/h]$. For $V > V_c$ there are V/V_c independent energy intervals each contributing average fluctuations $(e^2/h)V_c$ to the total current. Therefore, the current fluctuates on a scale $V \simeq V_c$ with an amplitude $\Delta I \simeq (e^2/h)\sqrt{VV_c}$. The fluctuations in the differential conductance

$$\delta G = \frac{\Delta I}{\Delta V} \propto \frac{e^2}{h}\sqrt{\frac{V}{V_c}}. \tag{3}$$

increase $\propto \sqrt{V/V_{Th}}$ for $eV > k_B T, E_{Th}$.

The voltage dependence of the fluctuation amplitude for two different 2000 nm long gold wires is shown in fig. 3. For both samples the voltage dependencies at low temperature ($T = 350$ mK) are rather similar. For $V > V_{Th}$ the rms amplitude of the UCF in both samples increases up to 2 mV for both low phonon temperatures ($\simeq 100$ mK) and 4.2 K. For $V > 2-3$ mV the UCF amplitude decreases. The increase of rms(G) with increasing voltage for both phonon temperatures can be explained by the contribution of $N = V/V_{Th}$ uncorrelated energy intervals to the total fluctuations of the differential conductance. This increase of the fluctuation amplitude with increasing voltage is the first experimental evidence for the theory of Larkin and Khmel'nitskiĭ in diffusive metalllic wires. The decrease for $V > 2-3$ mV is probably due to a reduction of the phase coherence length caused by phonon emission (increase of phonon density of states). The decrease of the rms amplitude for $T_{ph} = 0.35$ K for small voltages $V = 0-0.15$ mV (both samples) is not understood up to now.

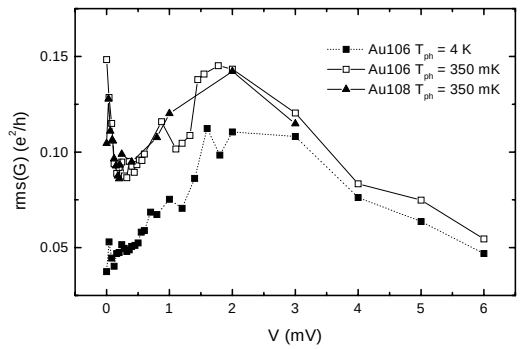

Figure 2: rms amplitude of conductance fluctuations vs voltage. Data have been obtained from magnetoconductance measurements.

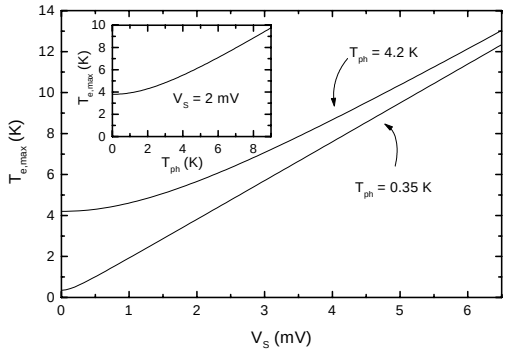

Figure 3: Electron temperature in the reservoirs $T_{e,max}$ vs voltage for $T_{ph} = 0.35$ K and $T_{ph} = 4.2$ K. The inset shows the dependence of $T_{e,max}$ on T_{ph} for $V = 2$ mV.

The approach of the curves for $T_{ph} = 0.35$ K and $T_{ph} = 4.2$ K for $V > 3$ mV in fig. 2 can be explained by heating of the electrons in the reservoirs and by heat diffusion. The electron temperature $T_{e,max}$ is shown in fig. 3 for $T_{ph} = 0.35$ K and $T = 4.2$ K. For voltages $V \geq 3$ mV the difference in the electron temperatures for $T_{ph} = 0.35$ K and $T_{ph} = 4.2$ K become small. This easily explains the convergence of the data in fig. 3.

References

[1] R. Landauer, IBM J. Res. Develop. **1**, 223 (1957).
[2] S. Washburn and R. A. Webb, Rep. Prog. Phys. **55**, 1311 (1992).
[3] S. Washburn and R. A. Webb, Adv. Phys. **35**, 375 (1986).
[4] A. I. Larkin and D. E. Khmelnitskii, Sov. Phys. JETP **64**, 1075 (1986).
[5] U. Murek, R. Schäfer, and W. Langheinrich, Phys. Rev. Lett. **70**, 841 (1993).
[6] R. Schäfer, K. Hecker, H. Hegger, and W. Langheinrich, Phys. Rev. B **53**, 15964 (1996).
[7] Y. M. Blanter and M. Büttiker, *cond-mat/9910158* (1999).
[8] T. Bauch, Ph.D. thesis, University of Cologne (2000).

Transport and Noise Characteristics of Submicron High-Temperature Superconductor Grain-Boundary Junctions

A. Marx, R. Gross [10]

Grain boundary junctions (GBJs) in high temperature superconductors (HTS) are widely used for the realization of Josephson junctions [1, 2]. Despite their simple fabrication there is up to now no consensus concerning the transport properties of GBJs [3]. The investigation of low frequency noise has turned out to be a valuable tool in clarifying the charge transport mechanism [4–11]. Numerous studies proved that the large amount of $1/f$-noise is due to a high density of charge trapping states in the grain boundary barrier. Unfortunately, there is up to now no detailed model for the microscopic nature of these traps. The analysis of the dynamics of individual charge traps provides valuable information to overcome this drawback [12, 13]. Due to the high density of traps in HTS Josephson junctions the fabrication of small area junctions is required to achieve a situation where only a single fluctuator is dominating the junction dynamics. Therefore, we have fabricated GBJs with a junction area down to $0.005\,\mu\mathrm{m}^2$ using electron beam lithography [14]. These junctions allowed for the investigation of individual fluctuators in a wide range of temperature and voltage.

Sample preparation and experimental techniques

$YBa_2Cu_3O_{7-\delta}$ thin films with a thickness of 20 to 30 nm were deposited on $SrTiO_3$ [001] bicrystal substrates using pulsed laser deposition. The as-prepared films showed a transition temperature T_c between 86 and 87 K. A 50 nm thick gold layer providing for contact pads was evaporated through a shadow mask. Bridges in a four probe geometry across the grain boundary with different widths were patterned using a multi-step optical and electron beam lithography process and ion beam etching. During the ion beam etching process the sample was cooled using LN_2 to reduce degradation of the film. In this way junctions with widths down to ~ 200 nm could be fabricated (see Fig. 1). After patterning we always observed a significant reduction of T_c and an increase of the junction resistance, which most likely is due to oxygen loss in the thin YBCO films, especially close to the grain boundary. This degradation was found to be caused by the baking of the electron beam resist (PMMA) at 160°C for 10 min and could be largely cancelled ($T_c > 81$ K) by an annealing process in 100 kPa pure oxygen for 1 h at 520°C.

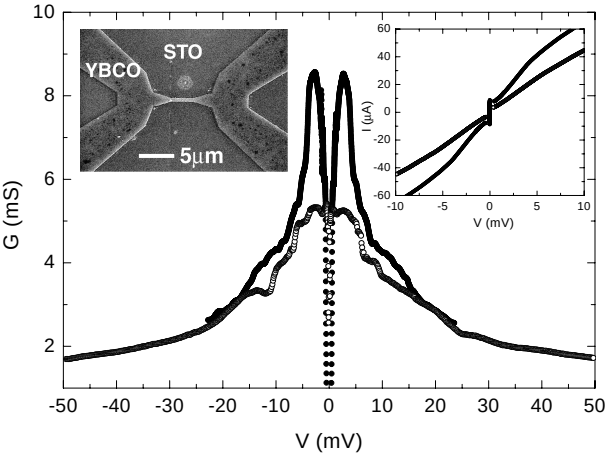

Figure 1: Differential conductance vs voltage of a $30 \times 600\,\mathrm{nm}^2$ bicrystal GBJ at $T = 6$ K. Right inset: Current-voltage curves. Left inset: scanning electron micrograph of a 600 nm wide GBJ.

Transport and noise properties

At 4.2 K junctions with widths down to 400 nm showed superconductivity with critical current densities of several $10^5\,\mathrm{A/cm}^2$. The inset of Fig. 1 shows typical current-voltage characteristics (IVCs) of a $30 \times 600\,\mathrm{nm}^2$ junction (full symbols measured immediately after preparation, open symbols after storage in vacuum for a few days). The differential conductance G is shown in Fig. 1. Both $G(V)$ curves reveal a strong increase of G with decreasing V. After the vacuum storage both I_c and G at $V \lesssim 15$ mV are noticeably reduced compared to the first run. This most likely is caused by oxygen loss close to the grain

[10] In collaboration with F. Herbstritt, T. Kemen, Universität zu Köln

boundary during vacuum storage. The increase of G below the gap voltage and the fine structure in the $G(V)$ curves can be qualitatively understood in terms of the model of Blonder, Tinkham, and Klapwijk (BTK), assuming a grain boundary barrier with high transmissivity [15–17].

The voltage fluctuations were measured with a low-T_c dc SQUID amplifier [10]. In Fig. 2 (c) and (d) two series of voltage noise spectra are shown which have been measured at 4.2 K for different junction voltages. Fig. 2 (a) and (b) display examples of time traces $\Delta V(t)$ recorded at the same temperature for $V = 2.5\,\mathrm{mV}$ clearly showing distinct random telegraph switching (RTS) signals. The two-level signals are most likely due to individual (ar a small number of strongly correlated) charge trapping centers in the barrier region randomly changing their occupation number. The most likely cause for the change in noise and transport properties is loss or redistribution of oxygen at the grain boundary

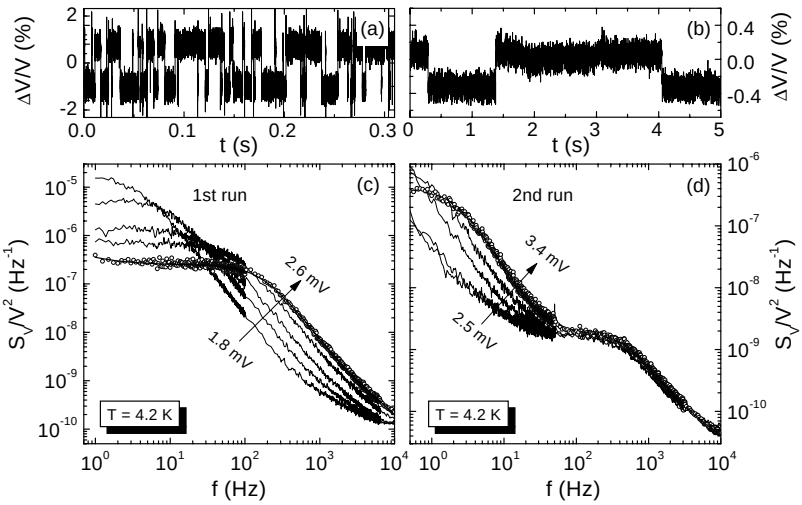

Figure 2: Voltage time traces ((a) and (b)) and noise spectra ((c) and (d)) before ((a) and (c)) and after ((b) and (d)) vacuum storage of the GBJ.

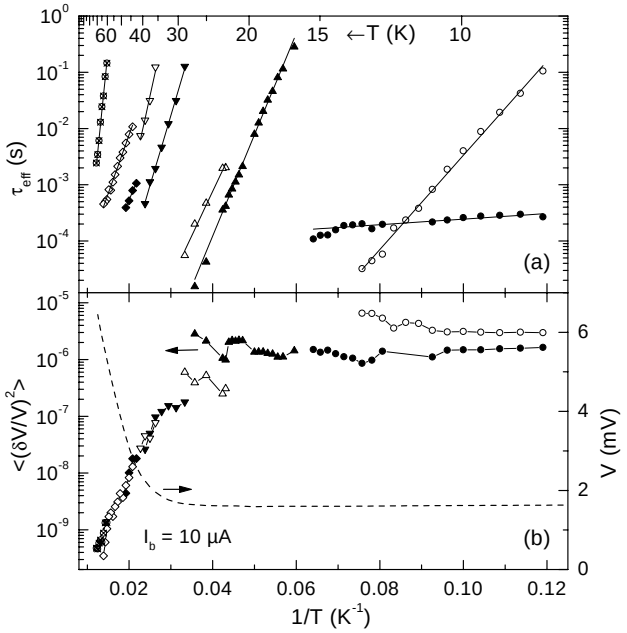

Figure 3: Effective lifetimes (a) and mean squared voltage fluctuations (b) of a series of TLFs over a broad temperature range. Identical symbols in both graphs correspond to the same fluctuator. Dashed line: junction voltage for $I_b = 10\,\mu\mathrm{A}$.

Within the accessible frequency range (0.5 to 2×10^4 Hz) all spectra could be well fitted with a superposition of a few ($n \leq 3$) independent Lorentzian components [18] together with a weak $1/f$-background. Each Lorentzian component represents the contribution of a single two-level fluctuator (TLF) with a switching amplitude ΔV_i and mean lifetimes τ_u and τ_l in the upper and lower resistance state, respectively. From the fits to the spectra we obtained the effective lifetimes $\tau_{\mathrm{eff}} = (\tau_u^{-1} + \tau_l^{-1})^{-1}$ as well as the mean squared fluctuation amplitudes $\langle(\delta V)^2\rangle$ of the underlying RTS signals.

Fig. 3 shows the temperature dependence of τ_{eff} and $\langle(\delta V/V)^2\rangle$ over a broad range of temperatures in an Arrhenius plot for a series of TLFs of a junction after the vacuum storage. All fluctuators show a thermally activated behavior in the temperature range from 8 to 80 K. The temperature dependence of $\langle(\delta V/V)^2\rangle$ as shown in Fig. 3 shows two striking features. Firstly, there is a crossover from an almost constant value below $\sim 30\,\mathrm{K}$ to an exponential decrease for $T > 30\,\mathrm{K}$. Secondly, the relative mean squared switching amplitudes $\langle(\delta V/V)^2\rangle$ of all fluctuators follow a common temperature dependence in spite of the broad scatter in the effective lifetimes without any systematic variation with temperature. This indicates that the pop-

ulation *dynamics* of a trap and its influence on the charge transport seem to be decoupled. From our measurements we conclude that the decrease of $\langle(\delta V/V)^2\rangle$ is to a large extent due to a decrease of the relative switching amplitude. It is further interesting to note that this decrease of $\langle(\delta V/V)^2\rangle$ would coincide with the decrease of the enhanced conductance in the low voltage regime which may be interpreted in a way that the noise centers in the junction mainly affect a distinct kind of conductance channels which are only active at low temperatures.

From a direct analysis of the voltage time traces the mean lifetimes τ_u and τ_l of both voltage states and the switching amplitude ΔV could be determined independently (this is not possible by analyzing the noise spectra without further assumptions. Usually, both lifetimes decrease exponentially with the applied voltage. Furthermore, the lifetimes of *both* voltage states are thermally activated with different kinetic parameters both lying in the same range found for the effective lifetimes for $T \geq 8\,\mathrm{K}$ whereas for $T \leq 8\,\mathrm{K}$ both switching times turn over to a T independent behavior indicating a tunneling-like switching in this temperature range.

In summary, the noise spectra and the voltage vs time traces were found to be dominated by random telegraph switching signals. The switching kinetics were found to be tunneling-like at $T \lesssim 8\,\mathrm{K}$ and thermally activated above this value up to T_c. At low T the mean lifetimes decrease exponentially with the junction voltage. These results confirm the assumption that the low frequency noise in high-T_c GBJs is caused by the stochastic capture and release of charge carriers at trapping centers within the barrier region. In addition, we found a similar mean squared switching amplitude for all two-level fluctuators in a sample which follows a common temperature dependence decaying exponentially above about 30 K.

References

[1] R. Gross, L. Alff, A. Beck, O. M. Froehlich, D. Koelle, and A. Marx, IEEE Trans. Appl. Supercond. **7**, 2929 (1997).
[2] D. Koelle, R. Kleiner, F. Ludwig, E. Dantsker, and J. Clarke, Rev. Mod. Phys. **71**, 631 (1999).
[3] L. Alff, S. Kleefisch, U. Schoop, M. Zittartz, T. Kemen, T. Bauch, A. Marx, and R. Gross, Eur. Phys. J. B **5**, 423 (1998).
[4] M. Kawasaki, P. Chaudhari, and A. Gupta, Phys. Rev. Lett. **68**, 1065 (1992).
[5] T. Kemen, A. Marx, L. Alff, D. Koelle, and R. Gross, Trans. Appl. Supercond. **9**, 3982 (1999).
[6] A. Marx, L. Alff, and R. Gross, Appl. Supercond. **6**, 621 (1999).
[7] A. Marx and R. Gross, Appl. Phys. Lett. **70**, 120 (1997).
[8] A. Marx, L. Alff, and R. Gross, IEEE Trans. Appl. Supercond. **7**, 2719 (1997).
[9] A. Marx, U. Fath, L. Alff, and R. Gross, Appl. Phys. Lett. **67**, 1929 (1995).
[10] A. Marx, U. Fath, W. Ludwig, R. Gross, and T. Amrein, Phys. Rev. B **51**, 6735 (1995).
[11] L. Hao, J. C. Macfarlane, and C. M. Pegrum, Supercond. Sci Technol. **9**, 678 (1996).
[12] K. S. Ralls and R. A. Buhrman, Phys. Rev. B **44**, 5800 (1991).
[13] C. T. Rogers and R. A. Buhrman, Phys. Rev. Lett. **55**, 859 (1985).
[14] F. Herbstritt, T. Kemen, L. Alff, A. Marx, and R. Gross, accepted for pubication in Appl. Phys. Lett. (2000).
[15] G. E. Blonder, M. Tinkham, and T. M. Klapwijk, Phys. Rev. B **25**, 4515 (1982).
[16] T. M. Klapwijk, G. E. Blonder, and M. Tinkham, Physica **109 & 110B**, 1657 (1982).
[17] T. Löfwander, G. Johansson, and G. Wendin, cond-mat/9908261.
[18] S. Machlup, J. Appl. Phys. **25**, 341 (1954).

Tunneling magnetoresistance in doped manganite grain boundary junctions

J. B. Philipp, L. Alff, A. Marx, R. Gross [11]

Ferromagnetic tunneling junctions have been studied intensively over the last years due to possible applications in magnetoelectronics devices. The tunneling magnetoresistance (TMR) between two ferromagnetic layers $i = 1, 2$ separated by a thin insulating barrier depends on the relative orientation of the magnetization and the spin polarization $P_i = 2a_i - 1$, where a_i is the fraction of majority spin electrons in the density of states at the Fermi level of layer i. Within the Jullière model [1], the TMR is estimated to

$$\frac{\Delta R}{R} = \frac{R_{\uparrow\downarrow} - R_{\uparrow\uparrow}}{R_{\uparrow\uparrow}} = \frac{2P_1P_2}{1 - P_1P_2}\,, \tag{1}$$

where $R_{\uparrow\uparrow}$ and $R_{\uparrow\downarrow}$ is the tunneling resistance for parallel and anti-parallel magnetization orientation. For parallel magnetization the tunneling resistance is significantly reduced, since the large density of occupied and empty states for either the majority or minority spin electrons in both junction electrodes allow for a large tunneling current. It is evident from (1) that a large TMR is obtained for high spin polarization. We note that in the Jullière model only elastic tunneling without any spin-flip processes is assumed and the junction electrodes are assumed to be single domain.

So far, most of the investigated TMR devices are based on transition metals and alloys such as Ni, Co, Fe, or $Co_{50}Fe_{50}$ with $P \leq 50\%$ limiting the available TMR effect (for recent overviews see Moodera *et al.* [2] and Parkin *et al.* [3]). In order to increase the TMT-effect a higher spin polarization close to 100% is desired. There are several candidates for materials with large P close to 100% such as the Mn-based Heusler alloys [4], the oxide ferromagnets as Fe_3O_4 or CrO_2, and the doped manganites of composition $La_xD_{1-x}MnO_3$ with D = Ca, Sr, and Ba. While for the former materials the high spin polarization is still under question [5], recently photoemission spectroscopy has provided direct evidence for the half-metallic nature of $La_{0.7}Sr_{0.3}MnO_3$ [6] with P close to 100%. Indeed, using doped manganites in ferromagnetic tunnel junctions and trilayer spin valve devices high TMR values above 450% at 4.2 K have been achieved [7, 8]. Within the Jullière model these TMR values correspond to a spin polarization above 80% [9, 10]. Recently, we have achieved a TMR effect above 1000% at 4.2 K corresponding to a spin polarization above 90% [11].

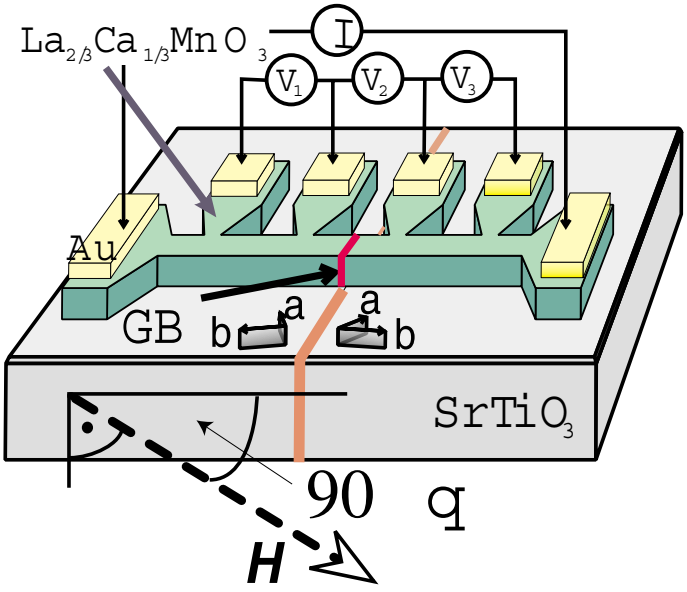

Figure 1: Sketch of the grain boundary junction geometry [19].

[11] In collaboration with S. Thienhaus and J. Klein (II. Physikalisches Institut, Universität zu Köln).

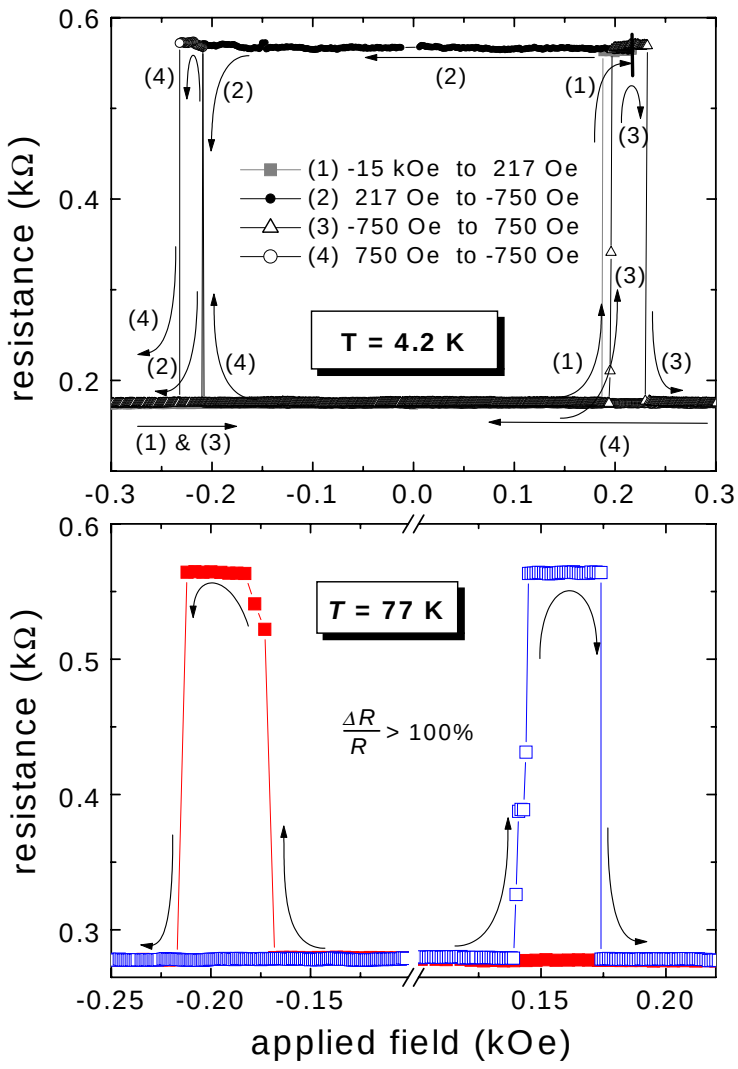

Figure 2: $R(H)$-curves of a $La_{2/3}Ca_{1/3}MnO_3$ GBJ for an angle $\theta = 0°$ between H and the GB barrier at 77 K. The direction of the field sweep is indicated by the arrows [19].

While most tunnel junctions rely on a planar structure based on multilayer thin films, one can also form ferromagnetic tunnel junctions by using well-defined individual grain boundaries (GBs) separating two ferromagnetic grains (see Fig. 1). Such grain boundary junctions (GBJs) can be achieved by growing epitaxial manganite films on a $SrTiO_3$ bicrystal substrates [12–16].

Fig. 2 shows as recent key development in the ongoing research namely the almost perfect two-level switching behavior of a manganite GBJ. Such dependence is required for magnetoelectronic memory devices [19]. The TMR effect at 77 K is still larger than 100%. At 4.2 K TMR effects above 500% have been achieved in our experiments demonstrating the high spin polarization in the doped manganites.

In our future work, we the main focus is on the fabrication of similar devices that can be operated at room temperature. For such devices materials with high Curie temperature well above room temperature and high spin polarization such as the double perovskites have to be used. With respect to the underlying physics, the spin polarized transport in such devices has to be clarified in detail. Here, in particular the effect of structural and magnetic disorder at the interfaces in magnetic tunnel junctions on the transport and noise properties has to be studied.

References

[1] M. Jullière, Phys. Lett. **A 54**, 225 (1975).

[2] J. S. Moodera and G. Mathon, J. Magn. Magn. Mater. **200**, 248 (1999).

[3] S. S. P. Parkin, K. P. Roche, M. G. Samant, P. M. Rice, R. B. Byers, R. E. Scheuerlein, E. J. O'Sullivan, S. L. Brown, J. Bucchigano, D. W. Abraham, Yu Lu, M. Rooks, P. L. Trouilloud, R. A. Wanner, and W. J. Gallagher, J. Appl. Phys. **85**, 5828 (1999).

[4] R. A. de Groot, F. M. Mueller, P. G. van Engen, and K. H. J. Buschow, Phys. Rev. Lett. **50**, 2024 (1983).

[5] K. P. Kämper, W. Schmitt, G. Güntherodt, R. J. Gambin, and R. Ruf, Phys. Rev. Lett. **59**, 2788 (1988).

[6] J.-H. Park, E. Vescovo, H.-J. Kim, C. Kwon, R. Ramesh, and T. Venkatesan, Nature **392**, 794 (1998).

[7] Yu Lu, X. W. Li, G. Q. Gong, Gang Xiao, A. Gupta, P. Lecoeur, J. Z. Sun, Y. Y. Wang, and V. P. Dravid, Phys. Rev. B **54**, R8357 (1996).

[8] J. Z. Sun, W. J. Gallagher, P. R. Duncombe, L. Krusin-Elbaum, R. A. Altman, A. Gupta, Yu Lu, G. Q. Gong, and Gang Xiao, Appl. Phys. Lett. **69**, 3266 (1996).

[9] M. Viret, M. Drouet, J. Nassar, J. P. Contour, C. Fermon, and A. Fert, Europhys. Lett. **39**, 545 (1997).
[10] Moon-Ho Jo, N. D. Mathur, N. K. Todd, M. G. Blamire, Phys. Rev **B 61**, R14905 (2000).
[11] Yafeng Lu, J. Klein, C. Höfener, B. Wiedenhorst, F. Herbstritt, L. Alff, and R. Gross, to be published.
[12] N. D. Mathur, G. Burnell, S. P. Isaac, T. J. Jackson, B.-S. Teo, J. L. MacManus-Driscoll, L. F. Cohen, J. E. Evetts, and M. G. Blamire, Nature **387**, 266 (1997).
[13] K. Steenbeck, T. Eick, K. Kirsch, K. O'Donnell, and E. Steinbeiß, Appl. Phys. Lett. **71**, 968 (1997).
[14] J. Klein, C. Höfener, S. Uhlenbruck, L. Alff, B. Büchner, and R. Gross, Europhys. Lett. **47**, 371 (1999).
[15] R. Gross, L. Alff, B. Büchner, B. H. Freitag, C. Höfener, J. Klein, Yafeng Lu, W. Mader, J. B. Philipp, M. S. R. Rao, P. Reutler, S. Ritter, S. Thienhaus, S. Uhlenbruck, B. Wiedenhorst, J. Magn. Magn. Mater. **211**, 150 (2000).
[16] C. Höfener, J. B. Philipp, J. Klein, L. Alff, A. Marx, B. Büchner, and R. Gross, Europhys. Lett. **50**, 681 (2000).
[17] B. Wiedenhorst, L. Alff, C. Recher, J. Klein, R. Gross, T. Walther, and W. Mader, subm. for publ. (2000)
[18] R. Gross, J. Klein, B. Wiedenhorst, C. Höfener, U. Schoop, J. B. Philipp, M. Schonecke, F. Herbstritt, L. Alff, Yafeng Lu, A. Marx, S. Schymon, S. Thienhaus, and W. Mader, SPIE Conf. Proc. Vol. 4058 (2000)
[19] J. B. Philipp, C. Höfener, S. Thienhaus, J. Klein, L. Alff, R. Gross, Phys. Rev. B **62**, R9248 (2000).

Heteroepitaxial growth of high-temperature superconductors and doped manganites in ramp type geometry

M. Schonecke, L. Alff, A. Marx, R. Gross [12]

The transport properties of heterostructures formed by superconductors and ferromagnets have been studied intensively in the context of spin-polarized tunneling [1]. Renewed interest in the field came along with the discovery of the cuprate high-temperature superconductors (HTS) and the colossal magnetoresistance (CMR) manganites, since their compatible crystal structures allow for the heteroepitaxial growth of multilayer structures (for a recent overview see [2]).

One important property of ferromagnet/superconductor junctions is the possible injection of spin polarized charge carriers into the superconductor causing nonequilibrium effects such as the reduction of critical temperature and critical current in the superconductor. The reason for these effects is the spin singlet state of the Cooper pairs in the HTS. It is well known that at normal metal/superconductor interfaces the process of Andreev reflection comes into play [3, 4]. Since this process can be described by a superposition of particle and hole like excitations with opposite spin directions, it is evident that the presence of spin polarization in the normal metal electrode will strongly modify the Andreev reflection. Since there is evidence that the charge carriers in doped manganites are fully spin polarized [5], doped manganites/HTS junctions are expected to be ideal candidates for the study of the effect of spin polarization on the Andreev scattering processes at superconductor/ferromagnet (S/FM) interfaces. Moreover, since the hole doped HTS have a $d_{x^2-y^2}$-wave symmetry of the superconducting order parameter with a sign change under $\pi/2$ rotation, zero-energy surface states (ZES) are formed with their spectral weight depending on the surface orientation [6–8]. These states are also called Andreev bound states because they are based on the Andreev reflection off the internal change of the order parameter. Spin polarization of the charge carriers will therefore also affect the presence of such bound surface/interface states. For a ferromagnet with 100% spin polarization, a complete suppression of the spectral weight of ZES is expected at HTS/FM interfaces [9].

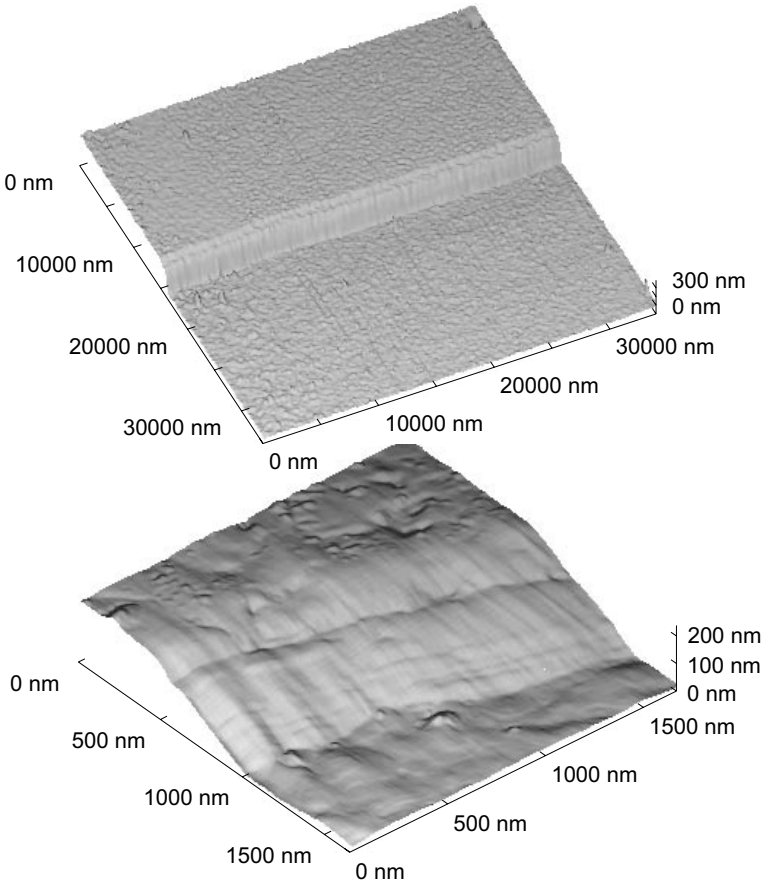

Figure 1: AFM images of a ramp surface processed with an *in situ* cleaning step at high temperatures. The parallel lines and the slight bending of the ramp structure in the lower image are due to artefacts of the measurement. [10].

[12] In collaboration with U. Schoop, S. Thienhaus, F. Herbstritt, J. Klein (II. Physikalisches Institut, Universität zu Köln).

A key technical issue with respect to manganite/cuprate heterostructures is the role of the interface between both materials. Firstly, one has to deal with *extrinsic* interfaces having properties that are strongly influenced by the fabrication process. In this context one has to keep in mind that the relevant length scales are associated to the very small superconducting and magnetic coherence lengths of the order of 1 nm. Therefore, atomic scale interface control is required. Secondly, even if the fabrication allows to obtain "perfect" interfaces, the related *intrinsic* interface properties may be significantly different from the bulk properties of the materials. Here, one has to consider the surface density of states, surface induced changes of the lattice parameters, surface induced magnetic disorder, etc. It is, for example, well known that the superconducting order parameter is strongly suppressed at surfaces of a $d_{x^2-y^2}$-superconductor. As for the doped manganites, even in the bulk there is a subtle and complex interplay between structural, spin, charge, and orbital degrees of freedom. At present, the knowledge on the surface or interface properties of the manganites is rather limited.

In our ongoing research we study different types of interfaces between doped manganites and the high-T_c cuprates, as well as between perovskite manganites with different Curie temperatures T_C. The interfaces are fabricated in ramp type geometry shown in Fig. 1.

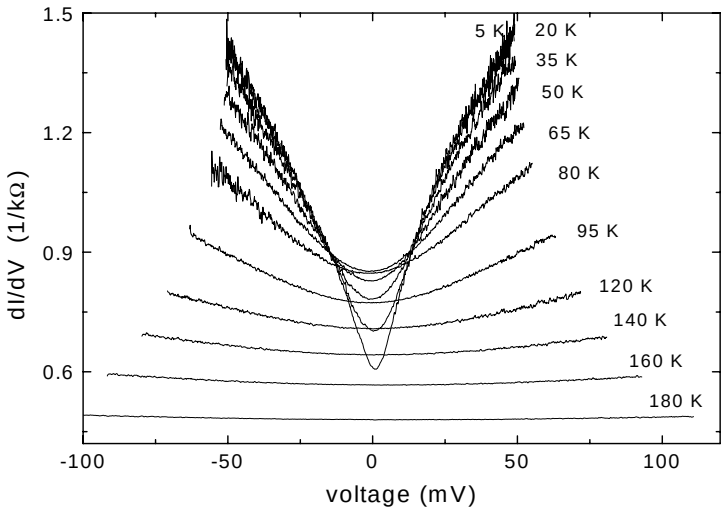

Figure 2: Differential conduction versus voltage of a low transparency $YBa_2Cu_3O_{7-\delta}/La_{2/3}Ca_{1/3}MnO_3$ junction (width: 2 μm) [10].

An important feature that has been observed in manganite/cuprate tunneling junctions is a zero bias conductance peak [11]. This can be understood in terms of Andreev bound states resulting from the $d_{x^2-y^2}$-wave symmetry of the superconducting order parameter. In [11] it is concluded from the experimental data that a 30% spin polarization is present in the $La_{2/3}Sr_{1/3}MnO_3$ electrodes. This surprisingly low spin polarization can be understood assuming strong spin-flip scattering in a low quality junction interface. The complete absence of a zero bias conductance peak in the tunneling spectra of the ramp type junctions in our studies (see Fig. 2) can have two reasons. Firstly, the junction interface is perfectly *a*- or *b*-axis oriented. For both cases no spectral weight of ZES is expected. However, due to the finite roughness of the ramp surface (see Fig. 1) a nonvanishing zero bias conductance peak is expected. Secondly, an obvious explanation is that the spin polarization of the manganite electrode is close to 100%. In the presence of a high quality interfaces with low spin-flip scattering this gives rise to a complete suppression of ZES as observed in our experiments. Moreover, spin polarized quasi-particles lead to a strongly suppressed peak in the density of states at the gap edge [9] in agreement with our data. The goal of our present work is to further clarify the correlation between interface properties and the transport behavior with well defined interfaces in both the tunneling and high transparency limit.

References

[1] R. Meservey and P. M. Tedrow, Phys. Rep. **238**, 173 (1994).
[2] A. M. Goldman, V. Vas'ko, P. Kraus, K. Nikolaev, and V. A. Larkin, J. Magn. Magn. Mater. **200**, 69 (1999).
[3] A. F. Andreev, Zh. Eksp. Teor. Fiz. **46**, 1823 (1964) [Sov. Phys. JETP **19**, 1228 (1964)].
[4] M. J. M. de Jong and C. W. J. Beenakker, Phys. Rev. Lett. **74**, 1657 (1995).

[5] J.-H. Park, E. Vescovo, H.-J. Kim, C. Kwon, R. Ramesh, T. Venkatesan, Nature **392**, 794 (1998).
[6] C. R. Hu, Phys. Rev. Lett. **72**, 1526 (1994); C. Yang and C. R. Hu, Phys. Rev. B **50**, 16766 (1994).
[7] Y. Tanaka and S. Kashiwaya, Phys. Rev. Lett. **74**, 3451 (1995); S. Kashiwaya, Y. Tanaka, M. Koyanagi, H. Takashima, and K. Kajimura, Phys. Rev. B **51**, 1350 (1995).
[8] L. Alff, H. Takashima, S. Kashiwaya, N. Terada, H. Ihara, Y. Tanaka, M. Koyanagi, and K. Kajimura, Phys. Rev. B **55**, R14757 (1997).
[9] S. Kashiwaya, Y. Tanaka, N. Yoshida, and M. R. Beasley, Phys. Rev. B **60**, 3572 (1999); I. Žutić and O. T. Valls, Phys. Rev. B **60**, 6320 (1999).
[10] U. Schoop, M. Schonecke, S. Thienhaus, S. Schymon, L. Alff, R. Gross, Physica C (in print); U. Schoop, M. Schonecke, S. Thienhaus, F. Herbstritt, J. Klein, L. Alff, R. Gross, Physica C (in print).
[11] A. Sawa, S. Kashiwaya, H. Obara, H. Yamasaki, M. Koyanagi, N. Yoshida, Y. Tanaka, cond-mat/9908431.

^{3}He/^{4}He dilution refrigerator with pulse tube refrigerator

K. Uhlig

In January the pulse tube refrigerator (PTR) described in last year's annual report was delivered to the WMI (Cryomech Co., N.Y.). It will be used to precool a new ^{3}He/^{4}He dilution refrigerator, and will replace the Gifford-McMahon cooler (GM) used so far. PTRs are closed-cycle-refrigerators for laboratory use which continuously reach temperatures below 4 Kelvin. For our application it is most significant that PTRs do not contain a cyclically moving piston like GM coolers, and so the vibrational amplitudes of PTRs are considerably smaller and their running quieter; consequently, the vibrational heat leak in the dilution unit is expected to be reduced in a DR precooled by a PTR, and the performance of the DR improved.

We measured the cooling power of the two stages of the PTR, and the specifications of the manufacturer were verified. In addition, the vibration spectrum of the PTR was recorded with an accelerometer. Then, based on the work with our GM-precooled DR, a new cryostat was designed which combines the PTR with one of our existing dilution units.

In the meantime, this cryostat has been completed in the machine shop of the WMI, and testing of the cryostat has begun.

^{3}He/^{4}He dilution refrigerator with Gifford-McMahon cooling

Experiments with our existing dilution refrigerator concentrated on a long-standing problem, the measurement of the heat leak into the mixing chamber caused by the vibrations of the GM cooler. Measuring its value is important as it influences the final temperature of the DR, and gives information about the efficiency of the attenuation of the GM cooler and about vibrational heat leaks which experiments cooled by the DR would be exposed to.

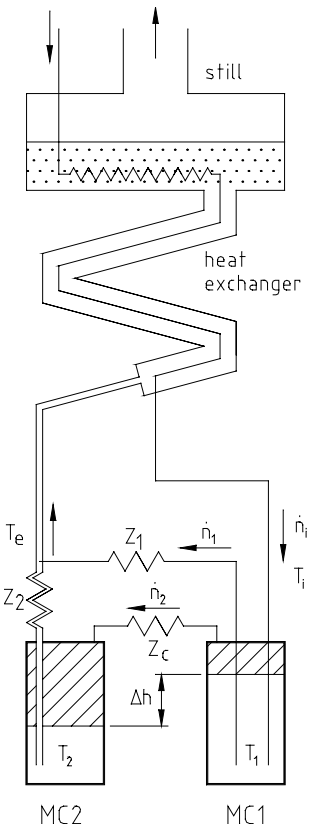

Because the dependence of the cooling power of DRs on temperature is quadratic in first order approximation, a small heat leak can be best determined with mixing chamber temperatures as low as possible. Additionally, the ^{4}He portion of the throughput should be small in order to exclude possible contributions of the ^{4}He to the heat leak (Niinikoski, 1978). An almost forgotten method, the so-called double-mixing-chamber (DMC; de Waele, 1976) should meet these requirements, and was (probably for the first time) utilized for determining the heat leak.

As depicted in the figure, liquid ^{3}He with temperature T_i runs from the concentrated side of the heat exchanger to the first mixing chamber MC1. One part, about half, of the ^{3}He stream is diluted in MC1, produces cooling, and flows through connecting tube z_1 to the return line of the heat exchanger. The remaining non-diluted part of the circulating ^{3}He is cooled very efficiently in MC1 to its temperature T_1 (no Kapitza-resistance), then flows through line z_c into the second mixing chamber, where it is also diluted and produces further cooling. Finally, the diluted ^{3}He flows through z_2 to the return side of the heat exchanger where it rejoins the dilute ^{3}He stream coming from MC1. Altogether, by using a DMC a temperature reduction of a factor of two can be gained in comparison with a single mixing chamber.

Dividing the original ^{3}He flow into two flows through MC1 and MC2 is achieved by choosing the right flow resistances of the connection lines z_1, z_2, and z_c; additionally, with different temperatures in MC1

and MC2, different osmotic pressures are connected, which give cause to different heights of the phase boundaries in MC1 and MC2 (see graph). Thus, not only the size of z_1, z_2, and z_c, but also the amount of ^{3}He/^{4}He used in the DR is critical. It is important that, caused by gravity, the ^{3}He leaving MC1 through z_c is purified of ^{4}He, and so the cooling power of MC2 should not be affected by ^{4}He contaminations.

The cooling power of a DR is derived from the enthalpy balance of the mixing chamber. For the second mixing chamber of a DMC we find

$$Q = Q_{hl} + Q_{ext} \quad = \quad 12 \cdot n_2 * t^*, \text{ with } t^* = 8 \cdot T_2^2 - T_1^2$$

with Q: cooling power; Q_{hl}: heat leak; Q_{ext}: applied heating; n_2: ^{3}He flow through MC2; $T_{1,2}$: temperatures of MC1 and MC2.

From a plot of Q_{ext} over t^* the heat leak Q_{hl} is found as the offset of a linear fit curve at $t^* = 0$. In the case of a GM precooled DR Q_{hl} is dominated by far by the vibrational heat leak. A value of 2 erg/sec of the heat leak can be taken from the figure, and from the slope of the fits the throughput n_2 can be calculated for each fit; values for n_2 were between 30 μmol/sec and 90 μmol/sec. It has to be pointed out that reliable thermometry is decisive for the experiment; T_2 was measured with a ^{3}He melting curve thermometer, and T_1 with two thick film resistors which were calibrated with the melting curve thermometer, before. Using the heat leak of 0.2 μWatt and a measured final temperature of T_2 = 7.2 mK we can calculate a final temperature without heat leak of $T_2 = 3.9$ mK.

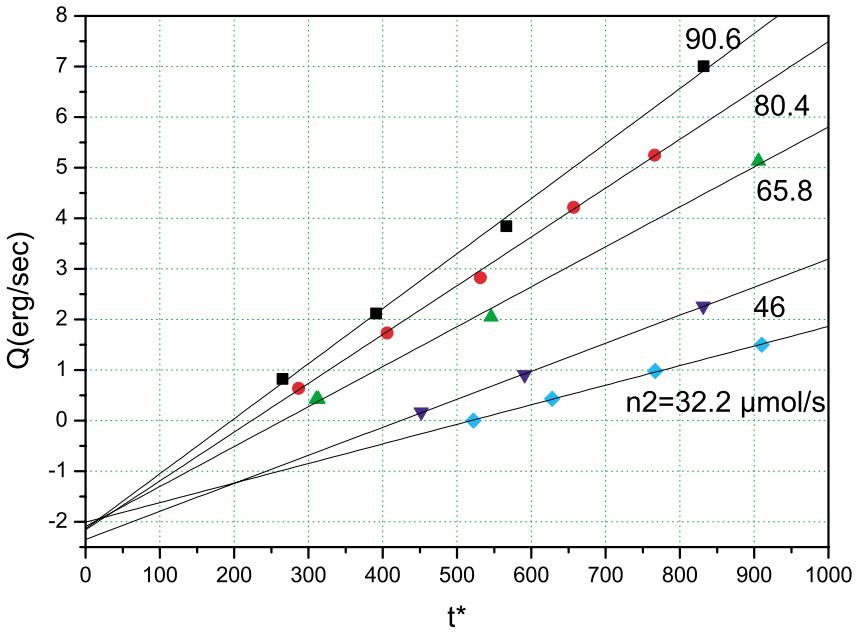

Our dilution unit with DMC is compatible with our new DR which is precooled by a pulsed-tube-refrigerator (described at the beginning of this report), and we aim to determine the reduced heat leak in the new apparatus with the highly sensitive DMC-method.

Epitaxial thin films of ordered double perovskite materials with magnetoresistance at room temperature

D. Reisinger, J. B. Philipp, L. Alff, A. Erb, A. Marx, R. Gross [13]

The material Sr_2FeMoO_6 [1] belongs to the group of the so-called 2116-double-perovskites [2], which includes a variety of interesting new materials. Among these materials there are some with high magnetic ordering temperature T_C. Furthermore, the phenomena of superconductivity, ferro(i)magnetism and colossal-magnetoresistance can be observed in this material class. The high Curie-temperature T_C and the high spin polarisation P make the double-perovskites attractive as the base material for magnetic sensors and for spin-electronic applications as for example MRAMs (magnetic random access memory). For example, for Sr_2FeMoO_6 a high Curie temperature of $T_C \simeq 420$ K was found and a high spin polarisation close to 100% is expected from theoretical calculations.

We have prepared epitaxial thin films of Sr_2FeMoO_6 on different substrate materials by pulsed laser deposition (PLD). The optimal growth parameters for this material still have to be found [3–6]. So far, three different growth-phases have been detected. Below a substrate temperature of 320°C, the films display a yellow colour and are insulating. Using higher substrate temperatures of up to 920°C, the films become semiconducting, and above 920°C they show a metallic behaviour. The film quality was investigated by X-ray analysis and by atomic force microscopy (AFM). The semiconducting films have a rocking curve with a narrow full width at half maximum (FWHM) of only about 0.04°. This shows the high epitaxial quality of the thin films. Moreover, AFM pictures show a smooth surface for these films. In contrast, the metallic films have a much wider rocking curve with a FWHM of about 0.20°. However, the detailed X-ray analysis usind a four-circle diffractometer shows a perfect ordering of the Fe-Mo sublattice for the metallic films. This is not the case for the semiconducting films. One can therefore conclude that the ordering of the Fe-Mo sublattice strongly influences the electrical transport properties. Test structures for measuring the electric transport properties have been patterned into the films using optical lithography and Ar ion beam etching. The magnetotransport properties have been measured in a standard cryostat between 4 and 500 K in applied magnetic fields up to 16 T.

Recently, we have applied in-situ reflection high energy electron diffraction (RHEED) to monitor the growth of the epitaxial thin films. Furthermore, the surfaces properties of the films can be studied by AFM without breaking the vacuum. We found that oxygen pressure, substrate temperature, the composition of the process gas, the details of the oxygenation process, the laser energy and pulse repetition rate are crucial parameters in the deposition process. In Fig. 1 the resistance vs. temperature behavior of several epitaxial Sr_2FeMoO_6 thin films is shown. The thickness of the films is 100 nm. These films have been fabricated by PLD using different process gases. The important result of our study is that the use of a reducing atmosphere containing H_2 allows the fabrication of thin films with metallic resistance vs. temperature curves at moderate substrate temperatures.

An important future task is the fabrication of tunnel junctions with electrodes of the double-perovskite materials. In a first attempt epitaxial Sr_2FeMoO_6 films will be grown on bicrystal substrates to introduce a well defined grain boundary that is expected to act as a tunneling barrier. These grain boundary junctions have to be compared to planar trilayer junctions employing an artificial tunneling barrier. Using such tunneling devices the spin polarization of the double perovskites can be determined experimentally and compared to the theoretically expected values.

The successful fabrication of room temperature magnetoresistive devices based on oxide materials such as the double-perovskites may have considerable impact on the field of spin-electronics in particular and for the so-called "oxide electronics" in general.

[13] In collaboration with F. Herbstritt, J. Klein (II. Physikalisches Institut, Universität zu Köln).

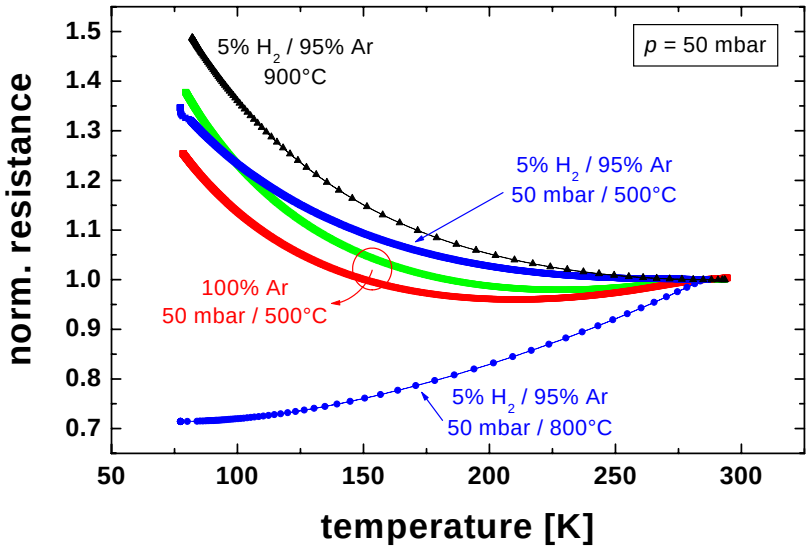

Figure 1: Normalized resistance vs. temperature for epitaxial Sr_2FeMoO_6 thin films as a function of the composition of the process gas.

References

[1] K.-I. Kobayashi, T. Kimura, H. Sawada, K. Terakura, and Y. Tokura, Nature **395**, 677 (1998).
[2] M. T. Anderson, K. B. Greenwood, G. A. Taylor, and K. R. Poeppelmeier, Prog. Solid State Chem. **22**, 197 (1993).
[3] T. Manako, M. Izumi, Y. Konishi, K.-I. Konishi, M. Kawasaki, and Y. Tokura, Appl. Phys. Lett. **74**, 2215 (1999).
[4] H. Asano, S. B. Ogale, J. Garrison, A. Orozco, Y. H. Li, E. Li, V. Smolyaninova, C. Galley, M. Downes, M. Rajeswari, R. Ramesh, and T. Venkatesan, Appl. Phys. Lett. **74**, 3696 (1999).
[5] H. Q. Yin, J.-S. Zhou, J.-P. Zhou, R. Dass, J. T. McDevitt, and J. B. Goodenough, Appl. Phys. Lett. **75**, 2812 (1999).
[6] W. Westerburg, D. Reisinger, and G. Jakob, Phys. Rev. B **62**, R767 (2000).

Crystal growth and bulk materials of transition metal oxides

Andreas Erb

One of the new research projects, which will be established at the Walther-Meissner-Insititute (WMI) is a lab dedicated to the preparation of bulk materials and crystal growth of transition metal oxides. For this purpose the rooms of the old carpentry has been completely liberated and transformed into lab for crystal growth. This required not only a complete renovation of the former carpentry, but also the planning and installation of the electrical power supply for a total maximum consumption of up to 100 KW electrical power for the furnaces and devices, the planning for a effective cooling system and a secure gas system for process gases (mainly Argon, Oxygen, N_2/Ar).
The goal is to be able to grow single crystals of the high temperature superconductors (HTSC), compounds showing collosal magneto resistance (CMR) and of other oxides of the transition metals.

This requires the development of adapted crystal growth methods for the different compounds: Czochralski growth, growth by zone melting, crystal growth from high temperature solutions, high pressure synthesis and containerfree crystal growth techniques.

Successful crystal growth experiments require the exact knowledge of the corresponding phase diagrams. Thus, it is planned to investigate the phase relationships and phase formation by means of differential thermal analysis, thermogravimetry and by x-ray phase analysis using a high temperature powder diffractometer. All these methods can be used in different atmospheres (vacuum, reducing and oxidising atmospheres)

The physical properties as well as the phase formation and phase stability of the compounds under study depend strongly on the oxygen content of the atmosphere during synthesis. For this reason equipment has been constructed to cover the whole range of oxygen partial pressures from high vacuum or even reducing atmospheres to up to 1kbar of pure oxygen atmosphere in temperatures up to 1800°C.
The absolute oxygen content of the produced samples can be determined by thermogravimetry in reducing atmospheres. Furthermore the oxygen diffusion coefficients can be determined both by thermogravimetry and by in situ resistivity measurements during the oxygenation / reduction of the samples.

Besides the more conventional x-ray characterization techniques for single crystals studies of magnetic flux pinning offer an excellent method to probe the samples for microstructural inhomogeinities on the nanometer scale in the case of high temperature superconductors. The understanding of the formation mechanism of such microstructural inhomogeinities is especially important for technical applications of these compounds and gives rise to tailored samples for both application and fundamental research.

Already installed and operational equipment:

- 2 chamber furnaces: $T_{max} = 1400^{\circ}C$
- 2 tube furnaces: $T_{max} = 1400^{\circ}C$,
  atmospheres: Vacuum, Ar, O_2 , Ar/H_2
- chamber furnace: $T_{max} = 1800^{\circ}C$
- simultaneous thermal analysis (DTA/TG) $T_{max} = 1600^{\circ}C$,
  atmospheres :Vacuum, Ar, O_2 ,Ar/H_2
- planetary ball mill for ultra fine milling
- laser granulometer for grain size measurements down to 0.1 μm
- cold isostatic press up to 4 kbar

Mössbauer Spectroscopic Investigation of Redox Reactions in Vermiculites from Santa Olalla (Huelva, Spain)

A. Lerf [14]

Natural clay minerals of the 2:1 type very often contain Fe ions in the octahedral and/or tetrahedral layers. It has been known for fifty years that at least the octahedral iron ions are easily accessible to redox reactions; a striking example for this are the colour reactions of some amines intercalated into smectites. Oxidation of the octahedral structural iron ions has also been considered as an important step in the weathering of micas to vermiculite. To evaluate the extent of redox reactions one needs to know the Fe^{2+}/Fe^{3+} ratio before and after the reaction. However, it is notoriously difficult to determine this ratio in natural and modified clay minerals by wet chemical methods. The most suitable method to derive reliable Fe^{2+}/Fe^{3+} ratios is Mössbauer spectroscopy.

We report here the Mössbauer parameters measured mainly at room temperature for the vermiculite of Santa Olalla, Huelva, Spain, before and after chemical modification. The emphasis is mainly on the determination of the Fe^{2+}/Fe^{3+} ratio. We investigated the oxidation by hydrogen peroxide and the reduction by sodium dithionite and hydrazine. In addition we applied p-phenylenediamine as a reducing agent which changes its color in the course of redox reactions.

Typical Mössbauer spectra of the starting material and a reduced sample are shown in Figures 1-2. With the exception of the fully oxidized sample, the spectra can be interpreted by a superposition of three quadrupole doublets and a broad background arising from slow relaxation of paramagnetic Fe^{3+}. One of these is attributable to Fe^{3+}, the other two to Fe^{2+}, all of them in octahedral positions. In agreement with the chemical formula we could not identify Fe^{3+} in tetrahedral sites. The data resulting from the least squares fits for the hydrazine and PDA treated samples are given in the Table.

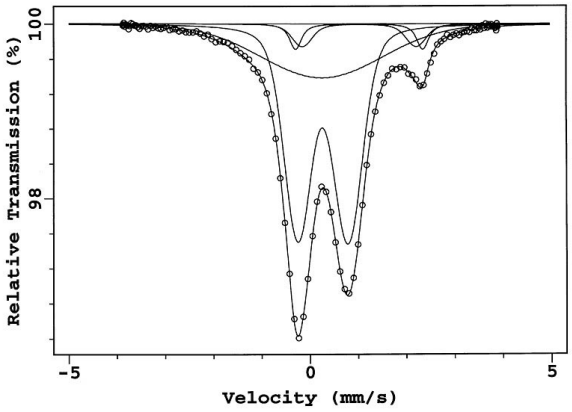

Figure 1: Mössbauer spectrum of the sodium form of the vermiculite from Santa Olalla.

The isomer shift (IS) and the quadrupole splitting (QS) of all iron sites in the samples under investigation vary only in small ranges of values: IS of Fe^{3+} 0.26-0.27 mm/s, IS of Fe^{2+} 1.00-1.04 mm/s ; QS of Fe^{3+} 0.89-1.05 mm/s, QS of Fe^{2+} 2.50-2.64 mm/s and 2.16-2.41 mm/s, respectively. These values are in excellent agreement with the parameters found previously for di- and trioctahedral micas and vermiculites. It should be noted that the quadrupole splitting of the Fe^{3+} site is exceptionally high for trioctahedral 2:1 clay minerals, but it decreases with the extent of reduction. For the hydrazine compounds with the highest degree of reduction the QS shows the lowest value observed in our experiments of about 0.89 mm/s.

Since there is no agreement in the assignment of these different iron positions to the structural features of the octahedral layers we restrict the further discussion to the Fe^{2+}/Fe^{3+} ratio, the parameter which shows the largest variations due to the chemical modifications we have carried out. To evaluate this parameter properly, one should have in mind the following two points. First, the distribution of the hyperfine parameters on the two Fe^{2+} sites should be considered with caution because the fitted values of the areas of the components and of the quadrupole splitting are strongly correlated. The total amount of Fe^{2+},

[14] In collaboration with F. E. Wagner, Physik-Department, TU-München, J. Poyato, Universität Sevilla

however, is not affected by this ambiguity of the data analysis. Secondly, in all spectra one observes a broad unresolved component that is assumed to result mainly from slow paramagnetic relaxation of Fe^{3+}. In the 4.2 K spectra the relaxing part is strongly enhanced and in addition a sextet appears for the starting material as well as for the reduced samples. It cannot be ruled out that part of the Fe^{2+} also undergoes a magnetic splitting at low temperatures. Therefore the accuracy in determination of the amount of Fe^{2+} sites cannot be improved by 4.2 K data. In addition, the amount of the relaxation background (difference of the sum of the relative areas of the resolved components to 100%, see table) depends on the velocity range in which the spectrum has been recorded. Therefore, the fractional areas for the background resulting from the data in the table are lower limits. These uncertainties in the determination of the slowly relaxing background do not affect the values of the Fe^{2+}/Fe^{3+} ratios deduced from the relative areas of the resolved Fe^{2+} and the Fe^{3+} quadrupole doublets. Therefore we can use this ratio as a measure of the changes due to the chemical manipulations carried out.

Applying the recipes used in previous studies of the redox reactions, we do not get any substantial changes in the Fe^{2+}/Fe^{3+} ratio with respect to the starting material. Major changes are achieved only if the concentration of the reagents is increased (H_2O_2), the reaction times extended (H_2O_2, dithionite) and/or the reaction solutions changed several times (dithionite). We ascribe such differences in behaviour to the particle size used in our experiment and conclude that these reagents react mainly at the outer surface of the crystals.

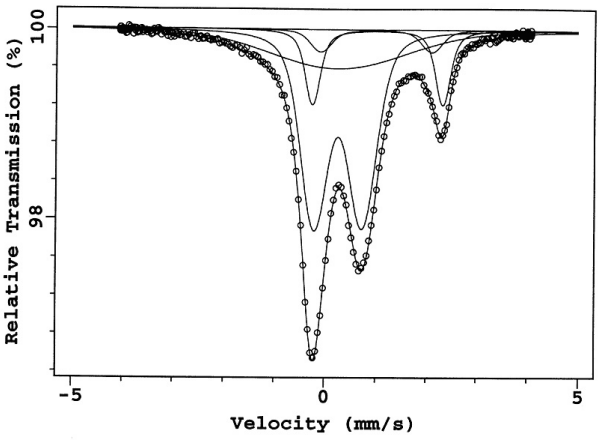

Figure 2: Mössbauer spectrum of the Na-vermiculite intercalated with PDA.

To check this hypothesis, the vermiculite has also been treated with reagents which can be inserted in the interlayer space by ion exchange. As reagents of this kind we chose hydrazine, which has also been used previously, and PDA. Carrying out the reduction with the latter reagent in solutions with pH 6-7 leads to an immediate reduction and color reaction indicating that the intercalation of the reducing agents shortens the reaction time dramatically. However, to get the maximum possible degree of reduction, the reaction conditions have to be optimized and we are not certain that we already have found the optimum conditions. The extent of reduction is influenced by the reaction times (we used 7 days for hydrazine) and by a repeated change of the reaction solutions (PDA). In addition there is some evidence that the degree of reduction is slightly higher for wet samples and that it depends also on the storage time of the dried samples.

One of the major factors determining the degree of reduction is the pH of the reaction solution. In the case of hydrazine, the extent of reduction is highest for pH 6.7 ($[\Sigma A(Fe^{2+}) = 24.8$ %), while there is nearly no reduction at pH 13. For PDA the extent of reduction also increases from pH 2 to pH 6.5. There is only a small degree of reduction in an aqueous PDA solution with pH = 8.5. One should note that the extent of reduction is not much lower than in the case of hydrazine despite the short reaction time chosen to avoid side reactions. These short reaction times may be responsible for the low uptake of PDA as shown by the chemical analysis. Applying more highly concentrated PDA solutions also seems to prevent reduction. Under such conditions the clay became deeply colored immediately. It is not clear at the moment whether the color is due to the intercalated radical ions or due to polymerized byproducts on the clay surface. It is worth mentioning that the addition of methanol to the aqueous PDA solutions increases the degree of reduction as well as the amount of PDA taken up. This may be correlated with the stabilizing effect of methanol on the PDA radical cation.

The low level of reduction by hydrazine and PDA at high pH may be caused by the following effects.

Table 2: Isomer shift (IS [mm/s], given versus the ^{57}Co:Rh source), quadrupole splitting (QS [mm/s]), and relative area (A [%]) of the different iron sites in the vermiculite from Santa Olalla after reduction with hydrazine and phenylenediamine under different reaction conditions. The relative areas do not add up to 100 %, the missing area being that of the broad background due to slow relaxation. The corresponding data of the starting material are also included for comparison.

Treatment	Fe^{3+}			Fe^{2+}						Comments
				1. site			2. site			
	IS	QS	A	IS	QS	A	IS	QS	A	
Santa Olalla, untreated	0.27	1.04	59.5	1.02	2.64	3.2	1.02	2.41	5.5	powder
	0.24	1.07	34.6	1.02	2.74	4.8	[§]-	[§]-	[§]-	at 4.2 K
	0.26	1.03	66.3	1.02	2.58	4.2	1.02	2.24	3.8	platelets
	0.26	1.02	62.8	1.02	2.54	2.9	1.02	2.37	5.0	platelets
24-26% N_2H_4 in H_2O/H_2O 1:1; pH11.1; 4h; 0.25/10	0.26	0.96	59.4	1.03	2.59	8.2	1.00	2.28	6.0	
0.15 N_2H_4-H_2SO_4; pH4; 7d; 0.25/100	0.26	0.96	58.2	1.03	2.59	17.7	1.00	2.16	5.8	
0.15 N_2H_4-H_2SO_4; pH6.7; 7d; 0.25/100	0.26	0.89	56.5	1.02	2.59	16.1	1.00	2.21	8.7	
0.15 N_2H_4-H_2SO_4; pH13; 7d; 0.25/100	0.27	1.05	62.8	1.03	2.64	3.6	1.00	2.39	6.8	
0.175 PDA; pH6.2; 2h; 0.5/25	0.26	0.93	62.7	1.01	2.50	13.6	[§]-	[§]-	[§]-	
as above, but measured at 4.2 K	0.19	1.05	31.7	1.16	2.47	5.8	[§]-	[§]-	[§]-	
0.175 PDA; pH4; 2h; 0.5/25	0.26	0.94	59.7	1.03	2.60	7.0	1.00	1.00	8.0	
0.1 PDA; pH6.5; 4h; 0.5/100	0.27	0.94	58.0	1.02	2.59	12.0	1.00	1.00	5.3	
as above; but 1+1+2h	0.26	0.95	57.8	1.03	2.57	12.8	1.00	1.00	5.3	
0.01 PDA; pH2; 4h; 0.25/100	0.26	0.94	68	1.03	2.60	5.9	1.00	1.00	9.9	
0.01 PDA; pH8.5; 24h; 0.25/100	0.26	0.98	62.8	1.03	2.60	5.9	1.00	1.00	7.9	
0.01 PDA pH2/MeOH (70/30); 0.25/100; 4h	0.26	0.94	65	1.04	2.59	6.2	1.00	1.00	10.1	
0.01 PDA; pH6; 24h; 0.25/100 + 0.01 PDA in MeOH(100ml); 22h	0.26	0.97	60.8	1.03	2.61	9.4	1.00	1.00	9.2	

0.15 N_2H_4 means that the solution used for sample treatment is 0.15 M in N_2H_4-H_2SO_4; 0.25/100 means 0.25 g of clay in 100 ml solution; 0.175 PDA means that the solution used for sample treatment is 0.175 M p-phenylenediamine (PDA); 0.5/25 means 0.5 g of clay in 25ml solution.

[§] the second Fe^{2+} cannot be resolved; the 1. Site therefore represents the total area of the Fe^{2+} quadrupole component.

First, only a part of the amine present is protonated, preventing the ion exchange and, hence, the uptake into the interlayer space. However, one would expect that reduction occurs at least on the outer crystal surfaces as is the case for dithionite reduction in particular, since the reducing power of hydrazine is comparable to that of dithionite. Thus, the following explanation could be of some importance: It is known that the oxidation of Fe^{2+} in trioctahedral micas is accompanied by proton loss from the structural OH groups to maintain the local charge neutrality. The low H^+ concentration at high pH could prevent the reverse process of Fe^{3+} reduction. The lower degree of reduction at low pH values is less clear. IR spectroscopic investigations of structural OH groups, which are presently underway, may help to elucidate effects of the redox reactions on the octahedral layers.

Electrochemical Intercalation of Alkylammonium Ions into the Isostructural Layered Dichalcogenides 2H-NbS_2 and 2H-TaS_2

A. Lerf [15]

It is clearly established that the intercalation of metal ions in the layered dichalcogenides is accompanied with a redox reaction of the solid, leading to negatively charged host lattice layers, and cations inserted in the interlayer galleries to compensate the negative charges [1]. However, the chemical mechanism of the molecular intercalation compounds is still a matter of debate. It seems to be established that the intercalation of ammonia and pyridine is also accompanied with a redox reaction and a simultaneous oxidative alteration of the nitrogen containing compounds. The resulting compounds are then also polyelectrolytes and described as $(MH^+)_xM_y[TaS_2]^{x-}$ (M = NH_3, pyridine) [2,3].

One should expect that N-containing Lewis bases forming stable protonated cations in aqueous solutions can be intercalated into the layered dichalcogenides by the same methods as the hydrated metal cations, for example by electrointercalation. Whereas the thermal intercalation of ammonia and alkylamines is documented well in literature [4-6], the uptake of alkylammonium ions is studied only sparely. These studies concentrate on the intercalation of tetraalkylammonium (alkyl = methyl to butyl) ions from the hydroxide solutions [7,8]. Only in one case the electrointercalation of tetrabutylammonium ions has been described [9].

We have performed for the first time a comparative study of the electrointercalation (galvanostatic conditions) of the series of methyl substituted ammonium ions $[H_{4-z}N(CH_3)_z]^+$ (with z = 0-4) into the isostructural dichalcogenides 2H-NbS_2 and 2H-TaS_2. The electrointercalation has been carried out in deaerated aqueous electrolytes. For the experiments with NbS_2 powder samples have been used (for $[H_3N(CH_3)]^+$ intercalation single crystals also), whereas in the case of TaS_2 single crystals has been intercalated exclusively. Using single crystals in the latter case allowed the continuous in-situ monitoring of the crystal expansion during the electrochemical intercalation process with a dilatometer. It is essential to control the current density used for intercalation to get reproducible results. In the case of TaS_2 the optimum value is about $2 \cdot 10^3$ μA/cm^2 for NH_4^+ and $2-6 \cdot 10^2$ μA/cm^2 for the alkyl substituted systems. For all compounds investigated the layer distance in the first stage phase has been determined. The extent of intercalation determined via Faraday's law has been proved by chemical analysis. In case of the Nb-compounds cyclovoltametric intercalation experiments and TG-DTA measurements have been made in addition.

The potential vs. charge transfer n curves obtained under galvanostatic conditions are shown in fig. 1. In all systems investigated the intercalation starts with at least one two-phase region, followed by a single phase region which can be assigned to a first stage compound. The two phase region varies dramatically with the type of alkylammonium ions, the host lattice and the current density used for intercalation. In case of $[H_{4-z}N(CH_3)_z]_xTaS_2$ we observed two two-phase regions: $0 < x < x_{onset}/2$, and $x_{onset}/2 < x < x_{onset}$ (with x_{onset} the lower limit of the concentration range of the first stage range). The crystal expansion is finished at x_{onset}, indicating that the intercalation proceeds near to equilibrium and that the diffusion within the opened interlayer spaces is fast with respect to the process of opening a new interlayer space. The intermediate state at $x_{onset}/2$ is a strongly disordered second stage phase. In the intercalation of $[H_3N(CH_3)]^+$ into NbS_2 system three two-phase regions has been observed: $0 < x < x_{onset}/3$, $x_{onset}/3 < x < x_{onset}/2$, and $x_{onset}/2 < x < x_{onset}$. The in-situ x-ray analysis shows that the intercalation starts also as a random opening of the interlayer galleries, but ends up in a more ordered sequence of staging ($NbS_2 \Rightarrow 3^{rd}$ stage $\Rightarrow 2^{nd}$ stage $\Rightarrow 1^{st}$ stage) than in the corresponding TaS_2 compound. With increasing number of methyl groups the intercalation process is getting more difficult, the clear features of staging disappeared and ends up in a single two-phase region.

[15] In collaboration with C. Ramos, Europäisches Patentamt, München, G. Badr, R. Schöllhorn, formerly: Institut für Anorg. und Anal. Chemie der TU Berlin

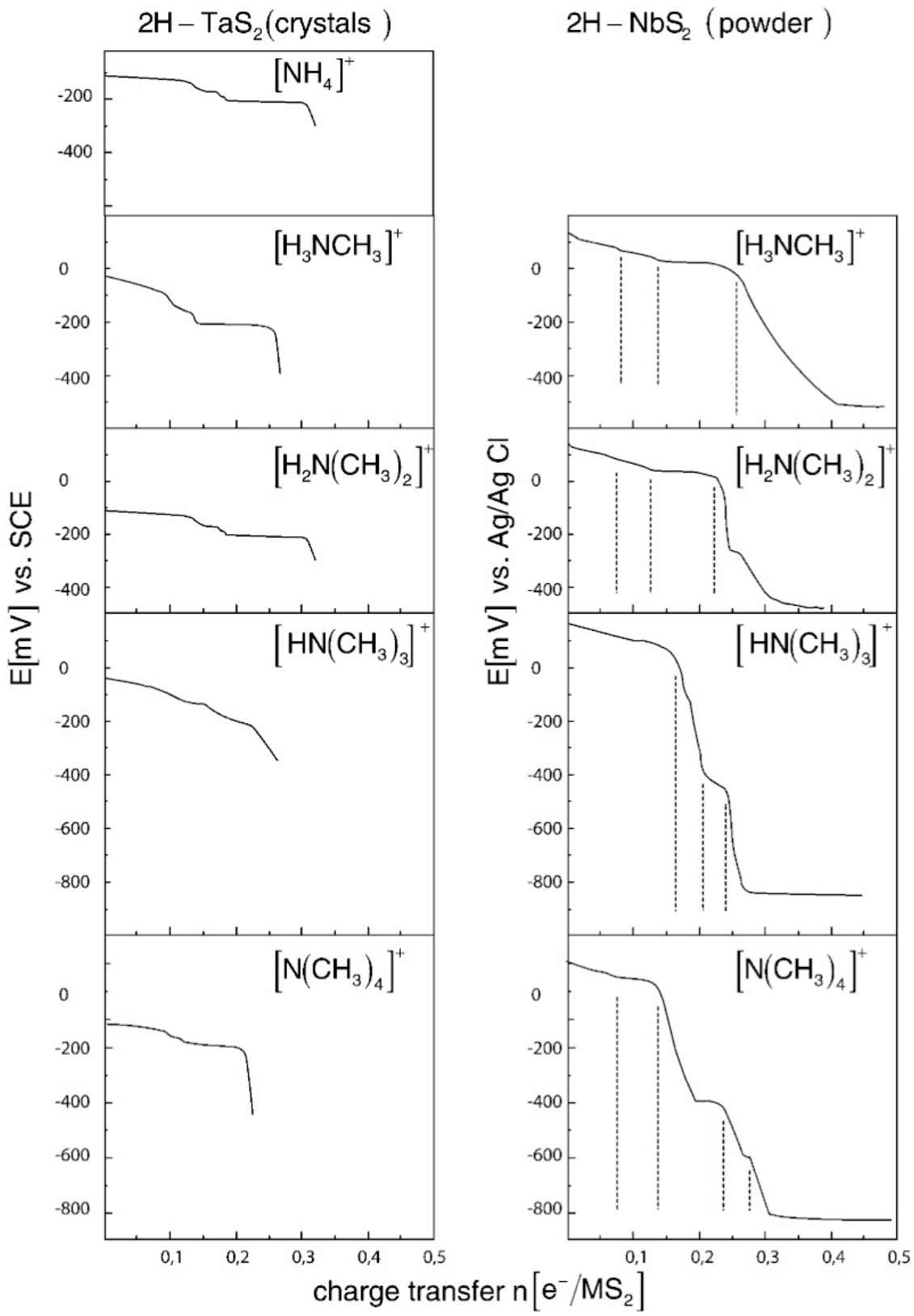

Figure 1: Potential vs. charge transfer n curves for the galvanostatic intercalation of methylated ammonium ions into 2H-TaS_2 and NbS_2

The lower limit of the single phase region varies with the type of the alkylammonium ions. It corresponds to a charge transfer n = 0.31 (because these ions are univalent n = x, the content of alkylammonium ions) for $NH_4^+TaS_2$ and decreases to n = 0.21 for $[N(CH_3)_4]^+$. For $[N(CH_3)_4]_xNbS_2$ we observed a lower value. Why there is such a strong difference in n_{onset} of the single phase regions is not clear, since the size of the inserted ions and the unit cell of both dichalcogenides within the layer planes are identical.

In case of the TaS_2-compounds the reaction is interrupted immediately after arriving the single phase regions to avoid the problems of water decomposition. In the NbS_2-compounds the reaction has been continued till the potential arrives at a constant value determined by the hydrogen evolution (water decomposition). There are regions of constant potential within the single phase region. Its origin is not known at present. This phenomenon and the above mentioned difference in the $x_{onset} = n_{onset}$ values in both series of compounds is the matter of present investigations.

The potential (measured vs. Ag/AgCl or SCE) at the onset of the first stage region is about 200 mV more negative for TaS_2 than for NbS_2, in excellent agreement with the higher oxidizing power of the latter one.

In case of the $[H_{4-z}N(CH_3)_z]_xNbS_2$ system chemical analysis and TG-DTA indicates that in addition to the charge compensating alkylammonium ions free amine and water are intercalated as solvating species.

References

[1] R. Schöllhorn, Angew. Chem. Int. Ed. Engl. **19**, 983 (1980).
[2] R. Schöllhorn, and H. D. Zagefka, Angew. Chem. Int. Ed. Engl. **16**, 199 (1977).
[3] R. Schöllhorn, H.D. Zagefka, T. Butz, and A. Lerf, Mat. Res. Bull. **14**, 369 (1979).
[4] F.R. Gamble, J.H. Osiecki, M. Cais, R. Pisharody, F.J. DiSalvo, and T.H. Geballe, Science **174**, 493 (1971).
[5] G. V. Subba Rao, and M. W. Shafer, in F. Levy (ed.), *Intercalated Layered Materials*, Reidel Publishing Company, Dordrecht (1979).
[6] P. Colombet, and V. Cajipe, Eur. J. Solid State Inorg. Chem. **26**, 255 (1989).
[7] G.V. Subba Rao, M.W. Shafer, and J.C. Tsang, J. Phys. Chem. **79**, 553 (1975).
[8] Y. Kanzaki, M. Konuma, and O. Matsumoto, J. Phys. Chem. Solids **41**, 525 (1980).
[9] B.M.L. Rao, and T.R. Halbert, Mat. Res. Bull. **16**, 919 (1981).

Computing, Network, and Internet Services

D. Guratzsch, J.B. Philipp, F. Venturini, M. Opel

In the previous year a lot of changes were made concerning computing and the network and internet services at the Walther-Meißner-Institut (WMI). The situation at the beginning of year 2000 was as follows. The local area network (LAN) consisted of single personal computers (PC) connected with each other via 10MBit Ethernet. They represented a simple peer-to-peer network (workgroup wmi) which had been set up during the previous five years together with the step-by-step introduction of "new" operating systems such as *Windows for Workgroups*, *Windows 95*, and *Windows NT*. This process led to an extremely inhomogeneous and confusing logical structure of the network place.

One of the main disadvantages of this workgroup-based network was the nonexistence of a common users' database. So each user always had to keep in mind different user names and passwords for each workstation in order to get access to the network resources such as shared folders or printers. At the beginning of the year we decided to set up a new, modern, domain-based internal network which is operated by a new server. This computer should provide both a users' and a computers' database and act as a domain controller. In addition, it should also provide file and print services. The remaining network services such as electronic mail, world wide web publishing, or backup and storage/archiving were taken over by the high-performance and high-reliable servers of the Leibniz-Rechenzentrum (LRZ) (Tab. 1).

Table 1: Network services

Service	operated by
domain controller	WMI
fileserver	WMI
printserver	WMI
mailserver	LRZ
webserver	LRZ
file backup	LRZ
file storage/archiving	LRZ

The first step was to select the new operating system. We decided to use the commercial system *Windows 2000 Server* as the WMI staff had gained some experience concerning Windows during the past years. Together with the services which should be provided this decision also fixed the hardware components necessary for the domain controller (Tab. 2). The computer is registered within the internet domain name service (DNS) as everest.wmi.badw-muenchen.de. It started operation in July 2000. Since then all PCs within our DNS name space wmi.badw-muenchen.de represent one single domain.

Table 2: Technical specifications of the domain controller

motherboard	ASUS P2B
number of CPUs	2 (Intel Pentium III, 650 MHz)
RAM	512 MByte
storage system	72 GByte (RAID level 5)
number of harddisks	3

The main advantages of this structure are:

- Each staff member has only one single user name with password which is valid for all computers and network resources within the WMI.
- Each user got an own home directory in the network. It is located on the network drive operated by the server and is backed up every night automatically by the LRZ using *Adstar Distributed Storage Management* (ADSM). In the case of data losses these home directories can be restored within a few minutes to the status of the previous night.
- Standard software which should be available on each PC within the WMI may be installed on the domain controller and then distributed among the network computers. This helps saving time and makes administration easier.

- The domain controller provides print services for shared printers. Windows operating systems are able to download the necessary printer drivers automatically when connecting to the server (*point-and-print* technology).
- Together with this reconstruction of the network a computer room was established in room No. 130. It is equipped with two shared printers, three workstations, one scanner, and one CD writer. All these machines may be used by all staff members and guests.

In the last years electronic mail (email) became an important tool for exchanging information within the WMI as well as between the WMI and other institutions. Together with the LRZ which operates our email service we could improve the situation in three ways. First, a new mail subdomain wmi.badw-muenchen.de (alias: wmi.badw.de) was registered within DNS. This made it possible to introduce easy-to-remember mail addresses of the form Firstname.Lastname@wmi.badw.de. Second, the LRZ increased the number of available mail accounts so that every staff member could get his/her own email address. Last, three email distribution lists were established. They provide an easy way to send messages to the scientific, non-scientific, or to all staff members by simply using one single address.

Last but not least, the presentation of the WMI in the world wide web (WWW) has been improved considerably in the past year. Since the beginning of the winter semester 2000/01 our updated and re-structured homepage is online. It is published by a virtual webserver of the LRZ under the uniform resource locator (URL) http://www.wmi.badw.de and offers information about the institute and its staff as well as about research and teaching. It is still growing and will be updated regularly.

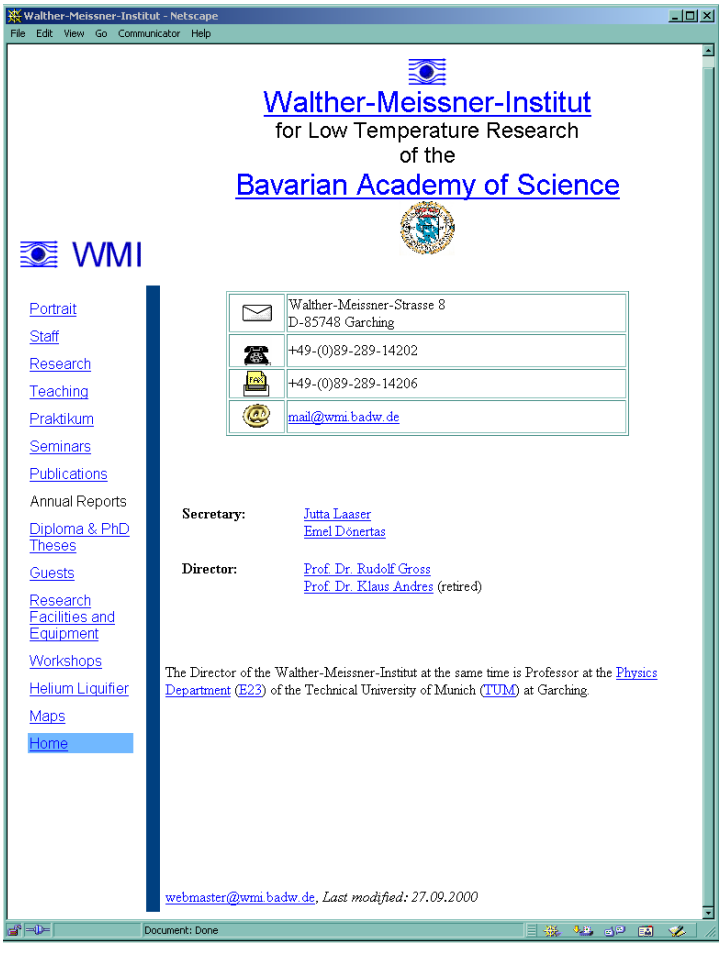

Figure 1: The new homepage of the WMI (http://www.wmi.badw.de)

In conclusion, the situation concerning computers, network, and internet services at the WMI has been improved considerably in the past year. After having set up the domain controller the administration of the internal network with all its resources will become easier in the future. The equipment of the computer room provides access to special devices like scanners and CD writers for all staff members. With the changes concerning electronic mail the people at the WMI now have uniform and easy-to-remember email addresses. Finally, after having updated our WWW homepage the Walther-Meißner-Institut is represented in a more fashionable and appropriate way within the world wide web.

Publications

1. **Large two-level magnetoresistance effect in doped manganite grain boundary junctions**
   J. B. Philipp, C. Höfener, S. Thienhaus, J. Klein, L. Alff, and R. Gross
   Phys. Rev. **B 62**, Rapid. Com., R9248 (2000).
2. **Local Magnetic Order in Manganite Thin Films Studied by $1/f$ Noise Measurements**
   P. Reutler, A. Bensaid, F. Herbstritt, C. Höfener, A. Marx, and R. Gross
   Phys. Rev. **B 62**, 11619 (2000).
3. **Role of ion beam etching in the fabrication of ramp-type junctions**
   U. Schoop, M. Schonecke, S. Thienhaus, S. Schymon, L. Alff, and R. Gross
   Physica **C**, accepted for publication (06/2000).
4. **Magnetoresistance of Coherently Strained $La_{2/3}Ba_{1/3}MnO_3/SrTiO_3$ Superlattices**
   Yafeng Lu, J. Klein, C. Höfener, B. Wiedenhorst, J. B. Philipp, F. Herbstritt, L. Alff, and R. Gross
   Phys. Rev **B**, accepted for publication (09/2000).
5. **Voltage-Flux-Characteristics of Asymmetric dc SQUIDs**
   J. Müller, S. Weiss, R. Gross, R. Kleiner, and D. Koelle
   IEEE Trans. Appl. Supercond., accepted for publication (09/2000).
6. **Transport and Noise Characteristics of Submicron High Temperature Superconductor Grain Boundary Junctions**
   F. Herbstritt, T. Kemen, A. Marx, and R. Gross
   Appl. Phys. Lett., accepted for publication (11/2000).
7. **Comparison of Josephson vortex flow transistors with different gate line configurations**
   J. Schuler, S. Weiss, T. Bauch, A. Marx, D. Koelle, and R. Gross
   Appl. Phys. Lett., accepted for publication (11/2000).
8. **Possible Pseudogap Behavior of Electron Doped High-Temperature Superconductors**
   S. Kleefisch, B. Welter, M. Naito, A. Marx, L. Alff, and R. Gross
   Phys. Rev. Lett., submitted for publication (10/2000).
9. **Canted Antiferromagnetism in $La_{0.94}Sr_{0.06}MnO_3$**
   J. Geck, M. Hücker, B. Büchner, R. Gross, L. Pinsard-Gaudart, and A. Revcolevschi
   Phys. Rev. **B**, submitted for publication (11/2000).
10. **Josephson Vortex Flow Transistors: Numerical Analysis and Experimental Results**
    J. Schuler, T. Bauch, S. Weiss, D. Koelle, R. Gross
    J. Appl. Phys., submitted for publication (11/2000).
11. **Magnetic Field-Temperature Phase Diagram of the Organic Conductor α-(BEDT-TTF)$_2$KHg(SCN)$_4$**
    P. Christ, W. Biberacher, M. V. Kartsovnik, E. Steep, E. Balthes, H. Weiss, and H. Müller
    JETP Letters 71, 303-306 (2000).
12. **Supraleitung und Suprafluidität**
    D. Einzel
    Essay für das Lexikon der Physik (2000).
13. **Suprafluidität in Wasserstoff**
    D. Einzel
    Physikalische Blätter 56, 13-14 (2000)
14. **Thermal excitations in (d + s)-wave superconductors**
    D. Einzel, I. Schürrer
    Physica B 284-288, 451-452 (2000)
15. **Heteroeptaxial Growth of Transation Metal Oxides Using UHV Laser Molecular Beam Epitaxy**
    R. Gross, J. Klein, B. Wiedenhorst, C. Höfener, U. Schoop, J. B. Philipp, M. Schonecke, F. Herbstritt, L. Alff, Yafeng Lu, A. Marx, S. Schymon, S. Thienhaus, and W. Mader

Superconducting and Related Oxides: Physics and Nanoengineering IV, D. Pavuna and I. Bosovic eds., SPIE Conf. Proc. 4058, 278-294 (2000).

16. **Mapping of the anomalous magnetotransport regime in the α-(BEDT-TTF)$_2$*M*Hg(SCN)$_4$ (*M* = K, Tl) organic conductors**
    M.M. Honold, N. Harrison, M.V. Kartsovnik, H. Yaguchi, C.H. Mielke, J. Singleton, N.D. Kushch, M. Kurmoo, and P. Day
    Phys. Rev. B 62, 7908-7919 (2000).
17. **Pseudogap and Superconducting Gap in $YBa_2Cu_3O_{6+\gamma}$: A Raman Study**
    M. Opel, M. Götzinger, Ch. Hoffmann, R. Nemetschek, R. Philipp, F. Venturini, R. Hackl, A. Erb, and E. Walker
    J. of Low Temp. Phys. 117, 347-351 (1999).
18. **Superconducting gap and pseudogap in Bi-2212**
    M. Opel, F. Venturini, R. Hackl, B. Revaz, H. Berger, and L. Forró
    Physica B 284-288, 669-670 (2000).
19. **Carrier relaxation, pseudopap, and superconducting gap in high-T_c cuprates: A Raman scattering study**
    M. Opel, R. Nemetschek, C. Hoffmann, R. Philipp, P.F. Müller, R. Hackl, I. Tüttö, A. Erb, B. Revaz, E. Walker, H. Berger, and L. Forró
    Phys. Rev. B 61, 9752-9774 (2000).
20. **Comment on "Contribution of small closed orbits to magnetoresistance in quasi-two-dimensional conductors"**
    V.G. Peschansky, M. V. Kartsovnik
    Phys. Rev. B 60, 11207-11209 (1999).
21. **Galvanomagnetic Phenomena in Layered orbits to magnetoresistance in quasi-two-dimensional conductors**
    V.G. Peschansky, M. V. Kartsovnik
    Phys. Rev. B 60, 11207-11209 (1999).
22. **Fermi Surface in the New Organic Quasi-Two-Dimensional Metal α-(BETS)$_2$TlHg(SeCN)$_4$**
    S.I. Pesotskii, R.B. Lyubovskii, V.I. Nizhankovskii, . Biberacher, M.V. Kartsovnik, K. Andres, J.A.A.J. Perenboom, N.D. Kushch, E.B. Yagubskii, and H. Kobayashi
    J. of Experimental and Theoretical Physics 90, 527-534 (2000).
23. **de Haas-van Alphen oscillations and angular magnetoresistance oscillations in the organic metal κ-(BETS)$_2$GaCl$_4$)**
    S.I. Pesotskii, R.B. Lyubovskii, M.V. Kartsovnik, W. Biberacher, N.D. Kushch, K. Andres, H. Kobayashi, and A. Kobayashi
    J. of Experimental and Theoretical Physics 88, 114-117 (1999).
24. **Quantum oscillations and phase diagram of α-(BEDT-TTF)$_2$TlHg(SCN)$_4$**
    C. Proust, A. Audouard, D. Vignolles, A. Kovalev, M.V. Kartsovnik, L. Brossard, and N. D. Kushch
    Phys. Rev. B 62, 2388-2396 (2000).
25. **Evidence for unconventional superconductivity in UPt_3 from magnetic torque studies**
    S. Schöttl, E.A. Schuberth, K. Flachbart, J.B. Kycia, W.P. Halperin, A.A. Menovsky, E. Bucher, and J. Hufnagl
    Phys. Rev. B 62, 4124-4131 (2000).
26. **Magnetic study of the UPt_3 superconducting phases**
    S. Schöttl, E.A. Schuberth, J.B. Kycia, and W.B. Halperin
    Physica B 280, 174 (2000).
27. **DC magnetic penetration depth of UPt_3 and Sr_2RuO_4**
    S. Schöttl, E.A. Schuberth, J.B. Kycia, W.B. Halperin, and T. Sasaki
    Journ. Magn. Magn. Mat., accepted for publication (2000).

28. **Platinum black sinters for the heat exchangers at very low temperatures**
    E.A. Schuberth, E.D. Adams, and Y. Takano
    Cryogenics 39, 799-801 (1999).
29. **Schwere Fermion Systeme**
    E. Schuberth
    Stichwortbeitrag zum Lexikon der Physik Bd 5, (2000)
30. **Destille am WMI**
    K. Uhlig
    Akademie Aktuell 1, 17 (2000).
31. **Klein und fein, neuer Mini-Kühler am Walther-Meißner-Institut**
    K. Uhlig
    Akademie Aktuell 2, 11 (2000).
32. **Collective modes and electronic Raman scattering in the cuprates**
    F. Venturini, U. Michelucci, T.P. Devereaux, and A.P. Kampf
    Physica C 341-348, 2265-2266 (2000).
33. **Collective spin fluctuation mode and Raman scattering in superconducting cuprates**
    F. Venturini, U. Michelucci, T.P. Devereaux, and A.P. Kampf
    Phys. Rev. B 62, 15204-15207 (2000).
34. **Direct observation of vortices in the organic superconductor κ-(BEDT-TTF)$_2$Cu(NCS)$_2$**
    L.Ya. Vinnikov, T.L. Barkov, M.V. Kartsovnik, and N.D. Kushch
    Phys. Rev. B 61, 14358-14361 (2000).
35. **Angle-dependent magnetoquantum oscillations in κ-(BEDT-TTF)$_2$Cu[N(CN)$_2$]Br**
    H. Weiss, M.V. Kartsovnik, W. Biberacher, E. Balthes, A.G.M. Jansen, and N.D. Kushch
    Phys. Rev. B 60, R16259-16262 (1999).
36. **Dilatometric investigations at graphite electrodes in lithium battery electrolytes**
    M. Winter, G.H. Wrodnigg, J.O. Besenhard, W. Biberacher, and P. Novák.
    J. Electrochem. Soc. 147, 2427-2432 (2000).
37. **Indication for an antiferromagnetically ordered state in the organic conductor κ-(BETS)$_2$FeCl$_4$**
    D. Zhang, K. Andres, Ch. Probst, W. Biberacher, N.D. Kushch, and H. Kobayashi
    Solid State Comm. 115, 433-437 (2000).

Completed Diploma and Ph.D. Theses

1. *Eigenschaften des Elektronensystems und seiner Wechselwirkungen in antiferromagnetischen und supraleitenden Kupraten: Eine Raman-Studie*
   Matthias Opel, Ph.D. Thesis (07/2000)

Research Projects and Cooperations

Deutsche Forschungsgemeinschaft

1. Elektronenmikroskopische Analyse von Defektstrukturen, lokalen strukturellen Eigenschaften und Ladungsordnungsph”anomenen in dotierten Manganaten
   (R. Gross, Az. GR 1132/3-1)
   Partner: Universität Bonn

2. Untersuchung des niederfrequenten $1/f$ Rauschens in Josephson-Kontakten aus Hochtemperatur-Supraleitern zur Charakterisierung elementarer Rauschzentren und Klärung der Transportmechanismen
   (A. Marx und R. Gross, Az. Ma 1953/1-1+2)

3. Vortex-Antidot-Wechselwirkung in dünnen Schichten aus Hochtemperatur-Supraleitern
   (R. Wördenweber, R. Gross und R. P. Hübener), Az. GR 1132/11-1, -2

4. Heteroepitaxie von Übergangsmetalloxiden
   (L. Alff und R. Gross, Az. Al 560/1-1+2)

5. Kristalline organische Metalle und Supraleiter: Synthese und elektronische Eigenschaften, gefördert von DFG und der russischen Stiftung für Grundlagenforschung (RFFI)
   (W. Biberacher, WMI, und N. Kushch, Institut für Probleme der chemischen Physik, Cernogolovka)

Bundesminister für Bildung, Wissenschaft, Forschung und Technologie

1. Verbundprojekt: Ultra-schnelle und ultra-verlustarme Informationstechnik-Komponenten; Teilvorhaben: Transport- und Rauscheigenschaften von Nano-SiGe-Bauelementen
   (R. Gross und A. Marx, Förderkennzeichen: 13N7902)
   Partner: DaimlerChrysler AG, AMO GmbH

European Union

1. Research and Training of Young Researchers on the Magnetic Properties of ^{3}He by Means of Neutron Diffraction
   (E. Schuberth; Kordination: Dr. Konrad Siemensmeyer, Hahn-Meitner Institut, Berlin)
   Partner: Hahn-Meitner Institut, Berlin, Univ. of Florida, Royal Holloway College, London, Univ. Liverpool, CNRS, Grenoble und Univ. Paris, Saclay

2. ESF-Netzwerk *“Vortex Matter at Extreme Scales and Conditions”*
   (R. Gross; Koordination: Prof. Moshchalkov, Univ. Leuven)
   Partner: Mehrere europäische Universitäten und Forschungseinrichtungen

3. High Field Infrastructure Cooperative Network
   (W. Biberacher)
   Partner: insgesamt 31 Teilnehmer, Federführung: CNRS Grenoble

Deutscher Akademischer Austauschdienst

1. Projektbezogener Personenaustausch mit Ungarn
   (R. Hackl)
   Ungarische Akademie der Wissenschaften, Institut für Festkörperphysik und Optik, Prof. Istvan Tüttő

2. Projektbezogener Personenaustausch mit Italien, Vigoni-Programm
   (R. Hackl)
   Universita di Roma La Sapienza, Instituto Nazionale di Fisica della Materia, Prof. Paolo Calvani

Invited Talks

Lambert Alff

1. **Symmetry of the order parameter in hole and electron doped cuprate superconductors**
   18th General Conference of the Condensed Matter Division of the European Physical Society (EPS), Montreux, Switzerland
   March 13 - 17, 2000.

2. **Symmetrie der Cooper-Paare in unkonventionellen Supraleitern**
   Großes Physikalisches Kolloquium, Universität Karlsruhe
   26. 06. 2000

3. **Supraleiter mit unkonventioneller Symmetrie des Ordnungsparameters**
   Seminar des Sonderforschungsbereich 252, Universität Mainz
   08. 06. 2000

4. **Physik der Korngrenzenkontakte in oxidischen dünnen Filmen: Von der Symmetrie des Ordnungsparameters in unkonventionellen Supraleitern zu spinabhängigem Transport in dotierten Manganaten**
   Universität Tübingen
   28. 07. 2000

Dieter Andres

1. **Effects of high magnetic field and pressure on the density wave state in the organic metal α-(BEDT-TTF)$_2$KHg(SCN)$_4$**
   Users' Meeting at the HFML in Grenoble
   09. 09. 2000

Dietrich Einzel

1. **Ballistischer Transport von ^{3}He in Aerogel**
   Kommissionssitzung des Walther-Meissner-Instituts, Garching
   15. 01. 2000

2. **Response and Transport in unkonventionellen Supraleitern**
   Festkörperphysik–Kolloquium, Freie Universität Berlin
   12. 05. 2000

3. **Knudsenströmung von normalfluidem ^{3}He in Aerogel**
   Kolloquium der Forschergruppe "*Transportphänomene und Supraleitern und Suprafluiden*", Universität Bayreuth
   21. 07. 2000

4. **Superonductivity and Superfluidity**
   Lecture at the Graduiertenkolleg *Struktur und Korrelationseffekte in Festkörpern*, Dresden
   03. 11. 2000

Rudolf Gross

1. **Kolossaler Magnetwiderstand in dotierten Manganaten: Physikalische Grundlagen und technische Anwendung**
   Kolloquium des Instituts für Festkörperforschung, Forschungszentrum Jülich
   19. 01. 2000

2. **Magnetoresistive Effekte in dotierten Manganaten: Physikalische Grundlagen und technische Anwendung**
   Festkörpertag, Universität Bonn
   11. 02. 2000

3. **Heteroepitaxial Growth of Transition Metal Oxides Using UHV Laser Molecular Beam Epitaxy**
   SPIE Conference on Oxide Nanoengineering: *Superconducting and Related Oxides*,
   April 24 - 28, 2000, Orlando, USA

4. **Oxidische Elektronik**
   Festkolloquium an der Universität Mainz
   19. 05. 2000

5. **Dotierte Manganate: Verspannungseffekte, Grenzflächen und magnetoelektronische Bauelemente**
   Kolloquium des Sonderforschungsbereichs 484, Universität Augsburg
   24. 10. 2000

Rudi Hackl

1. **Carrier relaxation, pseudogaps and gaps in cuprate systems**
   Universität Linz, Austria
   24. 01. 2000

2. **Gap excitations in superconductors**
   University of Illinois, Urbana-Champaign, USA
   18. 11. 2000

3. **A light-scattering study of charge excitations in copper-oxide systems**
   Simon Fraser University, Burnaby, Canada
   22. 11. 2000

4. **Carrier dynamics in differently doped cuprates as observed by inelastic light scattering**
   Institut für Festkörper- und Werkstofforschung, Dresden
   04. 12. 2000

Mark Kartsovnik

1. **B – T – P phase diagram of α-(BEDT-TTF)$_2$KHg(SCN)$_4$**
   International Conference on Science and Technology of Synthetic Metals (ICSM 2000), Bad Gastein (Austria)
   20. 07. 2000

2. **On the nature of the low-temperature electronic state in α-(ET)$_2$KHg(SCN)$_4$**
   Institute for Solid State Physics of the Russian Academy of Science in Chernogolovka, Russia
   20. 12. 2000

Achim Marx

1. **Noise measurements as diagnostic tool: Manganite thin films and HTS Junctions**
   Gesamttreffen des Leitprojekts Magnetoelektronik, Max-Planck-Institut für Mikrostrukturphysik in Halle
   December 05 - 06, 2000

Matthias Opel

1. **Raman-Spektroskopie an Hochtemperatur-Supraleitern**
   Seminar über aktuelle Probleme der Festkörpertheorie, Universität Augsburg
   14. 06. 2000

Erwin Schuberth

1. **Novel Magnetism in 3He Nanoclusters**
   18th General Conference of the Condensed Matter Division of the European Physical Society (EPS), Montreux, Switzerland, March 13 - 17, 2000.
2. **Heavy Fermion Systems at Very Low Temperatures**
   Department of Physics, University Sao Paulo, Brasil,
   August 11 - 20, 2000

Francesca Venturini

1. **Spin-fluctuation contributions to electronic Raman scattering**
   MPI für Festkörperforschung, Stuttgart
   19. 05. 2000

Seminars

1. **Magnetoresistance Studies of the Organic Metal α-$(ET)_2KHg(SCN)_4$ under Pressure**
   Dieter Andres, Walther-Meissner-Institut
   10. 01. 2000
2. **Study of Anomalies in the Normal State of Cuprates: Acoustic Measurements**
   Dr. Qing-ming Zhang, National Laboratory of Solid State Microstructures, Nanjing University, China
   21. 01. 2000
3. **Kryodetektoren zur Analyse von Röntgenstrahlung**
   Dr. Matthias Bühler, CSP Cryogenic Spectrometers GmbH
   28. 01. 2000
4. **Hochtemperatursupraleiter: Von der Physik zu neuen Anwendungen (mit Demonstationsexperimenten)**
   Prof. Dr. L. Schultz, Institut f. Metallische Werkstoffe, TU Dresden
   04. 02. 2000
5. **Magneto-quantum oscillations in the alkaline earth subnitride NaBa3N and the organic superconductor κ-$(BEDT\text{-}TTF)_2Cu[N(CN)_2]Br$**
   Dipl.-Phys. Herbert Weiss, High Magnetic Field Laboratory, Grenoble, France
   18. 02. 2000
6. **Pulsed-Laser Deposition of HTS Thin Films**
   Dr. Johannes Pedarnig, Abteilung für Angewandte Physik, Johannes-Kepler-Universität, Linz
   25. 02. 2000
7. **Neue Resultate an hochreinen 123-Einkristallen**
   Dr. Andreas Erb, Département de Physique de la Matiére Condensée, Université de Genéve
   03. 03. 2000
8. **Quantum oscillation experiments in the strongly 2D organic superconductor κ-$(BEDT\text{-}TTF)_2I_3$**
   Dr. E. Balthes, Universität Stuttgart und Hochfeld-Magnetlabor, Grenoble
   05. 05. 2000
9. **Electromagetic response in SDW systems**
   Prof. A. Virosztek, Research Institute for Solid State Physics and Technical University, Budapest
   12. 05. 2000
10. **Raman scattering in antiferromagnets**
    Dr. P. Knoll, Karl-Franzens-Universität, Graz
    19. 05. 2000
11. **Mid-Infrarot-Absorption in $YBa_2Cu_3O_6$: Versagen der Spinwellentheorie für Spin 1/2 in zwei Dimensionen**
    Dr. Markus Grüninger, Laboratory of Solid State Physics, MSC, University of Groningen und II. Physikalisches Institut, Universität zu Köln
    26. 05. 2000
12. **Infrared Studies of Symmetry Reduction in Polymeric Fullerenes and Fullerides**
    Prof. Dr. K. Kamarás, Research Institute for Solid State Physics and Optics, Hungarian Academy of Sciences, Budapest
    31. 05. 2000
13. **Festkörperphysik quo vadis? Teil II**
    Dr. Anton Lerf, Walther-Meissner-Institut
    09. 06. 2000
14. **Electro-mangetic response of the core of pancake vortices**
    Prof. Dr. D. Rainer, Universität Bayreuth

15. 06. 2000

15. **Superconductivity (some historical and other remarks)**
    Prof. Dr. V.L. Ginzburg, P.N. Lebedev Physics Institute, Moscow
    28. 07. 2000
16. **Dynamical redistribution of mean electron spin over the energy spectrum of quantum dots**
    Dr. V.K. Kalevich, Ioffe Physico-Technical Institute, St. Petersburg, Russland
    04. 08. 2000
17. **Präparation, Charakterisierung und Magnetotransportmessungen an dünnen Sr_2FeMoO_6-Schichten**
    Dipl.-Phys. Daniel Reisinger, Universität Mainz
    01. 09. 2000
18. **Relaxation and Pairing in High-Temperature Superconductors**
    Prof. Dr. E.G. Maksimov, P.N. Lebedev Physical Institute, Moscow, Russia
    11. 09. 2000
19. **Andreev bound states in high-T_c superconducting junctions**
    Tomas Löfwander, Chalmers University of Technology, Göteborg, Schweden
    15. 09. 2000
20. **The de Haas-van Alphen effect in quasi-two-dimensional metals**
    P. Grigoriev, L.D. Landau Institute for Theoretical Physics, Moscow
    18. 09. 2000
21. **Novel magnetism in 3He nanoclusters**
    Prof. Dr. E. Dwight Adams, MicroKelvin Facility, University of Florida
    06. 10. 2000
22. **Spinpolarisiertes Tunneln in Manganaten**
    Dipl.-Phys. B. Philipp, Walther-Meissner-Institut
    20. 10. 2000
23. **Unconventional Density Waves in a-(ET)2 Salts**
    Dipl.-Phys. Balźs Dóra, Institute of Physics, Technical University of Budapest
    23. 10. 2000
24. **De Haas-van Alphen oscillations in organic conductors: the coherent magnetic breakdown issues in periodic structures**
    Prof. Dr. V. Gvozdikov, Kharkov National University, Kharkov, Ukraine
    27. 10. 2000
25. **Tunnelspektroskopie**
    Dipl.-Phys. B. Welter, Walther-Meissner-Institut
    03. 11. 2000
26. **Angle-dependent magnetoresistance in layered organic metals**
    Dr. Mark Kartsovnik, Walther-Meissner-Institut
    06. 11. 2000
27. **Scanning Tunneling Spectroscopy studies of High Temperature Superconductors**
    Dr. I. Maggio-Aprile, Department of Condensed Matter Physics, University of Geneva, Switzerland
    10. 11. 2000
28. **Electronic Raman Scattering in Hg-based HTSC Compounds**
    Dr. A. Sacuto, École Sup'erieure de Physique et de Chimie Industrielle, Paris
    01. 12. 2000
29. **Microcalorimetry in extreme conditions of pressure (0 to 250 kbars) and/or of magnetic field (0 to 30 Tesla)**
    Dr. Ch. Marcenat, CEA/Grenoble, Departement de Recherche Fondamentale
    08. 12. 2000

30. **Coupling between lattice distortions and magnetism in manganite thin films**
    Dr. A. Vigliante, MPI, Stuttgart
    13. 12. 2000
31. **Elektronen-/Ionen Transferprozesse in Metalloxiden**
    Prof. Dr. R. Schöllhorn, Walther-Meissner-Institut
    15. 12. 2000
32. **Raman and infrared spectroscopy in manganites under high pressure**
    Dr. P. Postorino, Universitá di Roma La Sapienza
    20. 12. 2000

Staff of the WMI

Director

Prof. Dr. Gerhard Abstreiter (until 30. 06. 2000)
Prof. Dr. Rudolf Gross (since 01. 07. 2000)

Technical Director

Dr. Karl Neumaier

Administration/Secretary's Office

Jutta Laaser
Emel Dönertas

Scientific Staff

Dr. habil. Lambert Alff
Dr. Werner Biberacher
Dr. habil. Dietrich Einzel
Dr. habil. Andreas Erb
Dr. habil. Rudi Hackl
Dr. Mark Kartsovnik
Dr. habil. Anton Lerf
Dr. Achim Marx
Dr. Matthias Opel
Dr. Christian Probst
Dr. habil. Erwin Schuberth
Dr. Kurt Uhlig
Dr. habil. Edgar Umlauf
Dipl.-Phys. Dieter Andres
Dipl.-Phys. Boris Philipp
Dipl.-Phys. Daniel Reisinger
Dipl.-Phys. Mitja Schonecke
Dipl.-Phys. Jürgen Schuler
Dipl.-Phys. Francesca Venturini
Dipl.-Phys. Bettina Welter

Technical Staff

Joachim Geismann
Gabrielle Görblich
Ulrich Guggenberger
Dieter Guratzsch
Hermann Hagn
Wolfgang Hehn
Julius Klaus
Robert Müller
Roman Müller
Jan Naundorf
Georg Nitschke
Walter Nitschke
Christian Reichlmeier
Harald Schwaiger
Helmut Thies
Siegfried Wanninger

Assistants

Ingrid Freimuth
Sybilla Plöderl

Permanent Guests

Prof. Dr. B. S. Chandrasekhar
Dr. Robert Doll
Prof. Dr. Schöllhorn

Guest Researchers

1. Prof. Dr. B.S. Chandrasekhar
   permanent guest
2. Dr. Robert Doll
   permanent guest
3. Prof. Dr. Schöllhorn
   permanent guest
4. Dr. Qing-ming Zhang, Nanjing University, Nanjing, China
   03. 01. – 23. 01. 2000, 22. 10 – 31. 12. 2000
5. Dr. Attila Virosztek, Central Research Institute for Solid State Physics and Optics, Hungarian Academy of Sciences, Technische Universität Budapest, Budapest, Hungary
   08. 05. – 19. 05. 2000, 6. 11. – 17. 11. 2000
6. Prof. Dr. K. Kamaras, Central Research Institute for Solid State Physics and Optics, Hungarian Academy of Sciences, Technische Universität Budapest, Budapest, Hungary
   27. 05. bis 03. 06. 2000
7. Prof. Dr. A. Zawadowski, Technische Universität Budapest, Budapest, Hungary
   03. 07. – 16. 07. 2000
8. Dr. I. Tüttö, Central Research Institute for Solid State Physics and Optics, Eötrös Lorand University, Budapest, Hungary
   28. 07. – 18. 08. 2000
9. Prof. Dr. Juan Poyato Ferrera, Instituto de Ciencia de Materiales de Sevilla, Sevilla, Spanien
   03. 08. – 03. 09. 2000
10. Dr. F. Borondics, Central Research Institute for Solid State Physics and Optics, Budapest, Hungary
    23. 08. – 31. 08. 2000
11. Pavel Grigoriev, Hochfeld-Magnetlabor, Grenoble, France
    10. 09. – 21. 09. 2000
12. Dr. Sergei Pesotskii, Institut für Probleme der Chemischen Physik, Chernogolovka
    18. 09. – 17. 10. 2000
13. Dr. Nataliya Kushch, Institut für Probleme der Chemischen Physik, Chernogolovka
    03. 10. – 02. 12. 2000
14. Dr. Alessandro Nucara, Universitá di Roma ”La Sapienza”, Roma, Italy
    06. 10 – 14. 10. 2000
15. Dr. Alexei Kovalev, Institut für Festkörperphysik, Chernogolovka
    12. 10. – 11. 12. 2000
16. Balázs Dòra, Technische Universität Budapest, Budapest, Hungary
    19. 10 – 24. 10. 2000
17. Dr. Karol Flachbart, Institut für Experimentelle Physik, Slowakische Akademie der Wissenschaften, Kosice
    13. 11. – 10. 12. 2000
18. Prof. Paolo Calvani, Universitá di Roma ”La Sapienza”, Roma, Italy
    30. 11 – 03. 12. 2000
19. Prof. Dr. P. Capkova, Department of Chemical Physics and Optics, Karls-Universität, Prag
    04. 12. – 09. 12. 2000

Commission for Low Temperature Physics

Members of the Commission for Low Temperature Physics of the Bavarian Academy of Sciences:

Kaiser, Wolfgang, Leiter (Technische Universität München)
Brenig, Wilhelm, stellv. Leiter (Technische Universität München)
Landwehr, Gottfried (Universität Würzburg)
Hänsch, Theodor (Max-Planck Institut für Quantenoptik, Garching)
Koch, Frederick (Technische Universität München)
Kotthaus, Jörg Peter (Ludwig-Maximilians-Universität München)
Rainer, Dierk (Universität Bayreuth)
Renk, Karl Friedrich (Universität Regensburg)
Schwoerer, Markus (Universität Bayreuth)